



FAKULTÄT FÜR VERFAHRENS-  
UND SYSTEMTECHNIK

# File-based post-processing of DNS results for turbulent flames using MATLAB

**Dissertation**

zur Erlangung des akademischen Grades

**Doktoringenieur  
(Dr.-Ing.)**

von **Dipl.-Ing. Christiane Zistl**  
geb. am 05.03.1969 in München

genehmigt durch die Fakultät für Verfahrens- und Sytemtechnik  
der Otto-von-Guericke-Universität Magdeburg

Promotionskommission    Vorsitz:    Prof. Dr.-Ing. Ulrich Krause  
   Gutachter: Prof. Dr.-Ing. Dominique Thévenin  
   Gutachter: Prof. Dr.rer.nat. Ulrich Maas  
   Gutachter: Dr.-Ing. Renan Hilbert

eingereicht am:            29.09.2014

Promotionskolloquium:    28.04.2015

## Schriftliche Erklärung

Ich erkläre hiermit, dass ich die vorliegende Arbeit ohne unzulässige Hilfe Dritter und ohne Benutzung anderer als der angegebenen Hilfsmittel angefertigt habe. Die aus fremden Quellen direkt oder indirekt übernommenen Gedanken sind als solche kenntlich gemacht.

Insbesondere habe ich nicht die Hilfe einer kommerziellen Promotionsberatung in Anspruch genommen. Dritte haben von mir weder unmittelbar noch mittelbar geldwerte Leistungen für Arbeiten erhalten, die im Zusammenhang mit dem Inhalt der vorgelegten Dissertation stehen.

Die Arbeit wurde bisher weder im Inland noch im Ausland in gleicher oder ähnlicher Form als Dissertation eingereicht und ist als Ganzes auch noch nicht veröffentlicht.

## Acknowledgements

The present work was realized at the Institute of Fluid Dynamics & Thermodynamics at the University of Magdeburg "Otto-von-Guericke".

I convey my sincere thanks to Professor Dr.-Ing. Dominique Thévenin for having given me the chance to carry out this work at his institute, for his scientific support, his guidance and encouragement throughout this work.

I would like to thank Professor Ulrich Maas and Dr. Renan Hilbert for reviewing my thesis and for being present in the oral exam. Also I would like to thank Professor Ulrich Krause for taking the chair of the commission.

I would like to express my gratitude to Dr.-Ing. habil Gábor Janiga for many fruitful discussions especially in the beginning of my work. His excellent computer science background was a great help in numerous technical questions.

I am thankful to Dr.-Ing. Renan Hilbert for introducing me in post-processing of DNS data and in the existing part of the original MATLAB toolbox.

A particular thank goes to Dr.-Ing. Robert Schiefl (from the Institute of Technical Thermodynamics, Karlsruhe Institute of Technology) for the pleasant collaboration during our common publication concerning manifold methods.

I would like to thank Dr.-Ing Renan Hilbert, Dr.-Ing. Hemdan Shalaby and Dr. Gordon Fru. They provided me their DNS data in order to develop the tools introduced in Chapter 5 and to investigate the flames discussed in Chapter 6.

The main part of the MATLAB-runs were carried out at the linux cluster at the LRZ (Leibniz Rechenzentrum) in Munich, what is gratefully acknowledged.

# Contents

<b>1</b>	<b>Introduction</b>	<b>14</b>
1.1	Importance of combustion research . . . . .	14
1.2	Investigation of turbulent combustion . . . . .	15
1.3	Post-processing the results . . . . .	17
1.4	Intention of this work . . . . .	19
1.5	Structure of this work . . . . .	23
<b>2</b>	<b>Basic theory of turbulent combustion</b>	<b>24</b>
2.1	Phenomenological description of turbulence . . . . .	24
2.2	Phenomenological description of flames . . . . .	30
2.2.1	Categories of flames . . . . .	30
2.2.2	Premixed flames . . . . .	32
2.2.3	Non-premixed flames . . . . .	33
2.3	Balance equations for turbulent reactive flows . . . . .	35
2.4	Molecular transport processes . . . . .	37
2.5	Reaction kinetics . . . . .	42
2.6	Simplification of reaction mechanisms . . . . .	44
2.6.1	Reduction based on chemistry . . . . .	44
2.6.2	Reduction based on invariant manifolds . . . . .	45
2.6.3	Dimension of manifolds . . . . .	49
<b>3</b>	<b>Simulating and modeling turbulent flames</b>	<b>54</b>
3.1	Direct numerical simulation (DNS) . . . . .	55
3.1.1	Principles and limitations of DNS . . . . .	55
3.1.2	Classical simplifications to reduce computational costs . . . . .	57
3.1.3	Advantages and drawbacks . . . . .	59
3.1.4	Example for a 2D-direct numerical simulation of a partially premixed flame . . . . .	60
3.1.5	Example for a 3D-direct numerical simulation of a premixed flame . . . . .	61
3.2	Reynolds-Averaged Navier-Stokes-methods (RANS) . . . . .	63
3.2.1	Concept . . . . .	63

3.2.2	System of averaged balance equations . . . . .	63
3.2.3	Closure of unknown terms . . . . .	64
3.2.4	Advantages and Drawbacks . . . . .	65
3.3	Large Eddy Simulation (LES) . . . . .	66
3.3.1	Concept . . . . .	66
3.3.2	Advantages and drawbacks . . . . .	67
3.4	Probability-density function methods (PDF) . . . . .	67
3.4.1	Concept . . . . .	67
3.4.2	Advantages and drawbacks . . . . .	68
<b>4</b>	<b>Post-processed scales and quantities</b>	<b>69</b>
4.1	Scales and quantities characterizing turbulence . . . . .	69
4.1.1	Quantities derived from one-point statistics . . . . .	69
4.1.2	Quantities derived from two-point statistics . . . . .	70
4.1.3	Quantities characterizing the energy cascade . . . . .	74
4.1.4	Scales of 2-dimensional turbulence . . . . .	76
4.1.5	Table of available turbulent quantities and corresponding tools to post-process them	78
4.2	Scales and quantities describing flames . . . . .	79
4.2.1	Common quantities for all flames . . . . .	79
4.2.2	Quantities and scales to describe premixed flames . . . . .	84
4.2.3	Quantities and scales to describe non-premixed flames . . . . .	86
4.2.4	Table of available flame quantities and corresponding tools to post-process them	90
4.3	Scales and quantities describing probabilities . . . . .	92
4.3.1	Univariate probability . . . . .	93
4.3.2	Joint probability theory . . . . .	97
4.3.3	Conditional probability . . . . .	98
4.3.4	Table of available statistical quantities and corresponding tools to post-process them	99
<b>5</b>	<b>Post-processing tools for DNS data</b>	<b>101</b>
5.1	The program MATLAB . . . . .	101
5.2	The MATLAB Toolbox . . . . .	102
5.2.1	Overview on different groups of tools . . . . .	102
5.2.2	Tools for geometrical investigations . . . . .	104
5.2.3	Tools to investigate the flame structure . . . . .	107
5.2.4	Tools to investigate velocity field and turbulence . . . . .	110
5.2.5	Tools to investigate the interaction between turbulence and flames . . . . .	112
5.2.6	Tools for statistical investigations . . . . .	113
5.2.7	Tools to determine appropriate dimensions of manifolds . . . . .	115
5.2.8	Tools in batch mode and parallelized tools . . . . .	117

<b>6</b>	<b>Selected examples of applications</b>	<b>119</b>
6.1	Analysis of a cold flow field . . . . .	119
6.2	Analysis of flame properties . . . . .	123
6.2.1	Flame/turbulence interaction for a 2D non-premixed flame . . . . .	123
6.2.2	Flame/turbulence interaction for 3D premixed flames . . . . .	127
6.3	PDF modeling of a 3D nonpremixed hydrogen/air flame . . . . .	132
6.4	Chemistry reduction . . . . .	135
6.4.1	Flame configuration . . . . .	135
6.4.2	Results for detailed transport model . . . . .	136
6.4.3	Results for simplified transport model . . . . .	139
6.4.4	Analysis including temperature . . . . .	141
6.4.5	Neighbourhoods based on prescribed radius . . . . .	142
6.4.6	Impact of large neighborhoods . . . . .	143
6.5	Conclusion . . . . .	144
<b>7</b>	<b>Summary</b>	<b>145</b>
<b>A</b>	<b>Methods of taking averages</b>	<b>147</b>
<b>B</b>	<b>Geometrical quantities</b>	<b>148</b>
<b>C</b>	<b>Fourier transforms</b>	<b>151</b>
<b>D</b>	<b>MATLAB tools</b>	<b>154</b>

# Nomenclature

## Roman symbols

Symbol	Meaning	Dimension
$a$	speed of sound	(m s <sup>-1</sup> )
$a$	strain rate	(s <sup>-1</sup> )
$c$	reaction progress variable	(-)
$c_{p,k}$	specific heat capacity of species $k$ at constant pressure	(J kg <sup>-1</sup> K <sup>-1</sup> )
$c_v$	specific heat capacity at constant volume	(J kg <sup>-1</sup> K <sup>-1</sup> )
$C_k$	molar concentration of species $k$	(mol m <sup>-3</sup> )
$C_r$	molar concentration of reactive intermediates	(mol m <sup>-3</sup> )
$D$	extropy	(s <sup>-1</sup> )
$D_{kl}$	binary component diffusion coefficient	(m <sup>2</sup> s <sup>-1</sup> )
$D_k$	diffusion coefficient of species $k$	(m <sup>2</sup> s <sup>-1</sup> )
$D_T$	thermal diffusion coefficient	
$E_a$	activation energy	(J mol <sup>-1</sup> )
$f_i$	flame index	(-)
$F_l$	laminar flame surface area	(m <sup>2</sup> )
$F_t$	turbulent flame surface area	(m <sup>2</sup> )
$h_s$	sensible enthalpy	(J kg <sup>-1</sup> )
$h_{s,k}$	sensible enthalpy of species $k$	(J kg <sup>-1</sup> )
$H$	mean curvature	(m <sup>-1</sup> )
$k$	turbulent kinetic energy	(m <sup>2</sup> s <sup>-2</sup> )
$k_1, k_2$	principal curvatures	(m <sup>-1</sup> )
$k_B$	Boltzmann constant	(1.380662 · 10 <sup>-23</sup> J K <sup>-1</sup> )
$k_f, k_b$	kinetic rate coefficients	
$K$	Gaussian curvature	(m <sup>-2</sup> )
$l$	characteristic length	(m)
$l_k$	length scale of Kolmogorov	(m)
$L$	integral length scale	(m)
$L_f$	longitudinal integral length scale	(m)
$L_g$	lateral integral length scale	(m)
$L_d$	size of domain	(m)
$m_k$	mass of species $k$	(kg)
$N_r$	number of reactions	(-)
$N_S$	number of species	(-)
$\mathbf{n}$	normal vector to flame front	(-)
$p$	thermodynamic pressure	(Pa)

## Roman symbols

Symbol	Meaning	Dimension
$R$	perfect gas constant	$(\text{J mol}^{-1} \text{K}^{-1})$
$R_{ij}$	correlation tensor	$(\text{m}^2 \text{s}^{-2})$
$s_d$	displacement flame speed	$(\text{m s}^{-1})$
$S_\ell$	laminar flame speed	$(\text{m s}^{-1})$
$S_t$	turbulent flame speed	$(\text{m s}^{-1})$
$S$	shape factor	(-)
$t$	time	(s)
$t_k$	time scale of Kolmogorov	(s)
$T$	temperature	(K)
$T_b$	temperature of burnt gases	(K)
$T_u$	temperature of unburnt gases	(K)
$T$	integral time scale	(s)
$u$	characteristic velocity	$(\text{m s}^{-1})$
$u_i$	velocity component in the $i$ th direction	$(\text{m s}^{-1})$
$u_{rms}$	root mean square of velocity component	$(\text{m s}^{-1})$
$\mathbf{u}$	velocity vector	$(\text{m s}^{-1})$
$v_k$	velocity scale of Kolmogorov	$(\text{m s}^{-1})$
$V_{k,i}$	component of diffusion velocity of species $k$ in direction $i$	$(\text{m s}^{-1})$
$w$	molar reaction rate	$(\text{mol m}^{-3} \text{s}^{-1})$
$W$	molar mass of the mixture	$(\text{kg mol}^{-1})$
$W_k$	molar mass of species $k$	$(\text{kg mol}^{-1})$
$x_i$	spatial coordinate	(m)
$X_k$	mole fraction of species $k$	(-)
$Y_k$	mass fraction of species $k$	(-)
$Z'_i$	element mass fraction of element $i$	(-)
$Z$	mixture fraction	(-)



## Greek symbols

Symbol	Meaning	Dimension
$\alpha$	thermal diffusivity	$(\text{m}^2 \text{s}^{-1})$
$\beta$	temperature coefficient in Arrhenius law	$(-)$
$\delta_{ij}$	Kronecker's symbol	$(-)$
$\delta_L^0$	thermal flame thickness	$(\text{m})$
$\delta_L^t$	total flame thickness	$(\text{m})$
$\varepsilon$	rate of dissipation of kinetic energy	$(\text{m}^2 \text{s}^{-3})$
$\kappa$	wave number	$(\text{m}^{-1})$
$\lambda$	thermal conductivity	$(\text{W m}^{-1} \text{K}^{-1})$
$\lambda_k$	thermal conductivity of species $k$	$(\text{W m}^{-1} \text{K}^{-1})$
$\lambda$	Taylor length scale	$(\text{m})$
$\lambda_f$	longitudinal Taylor length scale	$(\text{m})$
$\lambda_g$	lateral Taylor length scale	$(\text{m})$
$\mu$	dynamic viscosity	$(\text{kg m}^{-1} \text{s}^{-1})$
$\mu_k$	dynamic viscosity of species $k$	$(\text{kg m}^{-1} \text{s}^{-1})$
$\mu_n$	moment of order $n$	
$\mu_D$	bulk viscosity	$(\text{kg m}^{-1} \text{s}^{-1})$
$\nu$	kinematic viscosity	$(\text{m}^2 \text{s}^{-1})$
$\nu_{k,j}$	stoichiometric coefficient of species $k$ in reaction $j$	
$\rho$	fluid mass density	$(\text{kg m}^{-3})$
$\rho_{ij}$	correlation coefficient	$(-)$
$\Phi_{ij}$	energy spectrum tensor	
$\tau_c$	chemical time scale	$(\text{s})$
$\tau_k$	time scale of Kolmogorov	$(\text{s})$
$\tau_{phys}$	physical time scale	$(\text{s})$
$\tau_{ij}$	components of viscous stress tensor	$(\text{Pa})$
$\sigma$	diameter of molecule	$(\text{m})$
$\chi$	scalar dissipation rate	$(\text{s}^{-1})$
$\omega$	vorticity	$(\text{s}^{-1})$
$\dot{\omega}_k$	mass reaction rate of species $k$	$(\text{kg m}^{-3} \text{s}^{-1})$
$\dot{\omega}_t$	heat release	$(\text{kg m}^{-3} \text{s}^{-1})$

## Dimensionless numbers

Symbol	Meaning
--------	---------

Da	Damköhler number
Le <sub>k</sub>	Lewis number of species <i>k</i>
Ma	Mach number
Re	Reynolds number
Re <sub>t</sub>	Reynolds number based on integral scale
Re <sub>k</sub>	Reynolds number based on micro-scale of Kolmogorov
Re <sub>λ</sub>	Reynolds number based on micro-scale of Taylor

## Zusammenfassung

Weltweit wird mehr als 80% der Primärenergie über die Verbrennung von fossilen Brennstoffen nutzbar gemacht. Diese Brennstoffe sind endlich beziehungsweise nur begrenzt wirtschaftlich abbauwürdig, während ihr Verbrauch stetig steigt. Zudem entstehen bei derartigen Verbrennungsprozessen umweltbelastende Schadstoffe und Treibhausgase. Klimakonventionen und Umweltschutzaufgaben verlangen jedoch eine Reduzierung derartiger Emissionen. Dies erfordert die Erforschung von Verbrennungsvorgängen zur Optimierung des Wirkungsgrades und der Leistungsausbeute und zur Minimierung des Verbrauchs und der ausgestossenen Schadstoffe.

Die Verbrennungsforschung gliedert sich in experimentelle Untersuchungen und numerische Simulationen. Bei den numerischen Simulationen unterscheiden wir:

- Direkte numerische Simulationen (DNS)
- zeitlich gefilterte Turbulenzmodellierung (RANS)
- Grobstruktur- oder Large Eddy Simulationen (LES)
- und PDF-Methoden mit Wahrscheinlichkeitsdichtefunktionen (Probability Density Functions).

Die direkte numerische Simulation löst die Navier-Stokes-Gleichungen ohne irgendeine Art von Mittelung, wobei alle räumlichen und zeitlichen Skalen aufgelöst werden. Eine Turbulenzmodellierung ist deshalb nicht notwendig. Dabei wird ein höchstmögliches Mass an Genauigkeit erreicht. Der Preis ist jedoch ein enorm hoher Aufwand an Rechenzeit und Speicherplatz, zunehmend mit Reynoldszahl und Anzahl der Speciesgleichungen. Das macht das Forschungswerkzeug DNS für die meisten praktischen Konfigurationen ungeeignet. Die detaillierten DNS Ergebnisse sind jedoch eine optimale Ausgangsbasis für die Entwicklung praxisnaher Modelle. Um sämtliche nützliche Informationen aus den immensen Mengen Rohdaten zu ziehen, müssen diese sorgfältig ausgewertet werden. Diese Informationen können dann genutzt werden, um

- RANS- und LES-Modelle
- PDF-Methoden
- oder Methoden zur Reduzierung von Reaktionsmechanismen

zu entwickeln, zu validieren oder zu verbessern.

Derartige Werkzeuge zur Auswertung dieser Daten stehen derzeit weder frei zur Verfügung noch sind sie auf dem kommerziellen Markt erhältlich. Jeder Nutzer entwickelt seine eigenen Werkzeuge. In der Hoffnung, diese Prozedur schneller und effizienter zu machen, wurde eine

Toolbox mit Skripts zu wichtigen Auswerteschritten entwickelt. Die Toolbox wurde in MATLAB geschrieben.

Sie erlaubt die Auswertung von

- 2D- und 3D Flammen,
- vorgemischten sowie nichtvorgemischten Flammen,
- Wasserstoff- sowie Kohlenwasserstoffflammen.

Mit Hilfe der Toolbox wurden wichtige Eigenschaften und Grössen sowohl von kalten Geschwindigkeitsfeldern als auch von Flammen untersucht. Zwei-dimensionale und drei-dimensionale turbulente Geschwindigkeitsfelder wurden verglichen. Die Wechselwirkung zwischen Turbulenz und Flammen wurde untersucht, sowohl für nicht vorgemischte 2D-Wasserstoff/Stickstoff/Luft-Flammen als auch für vorgemischte 3D-Methan/Luft-Flammen.

Bei Verwendung detaillierter Reaktionsmechanismen in einer DNS verursacht den grössten Aufwand die Lösung der zahlreichen Teilchenerhaltungsgleichungen und die Bestimmung der chemischen Quellterme. Zum Beispiel verursacht bei der Beschreibung einer Wasserstofflamme mit detailliertem Reaktionsmechanismus der Chemieteil etwa 70 % der Rechenzeit. Dieser hohe Aufwand erfordert Näherungsmethoden, mit denen man die Anzahl der Gleichungen im chemischen Reaktionssystem reduzieren kann, ohne die Genauigkeit wesentlich zu beeinflussen. Eine Möglichkeit, dieses Ziel zu erreichen sind die sogenannten Mannigfaltigkeitsmethoden. Diese versuchen, den Zustandsvektor durch eine niedrigdimensionale Version zu ersetzen, ohne dabei wesentlich an Genauigkeit zu verlieren.

Die meisten dieser Mannigfaltigkeitsmethoden arbeiten entweder mit einer fest vorgegebenen Dimension der Mannigfaltigkeit oder sie erwarten eine benutzer-definierte Angabe für die Dimension.

Im Rahmen dieser Arbeit wurde eine Methode entwickelt, um die geeignete Dimension einer Mannigfaltigkeit zu finden, damit ein vorgegebenes Mass an Genauigkeit erfüllt wird. Zu diesem Zweck wurde eine turbulente nicht vorgemischte Wasserstoff/Stickstoff/Luft-Flamme untersucht. Um den Einfluss von Chemie und Transport auf die Dimension der Mannigfaltigkeiten zu untersuchen, wurden zwei Fälle mit unterschiedlichen Transportmodellen betrachtet.

## Abstract

Today combustion of fossil fuels is the most important way to cover our energy needs. Presently, more than 80% of our energy requirement is produced by combustion of fossil fuels. Energy consumption is increasing rapidly, while fossil fuels are limited. Our air is influenced by emissions of pollutants and many governments impose limits on such emissions. Therefore, we have to improve efficiency in order to reduce fuel consumption and pollutant emissions.

The main strategies to investigate turbulent flames are experimental investigations and numerical simulations, relying in particular on:

- Direct numerical simulations (DNS),
- Reynolds-averaged Navier-Stokes equations (RANS),
- Large Eddy Simulations (LES),
- Probability density function methods (PDF).

In direct numerical simulations the complete Navier-Stokes equations are solved without any averaging. All spatial and time scales of turbulent motion are resolved. Turbulence modeling is not necessary any more. When DNS can be applied it is the "simplest" method of approach with the highest level of accuracy and description. On the other side DNS is time- and memory-intensive, increasing with Reynolds number and number of species equations. Therefore, DNS is not suitable for practical configurations. But DNS is an optimal method to foster model analyses and development for industrial needs. In order to gain all useful information from the huge amount of DNS data, they have to be post-processed carefully. This information can be used to develop, validate or improve:

- RANS- and LES-Models,
- PDF-Methods,
- Methods to reduce reaction mechanisms.

Such post-processing tools for turbulent reacting flows are not available (freely or commercially). Every user develops his own tools. In the hope to make this procedure faster and more efficient, a toolbox containing essential post-processing methods has been developed. The toolbox was written in MATLAB. The toolbox allows post-processing of:

- 2D as well as 3D results,
- Premixed as well as non-premixed flames,
- Hydrogen as well as hydrocarbon flames.

In this project the toolbox was used to investigate important properties of cold turbulent flow-fields as well as of turbulent flames. Two-dimensional and three-dimensional flow fields were compared. The interaction between turbulence and flames was investigated for non-premixed 2D-hydrogen/nitrogen/air-flames as well as for premixed methane/air-flames.

For combustion simulations with detailed reaction mechanisms, the large number of balance equations for chemical species and the computation of chemical source terms takes the main time and cost of the simulation. For example, describing chemistry with nine species and 37 reactions in a field of homogeneous isotropic turbulence, the supplementary costs of the chemistry part amount to about 70 % of the total computational costs. These high computer requirements make necessary simplification approaches based on reducing the number of chemical variables to a lower dimensional system without noticeably compromising the accuracy of the description. One possibility to achieve this goal are so-called manifold methods. These methods try to replace the state vector by a lower-dimensional version without noticeably compromising the accuracy.

Most of these methods work either with a predefined dimension of the manifolds or they expect a user-defined instruction for the dimension.

In this project we developed a methodology to find the appropriate dimension of low-dimensional manifolds for reaching a given level of accuracy. For that purpose a turbulent non-premixed  $\text{H}_2/\text{N}_2/\text{air}$  flame was investigated. In order to investigate the impact of chemistry and transport on the dimension of the manifold, two different transport models were considered.

# Chapter 1

## Introduction

### 1.1 Importance of combustion research

The evolution of mankind is directly connected to the domination of fire and the ability to ignite and to use it. Wood was the first and for many thousand years the only energy carrier. Fire could be used for cooking, for lightening and heating of caves, but also to produce tools to melt and forge (non-iron) metals. With raising temperatures the employment of more and better materials got possible. But wood was not only used as energy carrier but also to build housings, ships or vehicles or to produce paper. The raising consumption of wood led to damages in the environment. Secondly the scarcity of wood made it necessary to search for a new energy carrier.

In the middle of the 18th century in Europe wood was replaced by coal as energy carrier. Further evolution in industry and mining got possible. With the invention of the steam engine the industrial age could start. In the 20th century oil and natural gas became available as further energy carriers. With their utilization the development of combustion engines and gas turbines got possible. The drawback of this development was, that the environment was influenced through pollution of air and waters [123].

Today combustion of fossil fuels is still the most important and common process in our worldwide energy support. More than 80% of our energy requirement is produced by combustion of fossil fuels. Combustion systems are variously employed, for example for transport purposes in cars and ships [46] or airplanes [89], for power generation in stationary power plants [69], for heating of factories, residence homes and several other kinds of buildings, in industrial burners [124] for the production of steel or glass, or in heating processes in refineries. According to the International Energy Agency (IEA) we have to expect an explosive growth of energy consumption in the coming years at least till 2030.

On the other hand fossil fuels are limited and the quality of our air is influenced by emissions of pollutants, such as  $\text{NO}_x$ ,  $\text{SO}_x$ ,  $\text{CO}$ , greenhouse gases such as  $\text{CO}_2$  or particles such as soot. While the environmental problem started as a local one, meanwhile it has grown to a global

one. Environmental constraints are getting stronger and many governments impose limits on such emissions. Therefore, it is necessary to extend our knowledge of combustion processes in order to improve the efficiency of combustion engines, to reduce fuel consumption and pollutant emissions. In the future, fossil fuels and combustion of fossil fuels will have to be replaced by new energy sources or energy carriers and technologies to gain energy. One of the most important new carriers might be hydrogen or synthetic gas and, again for energy conversion, combustion will play a predominant role.

But we must not forget, when constructing sustainable, energy efficient buildings, infrastructure and transportation systems, that the safety of the public and the protection of property against losses due to fire must not be compromised [66].

## 1.2 Investigation of turbulent combustion

In spite of the great economic and technical importance of combustion, combustion science is a relatively young discipline. The reason is that combustion processes are a combination of several interrelated complex phenomena. The fundamentals of different processes had to be understood before several disciplines could merge to a science. According to Liñán and Williams, combustion science can be defined as *“the science of exothermic chemical reactions in flows with heat and mass transfer. As such, it involves thermodynamics, chemical kinetics, fluid mechanics, and transport processes.”*[76]

As dimensions of technical equipments are often large and processes are fast, most combustion processes take place in turbulent flow fields. There are two complementary ways to investigate turbulent reacting flows: an experimental and an analytical or numerical one. Experimental investigations of such flows are very interesting but difficult and time and cost intensive. The diagnostics must not affect the flow or the flame and have to be usable for example at high temperatures or velocities. Some variables are very difficult to measure. Therefore, there is increasingly the tendency to model additionally such flows by mathematical methods.

But the simulations can not replace the experiments completely and both are better seen as two complementary ways for the study of turbulent combustion [117]. For example experimental data are always required for validation of numerical models [1, 97].

The relationship among the various quantities occurring in many physical sciences such as combustion science can be expressed by a system of conservation equations. The system of equations to describe Newtonian fluid motion was introduced by Navier [90] in 1822 and Stokes [128] in 1845. At least for turbulent flows the complicated system of coupled non linear differential equations is not solvable by analytical methods. With the advent of electronic computers about one century later it became possible to solve the problem by numerical methods. For turbulent reacting flows the problem is much more complex because the two phenomena tur-



balance and chemical reactions as well as their interaction have to be considered. Balance equations for several species have to be solved additionally. Transport processes and reaction mechanisms have to be taken into account.

Power and memory capacities of modern computers are steadily increasing and with them the possibilities to solve extensive and complicated equation systems [151].

According to different requirements in research and practice in the industry there are different strategies to simulate turbulence as well as combustion processes with different levels of expense and accuracy. An overview about the numerical description of combustion phenomena, different modeling strategies, perspectives and progress in the last years is given for example in [12, 20, 21]. Today, pollutant formation and stability limits belong to the most important topics in combustion science [9]. In order to investigate these topics transport processes and multiple chemical reaction steps have to be considered. The impact of transport processes and reaction schemes is extensively reviewed in [49].

The main strategies to simulate turbulent flows and flames are:

- Direct Numerical Simulations (DNS),
- Reynolds-averaged Navier-Stokes equations (RANS),
- Large Eddy Simulations (LES)
- and Probability-density-function methods (PDF).

The DNS method consists in solving the full Navier-Stokes equations. All spatial and time scales of turbulent motion are resolved. No modeling is necessary. When DNS can be applied it is the "simplest" method of approach with the highest level of accuracy and description. DNS results contain very detailed information about the flow and its variables of interest. When the grids are fine enough DNS gives us nearly exact results and is also called "numerical experiment". On the other side DNS is time- and memory-intensive. For reacting flows, chemistry takes the main time and the main costs of the simulation. Even if the theory was well known, the application of DNS was not possible till the 70s of the last century, because of lack of computer power. DNS was published for the first time in 1972 [93]. DNS is not suitable for practical applications. But DNS appears to be in principle the best possible research tool [4, 88].

In industrial applications, mainly mean flow-fields, mean values and major trends are of interest, but not time-dependent fluctuations. The concept of the RANS approach is, following the proposal of Reynolds [109], to average out the unsteadiness from the instantaneous quantities and to solve for the mean values of all quantities. The balance equations for averaged quantities are obtained by averaging the instantaneous balance equations. However, this system is not closed any more and contains unknown quantities that need to be modeled. This means that turbulence models as well as turbulent combustion models (TCM) are required. Historically

the RANS method was the first possible approach because of less computer requirements and therefore, there are more years of experience compared to DNS.

The method of LES is a combination of DNS and RANS. LES started in the 1960s with the work of Smagorinsky [120]. The scales of turbulent motion are divided in large structures and small structures by a filter operation [72]. Large structures are resolved as in DNS, while the effects of the small structures need to be modeled as in RANS. The method of LES is quite established for non-reacting flows but for reacting flows there are still many unsolved issues.

The most important unknown terms in RANS and LES approaches are

- the Reynolds stresses in the momentum equations,
- the turbulent scalar transport in the energy equation
- and the chemical source terms in the species equations.

Closing properly the chemical source term is the key issue in combustion simulations.

Modeling of the chemical source term can be avoided by the use of probability density function (PDF) methods. Two types of PDF approaches can be distinguished: The transported PDF method of Pope [101] and the presumed PDF method.

Since in DNS the large number of chemical species and the computation of chemical source terms takes the largest time and cost of the simulation, simplification approaches based on reducing the number of chemical variables to a lower dimensional system without noticeably compromising the accuracy of the description are required. This goal can be achieved by methods based on physical considerations or by mathematical approaches such as manifold methods. An overview on manifold methods is given for example in [44, 83]. Manifold methods are based on the separation of fast and slow chemical timescales and a separate treatment of these processes. The system dynamics is then reduced to low-dimensional structures in state space where the slow dynamics occurs, the so called low-dimensional manifolds. Most of these methods work either with a predefined dimension of the manifolds or they expect a user-defined instruction for the dimension. In Section 2.6.3 we introduce a methodology to find the appropriate dimension of low-dimensional manifolds for reaching a given level of accuracy. In Section 6.4 we investigate dimensions of manifolds in a  $\text{H}_2/\text{N}_2/\text{air}$  flame.

### 1.3 Post-processing the results

DNS results produce a huge amount of raw data, which is increasing with increasing possibilities of numerical computation. For example for the 3D synthetic gas flame with 201 grid points per direction analyzed in Section 6.2.2 we obtain 1.8 GB of raw data per time output. For each species, the velocity components and the temperature we get information in more than

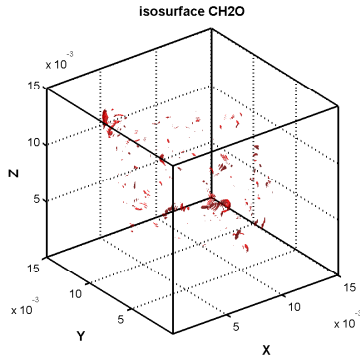


Figure 1.1: Isosurface of mass fraction of CH<sub>2</sub>O at 16 % of its maximum

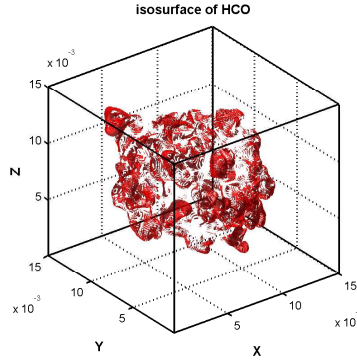


Figure 1.2: Isosurface of mass fraction of HCO at 16 % of its maximum

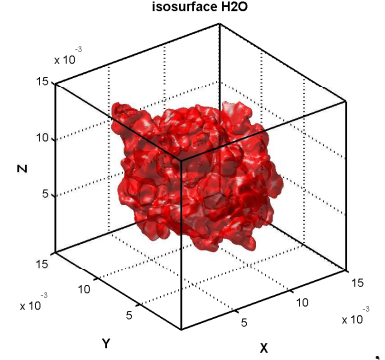


Figure 1.3: Isosurface of mass fraction of H<sub>2</sub>O at 16 % of its maximum

8 million grid points. Even when extracting the variables only along the flame front (see section 4.2.1) we still have information in nearly 160 000 points. The ranges of values the different variables can take are completely different. For example the temperature is running from 315 to 2168 K, while the velocity components are running from -19 to 29 m/s. The species mass fraction of CO<sub>2</sub> is running from 0 to 0.198, while the species mass fraction of OH is running from 0 to 0.005 in the whole domain and running from 0.0012 to 0.0031 along the flame surface defined by CO<sub>2</sub>. Isosurfaces of species mass fractions at the same level (relative to the maximum value) are looking completely different. While for CH<sub>2</sub>O we have only some small islands (see Figure 1.1), for HCO we obtain many larger islands (see Figure 1.2) and for H<sub>2</sub>O we have a complete coherent surface (see Figure 1.3). The necessity to post-process these data carefully in order to draw as much useful information as possible from them is obvious.

To cite Hamming:

*“The purpose of computing is insight, not numbers”* [45].

There are three possible concepts to do this:

- post-processing,
- co-processing,
- in-situ processing.

Current tools almost exclusively operate in a post-processing mode. This means that data are stored at run time, then pulled back onto the system later for analysis and visualization. This can be a problem as dataset sizes continue to grow.

Some scientists have moved to a co-processing approach. Co-processing is done using a dedicated visualization machine connected to the supercomputer. Simulation output is directly transferred to the visualization machine for immediate processing, and the resulting imagery is either stored to a disk or shipped to a desktop machine for viewing. In practice, however, this approach was seldom adopted because of two reasons: First, most scientists were reluctant to use their supercomputer time for visualization calculations. Second, it could take a significant effort to couple the parallel simulation code with the visualization code. In particular, the domain decomposition optimized for the simulation is often unsuitable for parallel visualization, resulting in the need to replicate data for speeding up the visualization calculations [86].

In situ-processing and visualization side-steps the deficiencies of both of these approaches by performing some analysis functions on the data during simulation run-time while it still resides on the system. The advantage is, these operations reduce the data size before the data is transferred to storage [85, 86]. But compared with a visualization in traditional post-processing fashion in-situ visualization also brings some unique challenges:

First of all, the visualization code must interact directly with the simulation code, which requires both the scientist and the visualization specialist to commit to this integration effort. To optimize memory usage, they have to find a way for the simulation and visualization codes to share the same structures to avoid replicate data. Second, visualization workload balancing is more difficult to achieve since the visualization has to comply with the simulation architecture and be tightly coupled with it. Unlike parallelizing visualization algorithms for standalone processing where one can partition and distribute data best suited for the visualization calculations, for in-situ visualization, data partition and distribution is dictated by the simulation code. Moving data frequently among processors is not an option for visualization processing. One needs to rethink to possibly balance the visualization workload so the visualization is at least as scalable as the simulation [86].

## 1.4 Intention of this work

Despite the huge dataset sizes we decided here to keep and store our results and do the post-processing afterwards. The main advantage is that we do not lose data and we can post-process every quantity or item at any time we need, even years after completing the DNS.

For this purpose a toolbox containing essential post-processing methods has been developed. The library contains flexible and efficient methods to investigate 2D as well as 3D results, premixed and non-premixed flames, hydrocarbon and hydrogen flames. A first description of parts of the toolbox was already published in [155]. The scripts are written in the language of the widely available commercial program MATLAB [87].

Employing this toolbox, the DNS results can be used as an optimal database in order to

- improve our physical understanding of combustion processes,

- develop, improve or validate RANS- or LES models,
- develop, improve or validate combustion models,
- develop, improve or validate PDF methods,
- develop, improve or validate methods to reduce reaction mechanisms.

Today (2015) the toolbox has users in more than 40 different universities and institutions in several countries in Europe, in America and in Asia. The users are listed in Table 1.1. Figure 1.4 shows how the different users are spread over the world.

<b>no</b>	<b>institute</b>	<b>country</b>
1	Istituto di ricerca sulla combustione, Napoli	Italy
2	Politecnico di Milano	Italy
3	Italian Aerospace Research Centre (CIRA)	Italy
4	Stork termeq	Netherlands
5	Eindhoven University of Technology	Netherlands
6	Leiden University, Medical Center	Netherlands
7	Lund University	Sweden
8	Chalmers University of Technology, Gothenburg	Sweden
9	University of Southampton	UK
10	Cranfield academy	UK
11	Cambridge University	UK
12	University of Western Macedonia	Greece
13	Ecole Centrale, Paris	France
14	University of Miskolc	Hungary
15	KIT, Karlsruher Institut für Technologie	Germany
16	TU Bergakademie Freiberg	Germany
17	Hochschule Bochum	Germany
18	TU-Braunschweig	Germany
19	RWTH-Aachen	Germany
20	Universität Duisburg-Essen	Germany
21	TU-Darmstadt	Germany
22	Deutsches Zentrum für Luft- und Raumfahrt (DLR)	Germany
23	Otto-von-Guericke Universität Magdeburg	Germany
24	Los Alamos National Laboratory	USA
25	North Carolina State University	USA
26	Stony Brook University, New York	USA
27	Stanford University, California	USA
28	Purdue University	USA

29	University of New Brunswick	Canada
30	Federal University of Paraná, Curitiba	Brasilia
31	Teheran university	Iran
32	K.N.Toosi university, Teheran	Iran
33	Rajamangala University of Technology Suvarnabhumi	Thailand
34	Zhejiang University, Laboratory of Clean Energy Utilization,	China
35	Zhejiang University, Institute for Thermal Power Engineering,	China
36	Yonsei University	South Korea
37	King Abdullah University of Science and Technology ( KAUST)	Saudi Arabia
38	Institute of chemical Technology, Matunga, Mumbai	India
39	JNCASR, Bangalore	India
40	Bandung Institute of Technology, Meteorology Department	Indonesia
41	Technological Institute of Israel, CS department	Israel

Table 1.1: Users of the toolbox (April 2015)

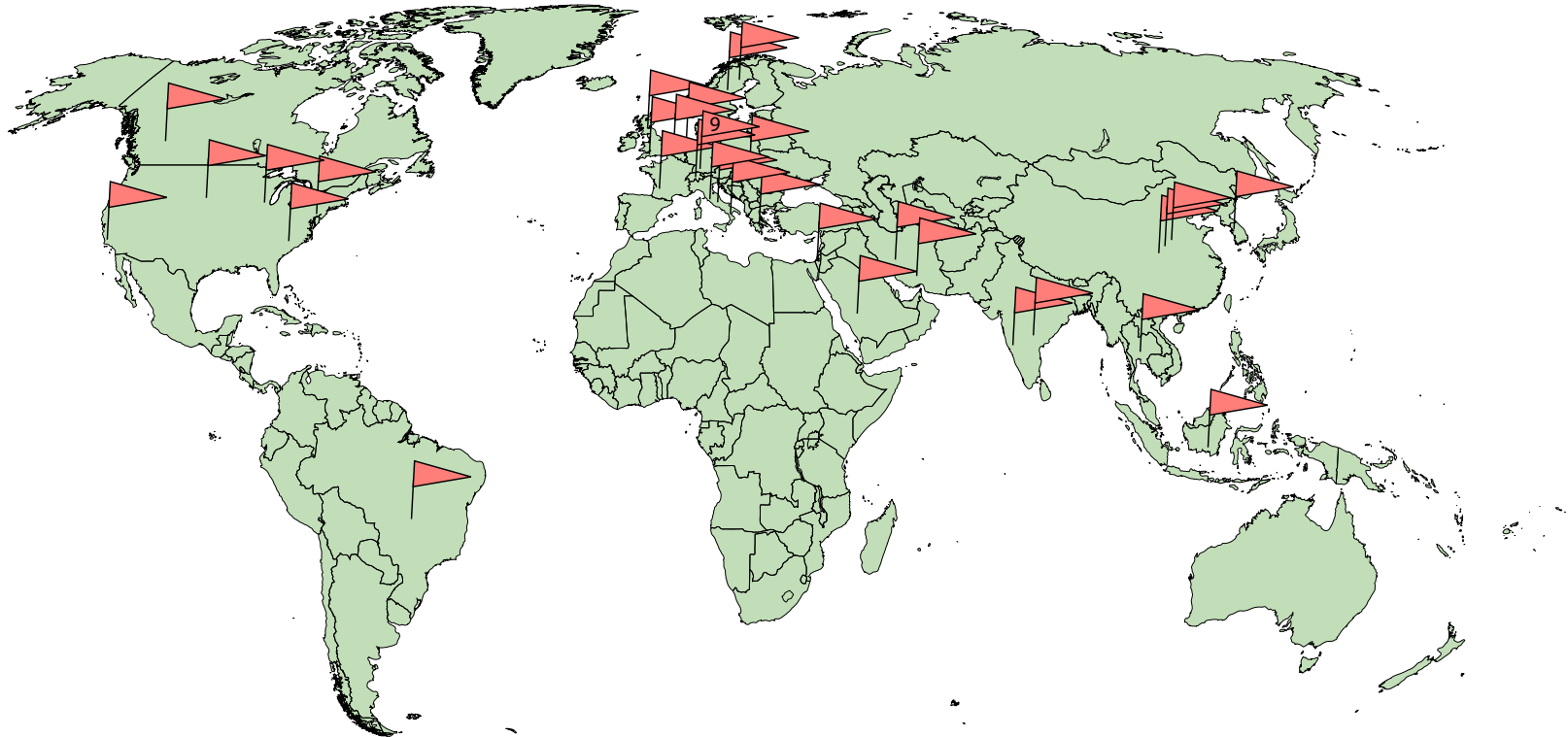


Figure 1.4: World map of Anaflame users

## 1.5 Structure of this work

This thesis is organized as follows:

The next chapter gives a basic introduction into the theory of turbulent combustion. In Sections 2.1 and 2.2 the phenomena connected to turbulence and flames are explained. The governing equations for turbulent combustion and transport processes are presented in Sections 2.3 and 2.4. Sections 2.5 and 2.6 deal with reaction kinetics and methods to simplify kinetics. Low-dimensional manifolds are discussed and a methodology to find the appropriate dimension of a low-dimensional manifold for reaching a given level of accuracy is introduced.

In Chapter 3 the most common modeling strategies of turbulent reacting flows are described. We compare what kind of information they need and what kind of information they give us. Advantages and limitations are discussed. As the toolbox is developed mainly for post-processing DNS data, the focal point of the chapter are direct numerical simulations. Principles and limitations of DNS are explained. Simplification methods to reduce computational costs are introduced. An impression is given about the huge amount of data produced by DNS. The necessity of post-processing them carefully is demonstrated for 2D as well as for 3D simulation results.

Chapter 4 deals with scales and quantities that are post-processed in the toolbox. Scales describing turbulence, scales describing flames and those describing probability are introduced.

Chapter 5 deals with the MATLAB toolbox for post-processing DNS data. First the program MATLAB is briefly introduced. The different kinds of tools to investigate turbulent flow fields, flames, interaction between turbulence and flames and dimensions of manifolds are demonstrated.

Chapter 6 discusses selected applications using the developed toolbox. 2D and 3D turbulent flow fields are analyzed, involving non-premixed as well as premixed flames. Their interaction with turbulence is investigated. A PDF analysis of a non-premixed flame is done. Finally, the appropriate dimension for a low-dimensional manifold is determined for a non-premixed turbulent  $\text{H}_2/\text{N}_2/\text{air}$  flame.

Chapter 7 closes the thesis with a summary and an outlook.



# Chapter 2

## Basic theory of turbulent combustion

Turbulent combustion is a complex phenomenon characterized by combining hydrodynamic turbulence, molecular transport, mixing and chemical reactions as well as by the interaction between turbulence and chemistry. The most important feature of turbulence concerning engineering applications is the ability to increase significantly properties of the flow like momentum-, heat- or mass transfer and to accelerate mixing rates by orders of magnitudes compared to molecular diffusion. In combustion devices it is important that mixing processes take place as fast and effectively as possible. Perfect mixing of the reactants is the presupposition of chemical reaction. Afterwards the pollutant streams have to be diluted and cooled before they are released into the atmosphere.

In Section 2.1 turbulence and its features are introduced. Section 2.2 gives an overview about combustion and a description of the different kinds of flames. The balance equations and transport terms are introduced in Sections 2.3 and 2.4. Finally Sections 2.5 and 2.6 deal with reaction kinetics and simplification methods for reaction mechanisms.

### 2.1 Phenomenological description of turbulence

Turbulence itself, even for non-reacting flows, belongs to the most interesting and complex phenomena of fluid physics, and is a focus of scientific research, too. An extensive discussion about several aspects of turbulent motion can be found among others in [50, 74, 103, 113, 118, 133]. Special information about homogeneous turbulence is given for example in [2]. Finally [65, 73, 146] deal with the special case of two-dimensional turbulence.

#### Laminar and turbulent flows

In fluid mechanics we can distinguish two kinds of flows, laminar flows and turbulent flows. Turbulent flows differ from laminar ones in some important items. Laminar flows consist of smooth and ordered layers. Disturbances are damped by viscous forces and the flows keep their regularity. In turbulent flows macroscopic fluid elements of different sizes, called eddies,

move more or less randomly forward, backward and across the layers. Turbulent flows are the

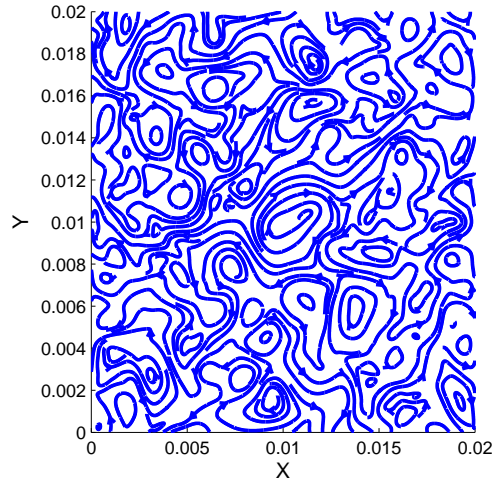


Figure 2.1: Turbulent flow field obtained by DNS at Re=1800

consequence of instabilities that can no longer be damped. Reynolds [108] introduced a dimensionless number to distinguish between laminar and turbulent flows, which bears his name today:

$$\text{Re} = \frac{lu}{\nu} \quad (2.1)$$

where  $l$  is a characteristic length,  $u$  a characteristic velocity and  $\nu$  is the kinematic viscosity (see Section 2.4). Figure 2.1 shows a turbulent flow field at a Reynolds number Re=1800. The Reynolds number Re can be considered as the ratio between inertia forces and viscous forces. For low Reynolds numbers the viscous damping forces are dominant, which means the flow is laminar. At a critical value of the Reynolds number inertia forces, leading to instabilities become dominant and a transition from laminar to turbulent flow takes place. When the Reynolds number is high enough we obtain a stable turbulent flow. In this thesis only turbulent flows are considered. The choice of characteristic length- and velocity scales depends on the specific problem considered. Therefore, we obtain different Reynolds numbers for different problems, and we have to take care which characteristic scales Re is based on.

### Properties of turbulent flows

There is no uniform definition of turbulence in the literature. According to Tennekes and Lumley [133], it is nearly impossible to give a definition of turbulence, it is only possible to list some characteristic items of turbulence:

- Irregularity and randomness,

- Diffusivity,
- Large Reynolds numbers,
- Rotational and three-dimensional,
- Dissipation.

The definition formulated by Hinze [50] reads: *“Turbulent fluid motion is an irregular condition of flow in which the various quantities show a random variation with time and space coordinates, so that statistically distinct average values can be discerned.”*

### **Turbulent scales**

The turbulent eddies mentioned above are characterized by a wide range of length- and time scales. The magnitude of the turbulent scales is bounded from above by the dimensions of the aperture where the flow occurs and bounded from below by viscosity effects. The smallest scales are decreasing in size with increasing velocity of the average flow. Some special scales play specific roles in the description of turbulent flows:

- Integral- or Macro-scales  
The integral length scale  $L$  can be considered as the size of the largest eddies or the distance a large eddy moves before dissolving. The magnitude of these scales depends on the geometry and the boundary conditions of the flow. The largest eddies do the main part of transport and mixing. The integral time scale  $T$  can be considered as the time the eddy uses to pass a certain point.
- Micro-scales of Kolmogorov  
The Kolmogorov scales  $l_k, t_k, v_k$  are the smallest scales occurring in turbulent motion. Viscous terms prevent the generation of infinitely small scales of motion by dissipating small scale energy into heat.
- Micro-scales of Taylor  
The Taylor micro-scale  $\lambda$  has no physical but a mathematical meaning. It can be used to determine other important properties of turbulence. Its size is between the Kolmogorov scale and the macro-scale.

How to calculate turbulent scales is introduced in Section 4.1.

### **Special kinds of turbulence**

If certain conditions are fulfilled the problem can be simplified and the velocity field can be considered as homogeneous or isotropic.

## Homogeneous turbulence

A velocity field is called homogeneous if it has quantitatively the same structure in all its parts and if its statistics are invariants under a shift in position.

## Isotropic turbulence

According to the definition of Hinze [50]: *"Isotropic turbulence is the simplest type of turbulence, since no preference for any specific direction occurs and a minimum number of quantities and relations are required to describe its structure and behavior. The condition of isotropy is defined by the invariance under rotation of the coordinate system and under reflection with respect to the coordinate planes of the statistically averaged properties of the turbulence."*

In real velocity fields global isotropy does not exist. The large scales indeed behave anisotropic. But there exist regions of small scales, which can be considered as locally isotropic, as explained below. The concept of isotropy plays an important role: The knowledge of the characteristics of isotropic turbulence can be used as a basis for research and understanding of actual, non isotropic turbulence. When treating non isotropic cases the assumption of isotropy can be used as first approximation. A huge part of turbulence theory is based on it, many simulations assume homogeneous isotropic turbulence, in many wind tunnel experiments great care is taken to reach isotropic conditions as far as possible. The assumption of homogeneous isotropic turbulence is often used as initial condition in this thesis.

## The energy cascade

A characteristic feature of turbulent motion is the well known energy cascade, pictorially described by Richardson [111] in a poem: *"Big whorls have little whorls that feed on their velocity, and little whorls have lesser whorls and so on to viscosity."* The concept of the energy cascade is that turbulent kinetic energy enters the turbulent system at the largest scales of motion. The Reynolds number  $Re$  is large and the effect of viscosity is negligible. The large eddies are quite unstable, break up and their energy is transferred to smaller and smaller eddies, whereby the eddies are stretching each other. This process continues until, at the smallest scales,  $Re$  is small enough so that the motion is stable and the energy gets dissipated into heat by viscous action. The rate at which this dissipation occurs is called dissipation rate  $\varepsilon$ . The dissipation rate  $\varepsilon$  depends on the eddies and the processes at the beginning of the cascade and is also the rate at which energy is transferred from larger to smaller eddies. If there is no continuous external source of energy at the beginning of the cascade, to keep up the turbulent motion and to compensate the dissipation at the end, turbulence and the turbulent kinetic energy will decay [103, 113, 133]. The smallest scales,  $l_k$ , introduced above were first identified by Kolmogorov [62] and bear his name today.

In Section 4.1 we calculate the turbulent kinetic energy and the dissipation rate. The question how the turbulent kinetic energy is distributed according to the different scales is discussed as well.

## Hypotheses of Kolmogorov

In connection with the energy cascade Kolmogorov formulated now-famous hypotheses:

### *Hypothesis of local isotropy*

The hypothesis of local isotropy says that in an arbitrary turbulent flow with a sufficiently high Reynolds number the turbulence can be considered as locally isotropic with good approximation in sufficiently small domains not lying near the boundaries of the flow or its singularities. A small domain means a domain whose linear dimensions are small in comparison with the size  $L$  of the largest eddies [62].

### *First hypothesis of similarity*

The first hypothesis of similarity says that for locally isotropic turbulence the statistical distributions are uniquely determined by the quantities  $\nu$  and  $\varepsilon$  [62]. This range of small scale motions is referred to as universal equilibrium range. In this range the energy generating processes get more and more unimportant.

### *Second hypothesis of similarity*

The second hypothesis of similarity says that if the scales are large in comparison with the Kolmogorov scale  $l_k$  but small in comparison with the large scales  $L$ , the statistical distributions are uniquely determined by the quantity  $\varepsilon$  and do not depend on  $\nu$  [62]. This part of the universal equilibrium range is called inertial subrange. In this range the transfer of energy takes place. Viscous effects are negligible. The second part is called dissipation range. Here all the

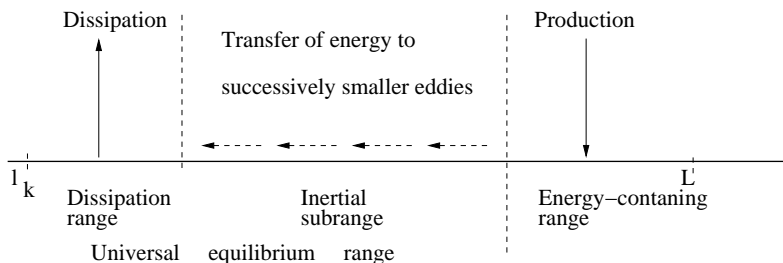


Figure 2.2: The energy cascade: Transfer of energy in different subranges

dissipation takes place. Figure 2.2 shows schematically the energy cascade with the transfer of energy and its different ranges.

### *Refinement of Kolmogorov hypotheses*

The original hypotheses of Kolmogorov are based on a uniform mechanism of transfer of energy from the coarser vortices to the finer ones and did not take into account the random character of this mechanism and the fluctuations of the dissipation rate  $\varepsilon$  about its mean value. The

interested reader can find refined theories in the papers of Kolmogorov [63] and Oboukhov [92].

### Different Reynolds numbers

As already mentioned we can define different Reynolds numbers depending on the characteristic scale we use:

- The Reynolds number based on the micro-scales of Kolmogorov  
The Reynolds number calculated for the micro-scales of Kolmogorov is one:

$$\text{Re}_k = \frac{v_k l_k}{\nu} = 1 \quad (2.2)$$

This means that viscous forces play a major role at this scale.

- The turbulent Reynolds number  
Knowing velocity fluctuations  $u_{rms}$  (see Eq. (4.3)):

$$\text{Re}_t = \frac{u_{rms} L}{\nu} \quad (2.3)$$

In scientific considerations as in this thesis the turbulent Reynolds number is based on the integral scale  $L$  in contrast to engineering problems where it is based on the size or the hydraulic diameter of the device. Typically, this scientific Reynolds number is about 0.01 times the macroscopic technical Reynolds number.

- The Reynolds number based on the micro-scale of Taylor  
In homogeneous turbulence the Reynolds number is often based on the (lateral) micro-scale of Taylor  $\lambda_g$ :

$$\text{Re}_\lambda = \frac{u_{rms} \lambda_g}{\nu} \quad (2.4)$$

### Properties of 2-dimensional turbulence

*"Two-dimensional turbulence has the special distinction that it is nowhere realized in nature or the laboratory but only in computer simulations"* [65]. For non-reacting flows turbulence is intrinsically three-dimensional. Only in a few special cases, for example for flames the shape of which is more cylindrical than spherical, turbulence can sometimes be considered as locally two-dimensional. Two dimensional simulations might still be suitable to investigate chemistry issues, to develop models for chemistry reduction or source terms.

The behavior of two-dimensional and three-dimensional turbulence is very different. The most important item is there is no vortex stretching in two-dimensional turbulence. The consequences of the missing vortex stretching on the energy cascade are discussed in Section 4.1.4.

Two-dimensional and three-dimensional turbulent velocity fields are investigated and compared later in Section 6.1.

## 2.2 Phenomenological description of flames

Combustion theory and phenomena in general considering several kinds of flames and fuels are extensively discussed for example in [22, 59, 67, 76, 96, 100, 145, 150, 152].

### 2.2.1 Categories of flames

The most important criteria to classify flames in flow fields are:

- premixed and non-premixed flames,
- flames in laminar and turbulent flow fields,
- flames with high or low effects of compressibility,
- flames with slow and fast chemistry.

#### Premixed and non-premixed flames

Depending on whether fuel and oxidizer are already mixed before they enter the combustion chamber or they are transported into the flame from opposite sides, flames can be divided into two main classes: premixed flames (Section 2.2.2) and non-premixed flames (Section 2.2.3).

#### Laminar and turbulent flames

The above groups can be further divided into laminar and turbulent flames, depending on the flow field. Turbulent flow fields were discussed in the previous section.

In most combustion equipments the flow in which combustion takes place is turbulent, but laminar flames are studied in order to have a basis for a better understanding of turbulent flames. For example numerically solving for laminar flames may be used to validate chemical models. In many turbulent combustion models laminar flames are the elementary building blocks of turbulent flames [95, 100]. Contrary to laminar flows, turbulent flows are characterized by fluctuations in velocity, which lead to fluctuations in density, temperature and mixture composition and so to reaction rates. Transport processes and mixing are enhanced compared to the laminar case.

According to [67, 150], compared to laminar flames the main features of turbulent flames are:

1. The flame surface is very complex and it is difficult to locate the various surfaces that are used to characterize laminar flames.
2. For premixed flames the turbulent flame speed is much greater than the laminar one because of the enhanced transport properties. It increases as the Reynolds number increases.
3. The height of a turbulent jet flame is smaller than that of a laminar one for the same flow rate and fuel to air ratio. It decreases as the turbulence intensity increases.

4. The reaction zones of turbulent flames are thicker than the reaction zones of laminar flames.

### Compressible and incompressible flows

We can distinguish three kinds of flows. The first ones are incompressible flows with constant density and constant pressure. Normally, reacting flows can not be considered as incompressible. The second ones are fully compressible flows with variable density and variable pressure. In the third ones the density is variable but independent of pressure, which means acoustic waves are filtered out. This assumption is also called low Mach number approximation. A measure for the compressibility is the Mach number, which is defined in the following manner:

$$\text{Ma} = \frac{u}{a} \quad (2.5)$$

The Mach number  $\text{Ma}$  compares the flow speed  $u$  and the speed of sound  $a$ . The speed of sound is the velocity at which disturbances of pressure spread. For low flame speeds and low Mach numbers it is allowed to neglect the influence of acoustic waves.

### Slow and fast chemistry

Turbulent combustion regimes can be further divided by considering the chemistry.

- Infinitely fast chemistry

Many chemical reactions take place so fast that the chemicals react to equilibrium as soon as they mix ("*mixed is burnt*") and the whole problem may be reduced to a mixing problem. The flame structure is not affected by turbulent motion and is similar to that of a laminar flame, wrinkled by turbulent motion. These regimes are called flamelets.

- Slow chemistry

If the time needed for chemical change is greater than the time needed for changes induced by fluid motion, nearly all turbulent eddies are embedded in the reaction zone. It is not possible any more to identify a clear flame front. This regime is called well-stirred reactor. The overall reaction rate is controlled by the chemistry.

- Finite-rate chemistry

However, real chemistries typically have a wide range of timescales for different species. Many problems like ignition processes and pollutant formation usually can not be described only by slow or infinitely fast chemistry.

The dimensionless number used to distinguish between fast and slow chemistry is the Damköhler number  $\text{Da}$ .  $\text{Da}$  is the ratio between a physical time-scale  $\tau_{phys}$  and a chemical time-scale  $\tau_c$  associated with the combustion reaction:

$$\text{Da} = \frac{\tau_{phys}}{\tau_c} \quad (2.6)$$



As physical time-scale often the turbulent integral time scale  $T$  is used.

For values of  $Da \gg 1$  the chemical time scale is shorter than the turbulent one. This limit defines the flamelet regime or fast chemistry.

For values of  $Da \ll 1$  the chemical time scale is larger than the turbulent one. This limit defines the well stirred-reactor or slow chemistry.

### 2.2.2 Premixed flames

Scientific research of turbulent premixed flames began with the experimental and theoretical investigations of Damköhler in 1940 [24]. Recent reviews especially on premixed flames can be found for example in [11, 102].

A premixed flame can occur when the fuel and oxidizer are mixed together before ignition. Mixing between fuel and oxidizer should be complete to the molecular level before combustion takes place. Fresh and burnt gases are separated by a thin reaction zone (about 0.1-1 mm). This zone, the flame front, has the ability to propagate towards the mixture of fresh gases. The rate of propagation is the most important property of premixed flames, since it quantifies the rate at which the flame can process reactants into products and hence describes the rate of heat release. For a laminar premixed flame the propagation rate is usually specified in terms of the laminar burning velocity  $S_\ell$  which is defined as the velocity of advance of the flame relative to the reactants, in the direction locally normal to itself and towards the reactants. If the laminar burning velocity  $S_\ell$  of the flat flame is smaller than the velocity of the unburnt gases the flame normally blows off. The propagation speed  $S_\ell$  depends on the equivalence ratio of the mixture, the temperature of the fresh gases and the pressure [22, 100, 145]. Different ways to define  $S_\ell$  can be found in [100].

Premixed flames are very sensitive to changes in product temperature, and even moderate heat losses from the products adjacent to the flame may cause rapid extinction [22].

The typical structure of a premixed flame is shown in Figure 2.3. Laminar premixed flames can be divided into two zones, a preheat zone where gases are heated by conduction and a reaction zone in which chemical enthalpy is converted into sensible enthalpy. Between burnt and fresh gases a strong temperature gradient is observed (the temperature ratio is about 5-7). Because of this gradient and the corresponding heat flux the fresh gases are preheated in the preheat zone before entering the most intense reaction zone where they start to burn [145].

A premixed flame is called stoichiometric if fuel and oxidizer consume each other completely. If there is an excess of fuel the system is called rich, if there is an excess of oxygen it is called lean.

Eddies of different length scales influence an initially laminar flame in different ways: Sufficiently large-scale eddies wrinkle the initially planar flame surface without significantly modifying its internal structure. The wrinkling leads to an increase in flame surface area and hence to faster propagation. The small-scale eddies primarily affect the local internal structure of the flame and the transport processes inside the flame [11, 24]. These regimes were first identified

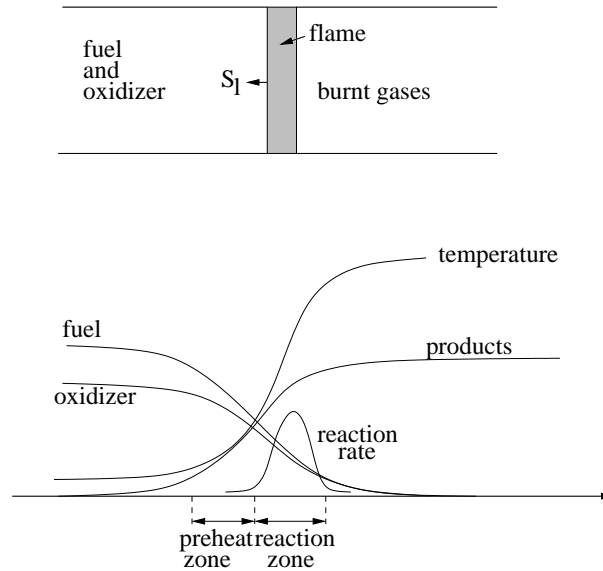


Figure 2.3: Structure of a premixed flame

by Damköhler. Today they are distinguished by the Damköhler number  $Da$ , introduced in Eq. (2.6).

In turbulent premixed flames the flame fronts propagate into a turbulent fluid flow with a turbulent propagation speed  $S_t$  higher than the corresponding laminar one. The increase of the turbulent flame speed  $S_t$  compared to the laminar flame speed  $S_\ell$  is mainly due to the increase of the turbulent flame surface area  $F_t$  compared to a laminar one  $F_l$  through the effect of wrinkling [24].

$$\frac{S_t}{S_\ell} = \frac{F_t}{F_l} \quad (2.7)$$

In some cases the turbulence may be strong enough to tear the flame sheet into pieces and to cause local extinction of the flame. Global extinction is possible with sufficiently intense turbulence.

An example for a laminar premixed flame is the flame of a Bunsen burner when the air intake is open. Turbulent premixed flames can be found for example in spark ignited automotive engines.

### 2.2.3 Non-premixed flames

Reviews especially dealing with non-premixed flames can be found among others in [6, 8, 144]. In non-premixed flames, fuel and oxidizer are initially separated and are mixed during the combustion process itself by convection and diffusion. Fuel and oxidizer diffuse towards the

flame zone where chemical kinetics convert them into products with liberation of energy. The product species and energy diffuse away from the flame zone into both fuel and oxidizer sides. Far away on each side of the flame, the gas is either too rich or too lean to burn. Chemical reactions can proceed only in a limited region, where fuel and oxidizer are mixed adequately. The flame can not propagate into the fuel without oxidizer or into the oxidizer without fuel. Thus, the flame front is fixed to the interface near the location of the stoichiometric composition and where the temperature is highest. Because non-premixed flames do not propagate, they can not be characterized directly by a propagation speed.

Non-premixed flames usually include more complex chemistry than premixed flames, because the whole range from pure air to pure fuel is covered and there is a strong interaction between mixing processes and chemistry. Non-premixed flames are safer to operate because they can not propagate or flashback. However their burning efficiency is reduced because mixing reduces the speed at which chemical reactions may proceed [100, 150].

The structure of a non-premixed flame is shown in Figure 2.4. The flame structure plotted

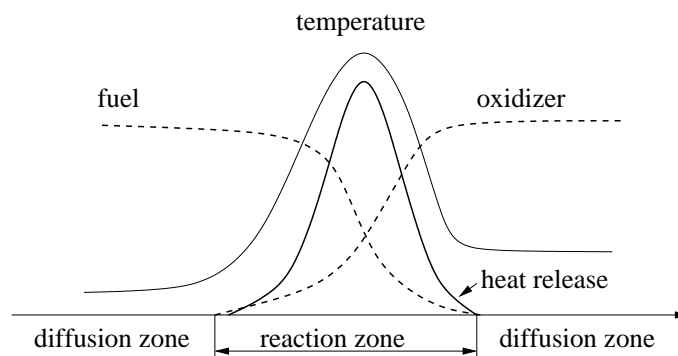


Figure 2.4: Structure of a non-premixed flame

in Figure 2.4 is steady only when strain is applied to the flame, i.e. when fuel and oxidizer streams are pushed against each other at given speeds.

Because they do not propagate, non-premixed flames are unable to impose their own dynamics on the flow field and are more sensitive to turbulence. Therefore, non-premixed flames are more sensitive to stretch than turbulent premixed flames: critical stretch values for extinction of non-premixed flames are one order of magnitude smaller than for premixed flames. Non-premixed flames are also more likely to be quenched by turbulent fluctuations [100].

An example for a laminar non-premixed flame is the flame of a candle. Turbulent non-premixed flames can be found for example in Diesel engines or in aircraft engines.

## 2.3 Balance equations for turbulent reactive flows

The physical processes in turbulent reactive flows described above phenomenologically can be described mathematically by a system of balance equations. This system consists of the classical Navier-Stokes equations for non reacting flows, which are supplied for example in [50, 91, 103, 113, 133]. As combustion involves multiple species reacting through multiple chemical reactions, the system needs to be completed by a set of balance equations depending on the species and reactions considered. The balance equations for turbulent multi-species reacting flows are supplied for example in [67, 100, 145, 152]. In the following equations we use the summation equation of Einstein for repeated indices.

### Balance equation for mass

The balance equation for mass is written [100]:

$$\frac{\partial \rho}{\partial t} + \frac{\partial(\rho u_i)}{\partial x_i} = 0 \quad (2.8)$$

where  $\rho$  is the fluid mass density and  $u_i$  is the  $i^{\text{th}}$  component of the fluid velocity. This equation is also well known as continuity equation.

### Balance equation for momentum

The balance equation for momentum is written [100]:

$$\frac{\partial(\rho u_j)}{\partial t} + \frac{\partial(\rho u_i u_j)}{\partial x_i} = -\frac{\partial p}{\partial x_j} + \frac{\partial \tau_{ij}}{\partial x_i} \quad (2.9)$$

where  $p$  is the thermodynamic pressure,  $\tau_{ij}$  is the viscous tensor for Newtonian fluids. (In this thesis, only Newtonian fluids are considered). The viscous tensor  $\tau_{ij}$  is then given by:

$$\tau_{ij} = \mu \left( \frac{\partial u_i}{\partial x_j} + \frac{\partial u_j}{\partial x_i} \right) + (\mu_D - \frac{2}{3}\mu) \frac{\partial u_k}{\partial x_k} \delta_{ij} \quad (2.10)$$

where  $\mu$  is the dynamic viscosity (see Section 2.4),  $\mu_D$  is the bulk viscosity and  $\delta_{ij}$  is the Kronecker symbol. Often  $\mu_D$  is neglected (according to the hypothesis of Stokes) and Eq. (2.10) becomes:

$$\tau_{ij} = \mu \left( \frac{\partial u_i}{\partial x_j} + \frac{\partial u_j}{\partial x_i} \right) - \frac{2}{3}\mu \frac{\partial u_k}{\partial x_k} \delta_{ij} \quad (2.11)$$

The balance equations for momentum are also well known as Navier-Stokes-equations.

### Balance equation for energy

There are several possibilities to formulate an equation for the energy or the enthalpy. Here

the equation for the sensible enthalpy is written [100]:

$$\frac{\partial(\rho h_s)}{\partial t} + \frac{\partial \rho u_i h_s}{\partial x_i} = \dot{\omega}_t + \frac{Dp}{Dt} + \frac{\partial}{\partial x_i} \left( \lambda \frac{\partial T}{\partial x_i} \right) - \frac{\partial}{\partial x_i} \left( \rho \sum_{k=1}^{N_S} V_{k,i} Y_k h_{s,k} \right) + \tau_{ij} \frac{\partial u_i}{\partial x_j} \quad (2.12)$$

where  $\dot{\omega}_t$  is the heat release due to combustion,  $T$  is the temperature,  $\lambda$  is the thermal conductivity (which is explained in the next paragraph),  $V_{k,i}$  is the diffusion velocity of species  $k$  in direction  $i$ ,  $Y_k$  is the mass fraction of the species  $k$  in the total mass,  $h_{s,k}$  is the sensible enthalpy of species  $k$  and  $N_S$  is the total number of chemical species. The mass fraction  $Y_k$  of a species  $k$  is defined:

$$Y_k = \frac{m_k}{m_{tot}} \quad (2.13)$$

where  $m_k$  is the mass of species  $k$  present in a given volume and  $m_{tot}$  is the total mass of gas in this volume.

The sensible enthalpy of species  $k$  is defined:

$$h_{s,k} = \int_{T_0}^T c_{p,k} dT \quad (2.14)$$

### Balance equation for species

In chemical reactions species are consumed and produced. Therefore, for each species a separate balance equation with source term exists [100] and has to be added to the above system:

$$\frac{\partial(\rho Y_k)}{\partial t} + \frac{\partial(\rho u_i Y_k)}{\partial x_i} = - \frac{\partial(\rho V_{k,i} Y_k)}{\partial x_i} + \dot{\omega}_k \quad (2.15)$$

where  $\dot{\omega}_k$  is the chemical rate of production of the species  $k$ .

By definition:

$$\sum_{k=1}^{N_S} Y_k V_{k,i} = 0 \quad \text{and} \quad \sum_{k=1}^{N_S} \dot{\omega}_k = 0 \quad \text{and} \quad \sum_{k=1}^{N_S} Y_k = 1 \quad (2.16)$$

### Relations to close the equation system

Obviously the above system is not closed. We need a relation between temperature, pressure and local composition, which is given here by the ideal gas equation:

$$p = \rho \frac{R}{W} T \quad (2.17)$$

where  $R=8\,314 \text{ J mol}^{-1}\text{K}^{-1}$  is the perfect gas constant and  $W$  is the mean molar mass of the mixture.  $W$  is given by:

$$\frac{1}{W} = \sum_{k=1}^{N_S} \frac{Y_k}{W_k} \quad (2.18)$$

with  $W_k$  the molar mass of species  $k$ . Additionally the system contains unknown variables:

1. the dynamic viscosity  $\mu$
2. the thermal conductivity  $\lambda$
3. the diffusion velocity  $V_{k,i}$
4. the chemical source term  $\dot{\omega}$

which need to be determined. Expressions for the first three variables are derived in Section 2.4. The source term  $\dot{\omega}$  is discussed in Section 2.5.

## 2.4 Molecular transport processes

In order to close the equation system of Section 2.3 relations for the transport processes for momentum, for the heat flux and for the transport of species are necessary. Molecular transport processes have in common that the corresponding physical properties are transported by the movement of the molecules in the gas. First we consider transport coefficients for single species gases, then we extend the results to mixtures. We follow now the explanations in [150]. For the interested reader more detailed information on the kinetic theory of gases and transport processes can be found in [10, 51].

### Transport of momentum

The viscous tensor  $\tau_{ij}$  in Eq. (2.11) contains as unknown value the dynamic viscosity  $\mu$ . Viscosity quantifies the transport of momentum caused by velocity gradients. Momentum is transported from regions of high velocity to regions of low velocity. The flux of momentum is proportional to the gradient of velocity.

$$j_{mv} = -\mu \frac{\partial u}{\partial x} \quad (2.19)$$

### Dynamic viscosity $\mu_k$ of a species $k$

The viscosity  $\mu_k$  of a pure species  $k$  can be estimated by the kinetic theory of gases:

$$\mu_k = \frac{5}{16} \frac{\sqrt{\pi m k_B T}}{\pi \sigma^2} \quad (2.20)$$

where  $m$  is the mass of the molecule,  $k_B$  is the Boltzmann constant,  $T$  is the temperature in K and  $\sigma$  is the diameter of the (spherical) molecule.

### Dynamic viscosity $\mu$ of a mixture

For mixtures as in combustion systems with many different species, empirical approximations are in use to calculate mixture-averaged values for  $\mu$ , like:

$$\mu = \frac{1}{2} \left[ \sum_{k=1}^{N_s} X_k \mu_k + \left( \sum_{k=1}^{N_s} \frac{X_k}{\mu_k} \right)^{-1} \right] \quad (2.21)$$

where  $X_k$  is the mole fraction of the species  $k$ .

When a higher accuracy is necessary the formula of Wilke (with the modification of Bird [10]) can be used [49]:

$$\mu = \sum_{k=1}^{N_s} \frac{X_k \mu_k}{\sum_{j=1}^{N_s} X_j \Phi_{kj}} \quad (2.22)$$

with

$$\Phi_{kj} = \frac{1}{\sqrt{8}} \left( 1 + \frac{W_k}{W_j} \right)^{-1/2} \cdot \left( 1 + \left( \frac{\mu_k}{\mu_j} \right)^{1/2} \left( \frac{W_j}{W_k} \right)^{1/4} \right)^2 \quad (2.23)$$

### Kinematic viscosity

In the previous section often the kinematic viscosity  $\nu$  was used. The connection between the dynamic viscosity  $\mu$  and the kinematic viscosity  $\nu$  is simply:

$$\nu = \frac{\mu}{\rho} \quad (2.24)$$

### Transport of heat

In Eq. (2.12) we have two terms of heat flux:

- the term  $-\lambda \frac{\partial T}{\partial x_i}$ , which is caused by heat conduction;
- the term  $\rho \sum_{k=1}^{N_s} V_{k,i} Y_k h_{s,k}$ , which is caused by the transport of enthalpies of different species.

In this thesis we neglect the radiative heat flux and the Dufour heat flux, which describes the energy transport caused by concentration gradients.

Heat conduction is the transport of energy caused by temperature gradients.

$$j_q = -\lambda \frac{\partial T}{\partial x} \quad (2.25)$$

The heat flux occurs from a region of high temperature towards a region with lower temperature. The coefficient  $\lambda$  is called thermal conductivity. Like the viscosity  $\mu$  it depends on the square root of the temperature and not on the pressure. Often a second quantity, the thermal diffusivity  $\alpha$  is used:

$$\alpha = \lambda / (\rho c_p). \quad (2.26)$$

### Conductivity $\lambda_k$ of a species $k$

The conductivity  $\lambda_k$  of a pure species  $k$  again can be estimated by the kinetic gas theory:

$$\lambda_k = \frac{25}{32} \frac{\sqrt{\pi m k T}}{\pi \sigma^2} \frac{c_v}{m} \quad (2.27)$$

where  $c_v$  is the molecular heat capacity at constant volume.

### Conductivity $\lambda$ of a mixture

In combustion processes where the gas is composed of many different species,  $\lambda$  of the mixture must be determined. The thermal conductivity of a mixture composed of  $N_S$  species can be calculated from the  $\lambda_k$ 's of the pure species in the following manner:

$$\lambda = \frac{1}{2} \left[ \sum_{k=1}^{N_S} X_k \lambda_k + \left( \sum_{k=1}^{N_S} \frac{X_k}{\lambda_k} \right)^{-1} \right] \quad (2.28)$$

### Transport of mass

The transport of mass caused by concentration gradients is called diffusion.

$$j_m = -D \rho \frac{\partial c}{\partial x} \quad (2.29)$$

The coefficient  $D$  is called diffusion coefficient.

### Diffusion coefficient $D$ of a species $k$

For a single species  $k$  the diffusion coefficient  $D_k$  can be calculated by:

$$D_k = \frac{3}{8} \frac{\sqrt{\pi m k T}}{\pi \sigma^2} \frac{1}{\rho} \quad (2.30)$$



### Diffusion coefficient $D$ in a mixture

In the most general case the diffusion velocities  $V_k$  of species  $k$  in Eqs. (2.12) and (2.15) are obtained by solving the system [100, 152]:

$$\begin{aligned} \nabla X_k = & \sum_{l=1}^{N_s} \frac{X_k X_l}{D_{kl}} (V_l - V_k) + (Y_k - X_k) \frac{\nabla p}{p} + \\ & \frac{\rho}{p} \sum_{l=1}^{N_s} Y_k Y_l (\mathbf{f}_k - \mathbf{f}_l) + \sum_{l=1}^{N_s} \left[ \left( \frac{X_k X_l}{\rho D_{kl}} \right) \left( \frac{D_{T,l}}{Y_l} - \frac{D_{T,k}}{Y_k} \right) \right] \left( \frac{\nabla T}{T} \right); \quad (k = 1, \dots, N_s) \end{aligned} \quad (2.31)$$

$D_T$  is the thermal diffusion coefficient.

$D_{kl}$  is the multi-component mass diffusion coefficient of the species.

For most combustion processes the following assumptions are allowed:

- The flux due to pressure gradients may be important for high-speed or rotating gases, but is negligible in most combustion processes.
- External body forces  $\mathbf{f}$  may occur for example through electric fields. This term is negligible, too, in most combustion processes. Gravity can be assumed to be the same for all species.
- The temperature gradient drives light molecules towards hot regions and heavy molecules towards cold regions of the flow. This effect is known as Soret effect. In many cases the mass flux due to temperature gradients can be neglected. But for light species like H, H<sub>2</sub> (as in hydrogen combustion) or for He it can be important [49].

Neglecting the last three terms Eq.(2.31) reduces to:

$$\nabla X_k = \sum_{l=1}^{N_s} \frac{X_k X_l}{D_{kl}} (V_l - V_k) \quad (2.32)$$

which is known as Stefan-Maxwell equation [152].

### Approximations for diffusion velocity and coefficients

The system in Eqs. (2.31) and (2.32) is of size  $N_s^2$  and must be solved in each direction at each point and at each instant for unsteady flows. Mathematically this task is difficult and costly. Therefore, approximations are often used.

The diffusion matrix  $D = (D_{kl})$  can be expanded in terms of convergent series. These series then yield approximate expressions for the transport coefficients. Different levels of approximation of the transport coefficients can be found depending on the order at which the expansion of the diffusion matrix is truncated. In what follows we give a short summary of the methods of

approximation. The interested reader can find detailed information and discussion for example in [49].

### First-order-approximation

The first two terms in the convergent series mentioned above are kept. This leads to the most accurate expression of the diffusion coefficients. Cross-diffusion, Soret effect and Dufour effect are accounted for.

### Zeroth-order-approximation

This approximation is also known as Hirschfelder-Curtiss approximation. The diffusion coefficient for species  $k$  in the mixture,  $D_k^*$ , is calculated as:

$$D_k^* = (1 - Y_k) \cdot \left( \bar{W} \sum_{l=1, l \neq k}^{N_S} \frac{Y_l}{W_l \mathcal{D}_{kl}} \right)^{-1} \quad (2.33)$$

Here  $\mathcal{D}_{kl}$  is the binary mass diffusion coefficient, depending on species pair properties, pressure and temperature. In the diffusion matrix only diagonal terms are accounted for. Cross-diffusion, Soret effect and Dufour effect are not considered. This approximation is equivalent to an approximation where only the first term of the series expansion is kept.

### Fick's law

The diffusion velocity of species  $k$  into the mixture is determined by:

$$Y_k \mathbf{V}_k = -D_k \nabla Y_k \quad (2.34)$$

where  $D_k$  is the diffusion coefficient of species  $k$  into the mixture.

### Constant Lewis number approach

First we have to introduce the Lewis number.

The laws of transport of momentum in Eq. (2.19), of transport of heat in Eq. (2.25) and of transport of mass in Eq. (2.29) are very similar. The dimensions of the diffusivity of momentum  $\nu$ , of the thermal diffusivity  $\alpha$  and of the diffusivity of mass  $D$  are the same:  $\text{m}^2 \text{s}^{-1}$ . Therefore, dimensionless numbers can be defined as the ratios made from different combinations of these diffusivities.

The Lewis number of species  $k$  is defined as the ratio between thermal diffusivity of the mixture and the mass diffusivity of the species:

$$\text{Le}_k = \frac{\lambda}{\rho c_p D_k} = \frac{\alpha}{D_k} \quad (2.35)$$

The Lewis number  $\text{Le}_k$  compares the diffusion speeds of heat and of species  $k$ .  $\text{Le}_k$  is a local quantity but, in most cases, it changes little from one point of the flame to another [100]. A

simple and attractive approach to express the diffusion coefficient  $D_k$  is to suppose that the Lewis number is constant for each individual species. The diffusion coefficient of species  $k$  in the mixture can then be expressed by:

$$D_k = \frac{\lambda}{\rho c_p Le_k} \quad (2.36)$$

This means that the knowledge of the value of the heat diffusion coefficient is sufficient to express the diffusion coefficients for all species. Different diffusion velocities of different species can be accounted for. The accuracy of this approximation depends on the configuration.

### Unity Lewis number approach

Going one step more is the assumption that all Lewis numbers are constant and equal to one. This means that for all species the diffusion coefficient is the same as the heat coefficient and therefore different diffusion velocities of different species can not be considered. The unity Lewis number approach is very useful for analytical developments. It is often a poor approximation, in particular for hydrogen combustion.

### Impact of diffusion models

The importance of an accurate description of the diffusion processes is demonstrated for example in [47, 48]. In [48] a turbulent non-premixed  $H_2$ /air flame was simulated twice using two different modeling levels for the diffusion velocities. Results for a zeroth-order approximation and for a unity Lewis number approximation are compared. Significant differences are shown for the flame temperature, for the heat release and for the scalar dissipation rate concerning peak values as well as distribution. In [47] a constant Lewis number approach is considered additionally. For example the flame structure is symmetric in the case of the unity Lewis number approach but when taking into account different diffusion velocities the flame structure is not symmetric any more.

In Section 6.4 we determine the dimension of a low-dimensional manifold of a non-premixed hydrogen/nitrogen/air flame twice, using either a zeroth-order approximation or a unity Lewis number approximation. For the detailed model we need one dimension more compared to the simplified model in order to reach the same accuracy. The first results were published in [156].

## 2.5 Reaction kinetics

The most important term in combustion research is the source term  $\dot{\omega}_k$  in the balance equation for species Eq. (2.15). In the case where chemical reactions are fast compared to the transport processes systems can be described by thermodynamics alone. But, in practice, the chemical reactions occur mostly on timescales comparable with that of the molecular transport processes.

Then, information is needed about the rates of chemical reactions to find expressions for the chemical source terms  $\dot{\omega}_k$  [150].

### Reaction rates and rate coefficients

The reaction rate may be expressed in terms of the concentration of the reactants. The rate of reaction depends on the conditions of the system, on the concentrations of the chemical compounds, temperature, pressure, presence of a catalyst or inhibitor [67].

For a reaction:



the reaction rate for the consumption of species A is:

$$\frac{d[A]}{dt} = -k[A]^a[B]^b \dots \quad (2.38)$$

where  $a, b, \dots$  are the reaction orders and  $k$  is the rate coefficient.

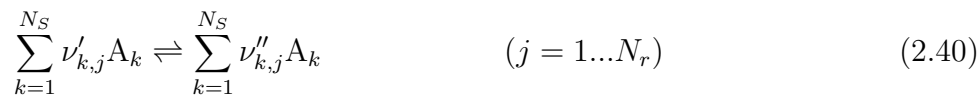
The rate coefficients strongly depend on the temperature according to an Arrhenius law which states: only molecules that possess an energy greater than the activation energy  $E_a$  will react and lead to products, following

$$k = AT^\beta \exp\left(-\frac{E_a}{RT}\right) \quad (2.39)$$

where the pre-exponential factor  $A$  represents the collision frequency and the exponential term represents the fraction of collisions that have high enough energy to react.  $E_a$  is the activation energy,  $R$  the perfect gas constant and  $T$  the temperature.

### Chemical reaction system

A complete chemical system consists of  $N_S$  species reacting through  $N_r$  reversible or irreversible elementary reactions. Each reversible elementary reaction can be written in the form:



where  $A_k$  denotes species  $k$  and  $\nu_{k,j}$  are the stoichiometric coefficients of species  $k$  in reaction  $j$ . The rate law for the molar formation rate  $w_j$  of the  $j$ th reaction is given by:

$$w_j = k_{f,j} \prod_{k=1}^{N_S} C_k^{\nu'_{k,j}} - k_{b,j} \prod_{k=1}^{N_S} C_k^{\nu''_{k,j}} \quad (2.41)$$

where  $C_k$  is the molar concentration of species  $k$ .  $k_f$  and  $k_b$  are the rate coefficients for the forward and backward reactions and are calculated by an Arrhenius law according to Eq. (2.39). For a mechanism consisting of a set of  $N_r$  reactions of  $N_S$  species the rate of formation of a

species is given by summation over the rate equations of all elementary reactions. Now the mass reaction rate  $\dot{\omega}_k$ , the source term in the balance equation for species, is given by:

$$\dot{\omega}_k = W_k \sum_{j=1}^{N_r} \nu_{kj} w_j \quad (2.42)$$

with  $W_k$  the molar mass of species  $k$ . In chemical reactions the total mass must be conserved. This is expressed by:

$$\sum_{k=1}^{N_S} \dot{\omega}_k = 0 \quad (2.43)$$

Therefore, all species, reactions and values of the Arrhenius parameters must be determined before computations can be carried out [49]. In the ideal case for each species involved in the combustion process a separate balance equation has to be solved. In many cases the complete reaction mechanisms consist of dozens of species leading to several hundreds of elementary reactions. This leads for example to consider roughly 10 species and 40 reactions for hydrogen combustion, or over 40 species and over 100 reactions for methane combustion [150]. Investigating such a system by a complete mechanism is very demanding in computing time and memory. In many cases, it is even impossible. Therefore, it is necessary to simplify the system. Corresponding methods are explained below. In this thesis reaction mechanisms and their simplification of gases like  $H_2$ , synthetic gas or methane are investigated. Reaction mechanisms and rate determining mechanisms for the combustion of coal particles are described for example in [125, 126].

## 2.6 Simplification of reaction mechanisms

Depending on the question of interest many reactions can sometimes be neglected in order to reduce the mechanism. A good description of the most common methods to analyze and simplify reaction schemes is given for example in [49, 67, 150]. In the sequel the most important ones are explained.

### 2.6.1 Reduction based on chemistry

#### Quasi steady-state approximation

The quasi steady state approximation is a simplification applied to the description of intermediates. Some intermediates are very reactive and therefore have a negligibly short lifetime. The rate of consumption of these intermediates is assumed to be approximately equal to the rate of formation and it can thus be written:

$$\frac{d[C_r]}{dt} \sim 0 \quad (2.44)$$

where  $[C_r]$  is the concentration of a very reactive intermediate species. These radicals can thus be removed from the complete scheme and the scheme gets simplified.

### Partial equilibrium

For high temperatures the reaction rates of forward and backward reactions of some intermediates are so fast that one obtains partial equilibrium for these reactions. In the equilibrium case forward and backward reaction rates are equal and the system may be simplified again by removing the corresponding intermediate radicals and expressing their concentrations in terms of the concentrations of the stable species. A drawback of this method is that partial equilibrium only occurs at relatively high temperature levels (above about 1600 K).

### Sensitivity analysis

Using this method, the rate limiting reaction steps are identified in the following manner: the parameters (for example the rate coefficients  $k_j$ ) of the system are changed slightly. Then, it is investigated how does the solution, that means the final concentrations, change.

If the change of the parameters  $k_j$  has little or no effect on the concentrations, quasi-steady state or partial equilibrium can be assumed. Reactions in which the change of the rate coefficients has large influence on the solution are the important rate-determining and limiting steps. The dependence of the concentrations on the parameters is called sensitivity.

## 2.6.2 Reduction based on invariant manifolds

The reduced mechanisms mentioned above normally are devised for certain conditions of temperature and mixture compositions and provide poor approximations outside these conditions. Using manifold methods, in contrast to conventional reduced mechanisms, no information is required concerning which reactions have to be assumed to be in partial equilibrium, nor which species are assumed to be in steady-state.

The idea of low-dimensional manifolds is the following: The thermo-chemical state of a homogeneous reacting system can be described by a  $(n=N_S+2)$ -dimensional vector  $Y = (Y_1, Y_2, \dots, Y_{N_S})$ , representing the mass fractions of  $N_S$  chemical species and two thermodynamic quantities as pressure and enthalpy. The system of governing equations for purely reacting flows can then be symbolically written [18]:

$$\frac{\partial Y}{\partial t} = F(Y) \quad Y \in R^n \quad (2.45)$$

where  $F$  is the chemical source term, representing the reaction mechanism. From a mathematical point of view, a model reduction based on a manifold is a reformulation process of Eq. (2.45) in an appropriate form by introducing a reduced space  $\theta=(\theta_1, \dots, \theta_m)$ ,  $m < n$  consisting of a new variable set, such that the solution of Eq. (2.45) will be accurately described by the reduced model:

$$\frac{\partial \theta}{\partial t} = \tilde{F}(\theta) \quad \theta \in R^m \quad (2.46)$$

In order to reduce the system one needs to determine the relation between these spaces. The reduced space can be represented in an explicit form:

$$M = \{Y = Y(\theta) \quad \theta \in R^m\} \quad (2.47)$$

by a low-dimensional manifold  $M$  embedded in the detailed system (2.45). Then, the system (2.45) can be projected onto the manifold, which means a transformation of the system to the new coordinates [18].

In [44, 83, 104, 107] several methods reducing chemistry via slow manifolds are discussed. In the following sections we introduce some specific manifold techniques considered in the rest of this work.

### Intrinsic Low-Dimensional Manifolds - ILDM

The method of Intrinsic Low-dimensional Manifolds (ILDM) was introduced by Maas [79, 80, 81]: Chemical reaction corresponds to a movement along a trajectory in the  $(N_S+2)$ -dimensional state space spanned by the enthalpy  $h$ , the pressure  $p$  and the  $N_S$  species mass fractions. Starting from different initial conditions, the reactive system evolves until it reaches

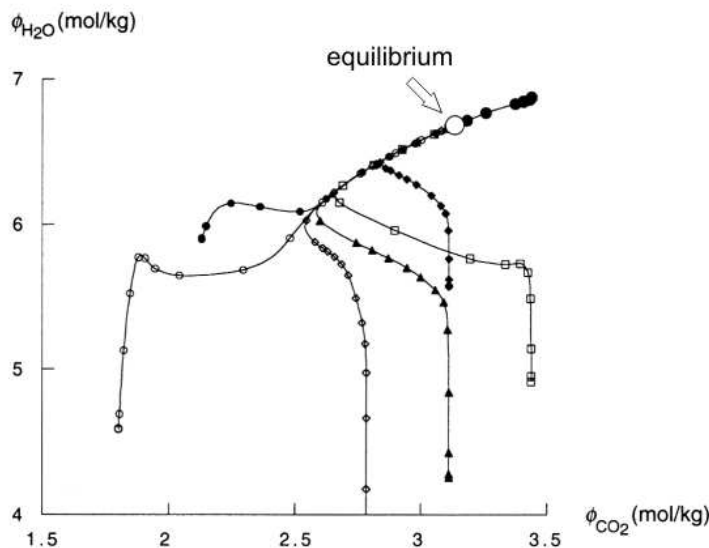


Figure 2.5: Trajectories in a system of methane oxidation in  $\text{CO}_2$  -  $\text{H}_2\text{O}$  plane [150]

the equilibrium point. Figure 2.5 shows an example of such trajectories for a stoichiometric  $\text{CH}_4$ -air system in the  $\text{CO}_2$  -  $\text{H}_2\text{O}$  plane.

The underlying governing processes occur at time scales that differ by orders of magnitude. The timescales of chemical reactions cover a much wider range than the time scales of physical

transport processes. The very fast timescales in chemical kinetics are usually responsible for equilibrium processes and they can be decoupled. From the system of  $N_S + 2$  equations an attractive subspace is then determined by looking at the eigenvalues and eigenvectors of the Jacobian matrix of the system of equations and by neglecting and cutting off fast timescales smaller than a given time limit. The inverse of the eigenvalue represents the corresponding chemical time scale. The complicated curves or surfaces in the state space can thus be reduced to simple ones. Depending on the cut off time scale, one, two or more coordinates of this state space are enough to accurately reproduce the kinetic properties of the full reactive system [79, 80, 81, 150]. Figure 2.6 shows a one-dimensional manifold obtained by neglecting the fastest time scales, (in this example the first  $50 \mu s$ ) in the above system. The number of

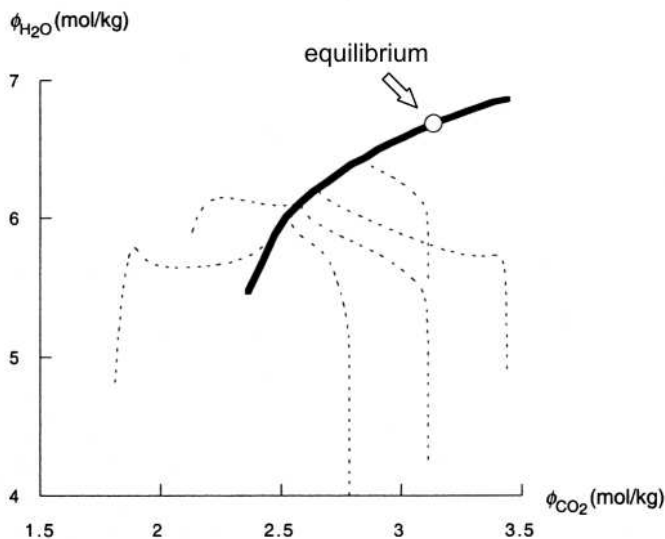


Figure 2.6: One-dimensional manifold [150]

the coordinates of the manifold corresponds to the minimum number of species  $m$  that need to be transported in order to describe with a sufficient accuracy the full reactive system. All other species, thermodynamic properties and reaction rates are obtained from a look-up table. Calculating the chemical rates of change directly would be much more time consuming [81]. After tabulating the resulting manifold, it becomes possible to use particle- (PDF) methods to model the chemical reactions in a turbulent flow.

### Drawbacks of ILDM

In the general case of non-homogeneous systems the system of governing equations for arbitrary



reacting flows can then be written [16, 17]:

$$\frac{\partial Y}{\partial t} = F(Y) - \bar{v} \cdot \nabla Y - \frac{1}{\rho} \text{div}(D \nabla Y) \quad (2.48)$$

where  $\bar{v}$  is the flow velocity and  $D$  is the diffusion matrix. The first term is related to the chemical source term (as before) and the second and third ones describe transport processes, convection and diffusion, respectively.

This means that there are two limiting cases: The first limiting case is a purely homogeneous system where the system dynamics are governed by the source term and chemical kinetics only. The second limiting case is a system without chemical source term, which is governed by convection and diffusion processes only. Originally, ILDM is designed for purely homogeneous systems where it gives good approximations. However there are two problems concerning the second case: The first is the low temperature zone, where the source term is negligible. The second is the coupling of some chemical modes with fast physical ones, which disturb the system from the low dimensional manifold. This means that a manifold which is defined on the basis of reaction processes only, cannot describe directly the coupling between reaction and transport processes [16]. Methods to overcome these problems are discussed below.

### Low temperature regions

As highly reduced ILDM manifolds cut off the fastest time scales, phenomena associated with these timescales, as the low temperature regions, can not be reproduced correctly. Treating the low temperature regions of a flame by increasing the number of dimensions of the manifold would increase computation time and memory requirements immensely. Therefore, one needs somehow to extend the ILDM manifold in these regions.

One solution to the problem is to model the manifold for the low temperature zone by the results of computations of a collection of one-dimensional freely propagating laminar (premixed) flames obtained with detailed reaction schemes. As a whole, this leads to a pre-tabulation of all species values and their thermodynamic coefficients as a function of a small number of coordinates (two to three), based on the data of a collection of laminar premixed flames. This database is then used instead of the classical ILDM manifold. There are two similar independently developed methods to do so: flame prolongation of ILDM (FPI) [40] and the flamelet-generated manifold method (FGM) [143].

In the original FPI method the first coordinate  $Y_Z$  is based on the mixture fraction and reproduces the local mixture between fuel and oxidizer whereas the second one is based on the reaction progress variable  $Y_c$  and represents the progress of reaction [40]. A third variable based on the enthalpy  $h$  can be added in order to reproduce enthalpy variations or heat losses [32]. FPI can also consider non-premixed and partially premixed flames [33]. An advantage of using FPI is, that a relative coarse grid step is possible, since only the coordinates of the look-up table have to be resolved on the computational grid. All other species will be deduced from these coordinates and do not directly lead to specific requirements for the grid resolution [134, 139, 140].

### Coupling between reaction and transport processes

One method for treating transport and diffusion processes relies on reaction-diffusion manifolds (REDIM). REDIM implements a relaxation process that is governed by an equation system of strongly coupled chemical and transport processes, Eq. (2.48). Then, it is supposed that for Eq. (2.48) there is again a reduced space  $\theta$  and a reduced model, as in Eq. (2.46), and a manifold  $M$ , as in Eq. (2.47) determining the reduced system dynamics as well. Then, the system in Eq. (2.48) is projected onto the new manifold. Now both reaction and diffusion influence the reduced model behavior through the manifold's structure. An initial solution of the approximate manifold is constructed using the extended ILDM method. The REDIM-Method is detailed in [16].

While FPI and FGM are based on physical considerations, the REDIM method, similar to ILDM, is based on a rigorous mathematical approach and is therefore independent of the flame topology.

### 2.6.3 Dimension of manifolds

Most manifold methods are either working only for a certain dimension of the manifold or they expect that the user already knows the required dimension. We have developed in this work a method to determine the appropriate dimension of a low-dimensional manifold for reaching a defined level of accuracy. This method is described in [156].

The DNS simulations deliver, at each spatial and temporal point, a state vector  $Y$  as described in Section 2.6.2, which contains, besides other variables (for example temperature) the species mass fractions

$$Y_k \quad (k = 1, 2, \dots, N_S) \quad (2.49)$$

as its components. With an appropriate species numbering scheme, the index  $k$  can simply run over numbers,  $k = 1, \dots, N_S$ , where  $N_S$  is the number of chemical species. To ascertain how well the DNS-data can be described by low-dimensional manifolds, the following procedure was taken:

For a selected data point (state vector  $Y$ ) from the DNS data matrix, a set of  $N$  nearest neighbor points was determined, based on the distance to this point in state space, similar to the method used by Maas and Thévenin [82]. The distance between two points  $a = (Y_{k,a})$  and  $b = (Y_{k,b})$  was determined as

$$d_{a,b} = \sqrt{\sum_{k=1}^{N_S} \left( \frac{Y_{k,a} - Y_{k,b}}{w_k} \right)^2} \quad , \quad (2.50)$$

where the  $w_k > 0$  are scaling factors; the significance of these will be studied later.

The  $N$  nearest neighbors form a small "cloud" of points in state space; note that they need

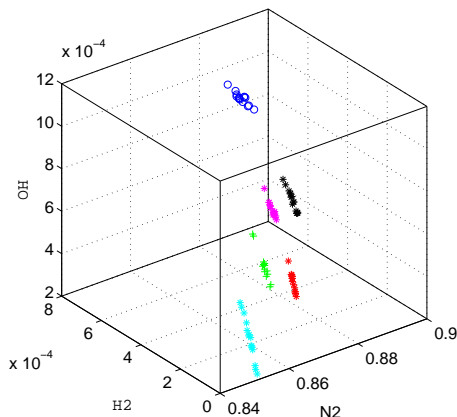


Figure 2.7: Clouds of nearest neighbors

not be close in geometrical space, i.e., points in a state-space neighborhood can stem from very different locations in the turbulent flame. Figure 2.7 shows some clouds of nearest neighbors in the  $N_2$ - $H_2$ - $OH$ -space.

Alternatively, instead of considering species mass fractions only it is also possible to consider temperature as an additional state vector component when searching for nearest neighbors.

A third method to find clouds of nearest neighbors is not to define a certain number of neighbors but to define a prescribed radius (in state space) of the clouds.

In the next step it is checked how well this cloud can be approximated by a linear subspace of a given dimension.

In all cases first the data points in the cloud are centered by subtracting the cloud mean from each species, and then divided by the weights  $w_k$ . This results in a centered and scaled version ( $x_{k,l}$ ) of the data in the cloud:

$$x_{k,l} = \frac{Y_{k,l} - \bar{Y}_k}{w_k} \quad (k = 1, \dots, N_S, l = 1, \dots, N) \quad (2.51)$$

where  $\bar{Y}_k = \frac{1}{N} \sum_{m=1}^N Y_{k,m}$  is the cloud mean of the  $k$ -th species.

The representability of the  $(x_{k,l})$  by low-dimensional linear subspaces is assessed by a singular value decomposition (SVD) [43]. The SVD decomposes the  $N_S - \text{by} - N$  matrix  $(x_{k,l})$  into the product of two orthonormal matrices  $u$  and  $v$  and a diagonal matrix  $\sigma$  with non negative components according to

$$(x_{k,l}) = (u_{k,j})(\sigma_{k,l})(v_{l,m})^T \quad (k, j = 1, \dots, N_S, l, m = 1, \dots, N) \quad (2.52)$$

The entries  $(\sigma_{k,k} \geq 0, k = 1, \dots, n_s)$  along the diagonal, called singular values, are decreasing. The columns of  $u$  are mutually orthonormal; they form a basis of the composition space, which

can be used alternatively to the conventional species basis. The matrix  $q$  obtained from the matrix product of  $\sigma$  and  $v^T$ ,  $q_{k,l} \equiv (\sigma_{k,l})(v_{l,m})^T$  can then be interpreted as coordinates of the data points, expressed in the basis formed by the columns of  $u_{k,j}$ :

$$x_{k,l} = u_{k,1}q_{1,l} + u_{k,2}q_{2,l} + \dots + u_{k,N_S}q_{N_S,l} \quad (k = 1, \dots, N_S) \quad (2.53)$$

The significance of the SVD is, loosely speaking, that the new basis defined by  $u$  is, among all possible orthonormal bases of composition space, the one that is "optimally aligned" with the trend of the data in the local neighborhood. The first basis vector in  $u$  points in the direction in state space of maximum variance, so that the first contribution  $u_{k,1}q_{1,l}$  conveys most of the information about the data in  $x$ , while the second term  $u_{k,2}q_{2,l}$  contains more information than the third, and so on.

By truncating (2.53) after the first term, the best (in a least squares sense) one-dimensional linear approximation ( $x_{k,l}^{(1)}$ ) of  $x_{k,l}$  can be obtained:

$$x_{k,l} \approx (x_{k,l}^{(1)}) = u_{k,1}q_{1,l} \quad (k = 1, \dots, N_S) \quad (2.54)$$

Including more terms from (2.53), yields increasingly better approximations of successively higher dimension  $d \leq N_S$ :

$$x_{k,l} \approx (x_{k,l}^{(d)}) = u_{k,1}q_{1,l} + \dots + u_{k,d}q_{d,l} \quad (k = 1, \dots, N_S), \quad (2.55)$$

until at  $d = N_S$ , the data in  $x$  are reproduced exactly.

The reconstructed mass fractions can be obtained from the  $d$ -dimensional reconstruction  $x_{k,l}^{(d)}$  via

$$Y_{k,l}^{(d)} = \bar{Y}_k + x_{k,l}^{(d)}w_k$$

Note that there is the degenerate case of  $d = 0$ , with

$$Y_{k,l}^{(0)} = \bar{Y}_k$$

where the whole cloud is approximated by one single point, the cloud mean.

For illustration, Figure 2.8 shows on the left a set of artificially generated data points, two center points (red +), the local neighborhood for each point (marked with red o), and the corresponding singular vectors describing the local neighborhood. Note how, for both clouds, the first basis vectors  $u(:, 1)$  align with the local trend of the data, and provide locally one-dimensional linear representations of the small neighborhoods. However, a one-dimensional linear structure could not *globally* represent the *nonlinear* dataset well. The right figure shows a detail from the leftmost cloud. Even though the data points reside in 2D-space, they can locally be approximated by a one-dimensional linear structure (broken line, spanned by the first vector,  $u(:, 1)$ ). The projected points (reconstruction based on one dimension) are depicted as black stars.

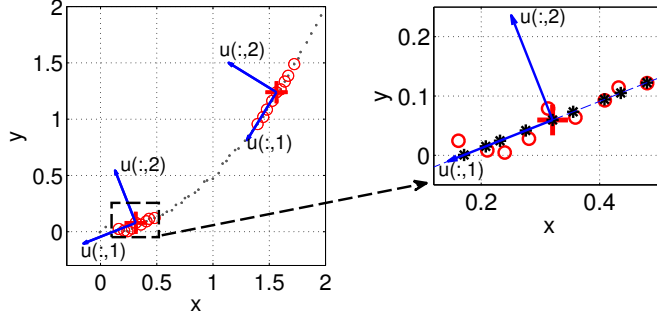


Figure 2.8: Left: Artificial dataset in 2D-space, with two local clusters, for illustrating the procedure. ‘.’: data points, red ‘+’: centers, red ‘o’: local neighborhoods (clouds) around to the two centers, arrows: local basis vectors. Right: Detail around the left cloud, with projections (black stars) onto a one-dimensional linear manifold.

The dimension  $d$  is then varied, and the deviation  $\Delta_{k,l}^{(d)} = |x_{k,l} - x_{k,l}^{(d)}|$  between the  $d$ -dimensional approximation and the original data is determined for all points in the cloud.

To obtain a simple overall measure of the deviation between original and low-dimensional reconstruction for each species, two quantities were considered. First, the sum of the deviations over all points,  $\sum_{l=1}^N |x_{k,l} - x_{k,l}^{(d)}|$  was normalized by that sum for reconstruction with dimension 0, leading to

$$\delta_k^{(d)} = \frac{\sum_{l=1}^N |x_{k,l} - x_{k,l}^{(d)}|}{\sum_{l=1}^N |x_{k,l} - x_{k,l}^{(0)}|} \quad (2.56)$$

as a cloud-global, normalized deviation measure for species  $k$ . Note that the  $\delta_k^{(d)}$  are independent of the cloud size (extent in state space).

Additionally, the correlation coefficient between original and reconstructed values has been computed for each species as well:

$$\frac{N \sum x_{k,l} x_{k,l}^{(d)} - \sum x_{k,l} \sum x_{k,l}^{(d)}}{\sqrt{\left(N \sum x_{k,l}^2 - \left(\sum x_{k,l}\right)^2\right) \left(N \sum \left(x_{k,l}^{(d)}\right)^2 - \left(\sum x_{k,l}^{(d)}\right)^2\right)}, \quad (2.57)$$

where the summation again is over index  $l$  (the points in the clouds). We first calculate the correlation coefficients for each cloud and then we determine the mean value of all correlation coefficients.

This analysis is repeated for about 3000 to 4000 locations (cloud centers) scattered throughout state space, and information about the approximation quality of linear subspaces of various dimension is obtained. The procedure relies on the notion of a distance in composition space.

Since some species mass fractions are typically very small (minor radicals), they hardly contribute to the distance between two given points, which is therefore determined almost entirely by the major species. This imparity causes a statistical bias towards the major species in the method, first, for neighborhood selection, and then also for the SVD analysis. This can be mitigated by adjusting the scaling weights  $w_k$  in Eq.(2.50). Two cases were studied:

- The weights  $w_k$  were set to one for all species, i.e., the original mass fractions were used.
- The weights were set to the difference between maximum and minimum of each species in the DNS dataset:  $w_k = \max_l(Y_{k,l}) - \min_l(Y_{k,l})$ . This removes the imparity in magnitude of minor and major species mass fractions. All species then occupy the whole interval  $[0,1]$ .

The MATLAB tools to determine in this way manifolds dimension are introduced in Section 5.2.7. In Section 6.4 we investigate the resulting dimensions of a diluted hydrogen air flame.

# Chapter 3

## Simulating and modeling turbulent flames

The complicated system of coupled nonlinear differential equations given in Section 2.3 is not solvable by analytical methods in general. Therefore, the system has to be solved by numerical methods. According to different requirements in research and practice in the industry there are different strategies to do so, in particular:

- Direct numerical simulation (DNS),
- Reynolds-Averaged-Navier-Stokes-Methods (RANS),
- Large-Eddy-Simulations (LES),
- Probability-density-function (PDF) Methods.

The advantage of one is the drawback of the others and vice versa. In this chapter the different concepts are introduced and advantages and drawbacks are compared. Further discussions can be found among others in [31, 103] for non reacting flows, and in [34, 100] for reacting flows. In Section 3.1 principles and limitations of direct numerical simulations are introduced. Methods to reduce computational costs are explained. The huge amount of data produced by direct numerical simulations and the necessity of post-processing DNS results carefully is demonstrated. In Section 3.2 RANS-methods, averaged balance equations and models to close the unknown terms are introduced. Section 3.3 deals with Large-Eddy-simulations and Section 3.4 with PDF-methods. In this short chapter, only aspects relevant for the present study are discussed.

## 3.1 Direct numerical simulation (DNS)

### 3.1.1 Principles and limitations of DNS

#### Concept

The concept of DNS for non reacting flows is extensively discussed for example in [14, 88] and for reacting flows in [4]. In direct numerical simulations the full instantaneous Navier-Stokes equations are solved. All scales of motion from the largest turbulent eddies which are in the order of the macro-scale to the smallest scales, where dissipation takes place, the micro-scale of Kolmogorov,  $l_k$ , are resolved without any turbulence model. Therefore, the computational domain must be at least a few times as large as the integral scale and on the other hand the cell size of the grid must not be larger than the micro-scale of Kolmogorov. However, according to Moin and Mahesh [88] this criterion is too stringent and it is enough to resolve scales in the order of magnitude of  $l_k$ .

#### Limitations

The Kolmogorov scale can be estimated in terms of the macro-scale and the turbulent Reynolds number:  $\frac{L}{l_k} \simeq \text{Re}_t^{3/4}$ . This means that for one direction the number of nodes  $N$  grows proportionally to  $\text{Re}_t^{3/4}$  [20, 21]:

$$N \propto \text{Re}^{3/4} \quad (3.1)$$

which limits the possible Reynolds number in a DNS. Since turbulence is three-dimensional this number of points must be employed in each direction, which leads to a total of  $N \propto \text{Re}^{9/4}$ . Additionally with increasing Reynolds numbers the characteristic timescale decreases with  $\text{Re}^{-1/2}$ . Thus, on the whole the expend of simulation increases proportionally to  $\text{Re}_t^{11/4}$  [14, 20, 21].

In a reactive case the inner flame structure has to be resolved additionally by at least  $Q = 10$  grid points [20, 21]. Considering a premixed flame in term of the flame thickness  $\delta$ , the size of the computational domain  $L_d$  is then given by  $L_d \simeq (\frac{N}{Q})\delta$ . The condition that the integral length scale  $L$  must be smaller than the domain size  $L_d$  leads to the inequality:

$$\frac{L}{\delta} < \frac{L_d}{\delta} < \frac{N}{Q} \quad (3.2)$$

With the Damköhler number  $\text{Da} = \frac{T}{\tau_c}$ , where  $T = \frac{L}{u'}$  and  $\tau_c = \frac{\delta}{S_\ell}$  and  $\delta \simeq \frac{\nu}{S_\ell}$ , the product of the Reynolds by the Damköhler number is:

$$\text{ReDa} = \frac{L^2 S_\ell}{\nu \delta} = \left(\frac{L}{\delta}\right)^2 \quad (3.3)$$

leading to the computational grid condition for a premixed flame [20, 100]:

$$\text{ReDa} < \left(\frac{N}{Q}\right)^2 \quad (3.4)$$



Thus, DNS for turbulent reacting flows is limited to low Reynolds and low Damköhler numbers and laboratory conditions. For example for a two dimensional domain with a number of grid points of  $1000 \times 1000 = 10^6$ , one would have  $Re < 10^4$  for resolving all turbulent scales. When resolving the flame front by 10 cells the product  $ReDa$  is  $(1000/10)^2 = 10^4$ . To reach a Damköhler number of 10 it will be necessary to limit the Reynolds number to 1000 [20, 21]. A Reynolds number of 1000 seems small but in scientific computations the Reynolds number

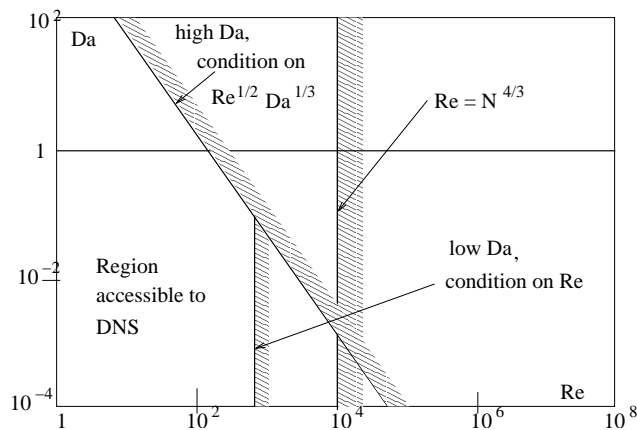


Figure 3.1: Limitations of DNS for non-premixed flames [21]

is usually built using the macro-scale and not the dimensions of the device, like in industrial cases. Macro-scale-based Reynolds numbers are typically 10 to 100 times smaller than the diameter-based Reynolds number for the same conditions [100].

For non-premixed flames the condition associated with a correct resolution of the reactive layer is even more stringent [20, 21]. Figure 3.1 shows the Damköhler- and Reynolds number limitations in a combustion diagram.

Since in direct numerical simulations the solution depends on the initial conditions, it is necessary to repeat the computations and to average it. This means that the needed computing time is increasing immensely. Working with parallel super computers seems the only possible solution to investigate more complicated problems at acceptable costs [136, 138].

### Boundary conditions

The choice of initial and boundary conditions introduces additional difficulties because the classical Dirichlet and von Neumann conditions do not work for compressible DNS. Another technique, called Navier-Stokes Characteristic Boundary conditions (NSCBC) is generally used for compressible simulations. These boundary conditions are out of scope of this work. For the interested reader they are explained in [5, 99, 137].

## Discretization

The conservation equations of Section 2.3 are very complex and difficult to solve, because they are non linear and normally fully coupled. In most cases they can not be solved analytically and numerical methods are necessary. This means that the differential equations must be approximated by a system of algebraic equations which can be solved by a computer. The approximations are applied to small domains in space and time. Thus the numerical solution provides results at many discrete locations in space and time [31]. The most important discretization approaches are the finite difference, the finite volume, the finite element and spectral methods.

The accuracy of the solution depends on the quality of the discretization. We need a scheme with very high accuracy, low dissipation, and low numerical diffusion. As explained for example in [31] upwind methods are dissipative. That means, they naturally include a diffusive term that will dissipate energy in a time dependent calculation. When these methods are used in DNS, the dissipation produced is often much greater than that due to physical viscosity and the results obtained often have little connection with the physics of the problem. Therefore, due to precision requirements, direct numerical simulation techniques often use centered schemes for spatial derivatives and provide only a very small amount of numerical damping. The behavior in time must be modeled as accurately as the behavior in space, which means we need very small time steps. The discretization errors in space and time should be as equal as possible. Therefore, for the integration in time high precision methods are required, too. For large time steps explicit methods can get instable [31, 91]. But the small time steps necessary in our case lie within the stable range. Compared to implicit methods, explicit formulations are easy to parallelize, need relative low memory storage and have easy access to high-order discretization, so that they will be used in this work [138].

For the interested reader more about discretization methods in space and time can be found for instance in [14, 31]. The code used to conduct the DNS calculations post-processed in this thesis is called Parcomb. The original version is described in [136, 138]. Parcomb uses sixth-order central derivatives in space and a fourth order fully explicit Runge-Kutta integration in time. Many additions and new developments have been implemented in Parcomb during the last fifteen years [36].

### 3.1.2 Classical simplifications to reduce computational costs

In order to get acceptable computational costs simplifications are often necessary to reduce the complexity. This is especially true for 3D-simulations. Classical methods used to reduce the computational costs are:

## Methods to reduce the physical complexity

- by considering incompressible flows:  
In this simplification the density is considered as constant and independent of pressure and temperature. Flame-induced flow modifications due to heat release can not be taken into account, which is a major limit.
- by using a low Mach number approximation  
Like in the incompressible case, flame acoustic/interactions are not captured and the density is independent of pressure. But the density may still change due to temperature variations, for example because of heat release. For most applications of interest, such as for example furnaces and boilers, but also inside the combustion chambers for automotive or aeronautical/aerospace applications, the maximum Mach number is generally quite small, at least in the region where combustion takes place. It is then unnecessary and inefficient to employ a fully compressible formulation to investigate numerically such configurations. The low Mach number approximation allows an important speedup, since the stability restrictions associated in particular with the Courant-Friedrichs-Lewy condition are practically released [134, 140]. Moreover, the equations are considerably simplified since several viscous terms become negligible, in particular in the energy equation [139].
- by considering chemical reactions without heat release.

## Methods to reduce the space dimensions

As mentioned above the grid size is mostly determined by the number of cells within the flame front. Thus, flame fronts with a thickness of 0.1 mm require mesh sizes of the order of microns. For example, a DNS simulation of a three-dimensional turbulent flame at atmospheric pressure typically requires at least 1 to 2 million grid points for a computational box corresponding to a physical size of  $5 \times 5 \times 5 \text{ mm}^3$  [100]. One way to simplify the problem is to perform reacting flow simulations in two dimensions. Of course all three-dimensional effects of real turbulence get lost. This approximation is generally not suitable for non reacting flows because turbulent fluctuations are intrinsically three-dimensional.

For premixed combustion, however, some direct simulations show that the probability of finding locally cylindrical 2D flame sheets is higher than the probability of finding 3D spheroidal flame surfaces. Two-dimensional flames appear more probable even though the flow field ahead of these flames is fully three-dimensional. Considering the prohibitive costs of three-dimensional reacting flow computations, two-dimensional simulations remain quite valuable, in particular for systematic studies.

## Methods reducing the chemical schemes

As explained in Section 2.6 chemistry is the most complex and expensive part of the simulation. In order to reach realistic simulation times reduction techniques are often used. The most important techniques leading to a reduced mechanism were explained in Section 2.6. For

example, combining the low-Mach number approach and the chemistry reduction using FPI leads to a typical speed-up of two orders of magnitude compared to a fully compressible formulation employing complete reaction schemes [21, 135]. Thanks to this considerable acceleration, three-dimensional DNS become feasible for computational costs comparable to those of present two-dimensional compressible direct simulations with detailed chemistry.

### 3.1.3 Advantages and drawbacks

#### Advantages

When DNS can be applied it is the simplest method with the highest level of accuracy and description. As no models for turbulence and combustion are required all effects can be simulated where other methods fail, like ignition and extinction or flame-turbulence interaction.

The flow field obtained can be seen as the result of a "numerical experiment". Often, the DNS data are even resolved better than in any experiment. Some data like for example high-order correlations can be determined far more accurately by DNS than in an experiment. Additionally, experiments often are even more cost and time intensive than simulation by DNS.

The DNS results contain very detailed information about the flow and its variables of interest like for example velocity. With this information the flow can be analyzed quite exactly: A physical understanding of the flow becomes possible. The information obtained by DNS can then be used to model similar flows or the results can be used to improve existing or to validate new RANS-models, subgrid scale models for LES or methods to reduce chemical reaction schemes.

#### Drawbacks

One major problem of DNS is how to handle and store all these data in a reasonable manner. The costs of DNS are extremely high and computing time and computer requirements increase immensely with increasing Reynolds numbers. Thus, DNS is limited to low Re numbers and to laboratory conditions. On the whole the cost of DNS increases proportionally to  $Re^{11/4}$  [14, 21], as explained previously.

The statistical evaluation of all the data obtained by DNS takes a lot of time, too. Normally DNS is too expensive to be used as a design tool.

For combustion simulations, where chemical reactions take place and a balance equation for each species has to be considered additionally, the computing time increases even more. For example, describing chemistry with 9 species and 37 reactions in a field of homogeneous isotropic turbulence, the supplementary costs of the chemistry part amount to about 70 % of the total computational costs [21].

Therefore, DNS is mainly a research tool, but a very interesting one. Now, the main question remains: how can we extract as much information as possible from a DNS?

### 3.1.4 Example for a 2D-direct numerical simulation of a partially premixed flame

As already mentioned a lot of data is produced by DNS. In fact the main problem is how to handle and store all these data in a reasonable manner. This detailed information about the flow- and species field and all variables of interest like for example velocity, temperature, heat release or concentrations need to be post-processed. In order to extract as much useful data as possible from the raw variables the commercial program MATLAB is used in the present work. The most important post-processed variables are introduced in Chapter 4. The post-processing procedure and the post-processing tools, which have been developed during this work are explained in detail in Chapter 5. Here, we give a first impression about the extent of

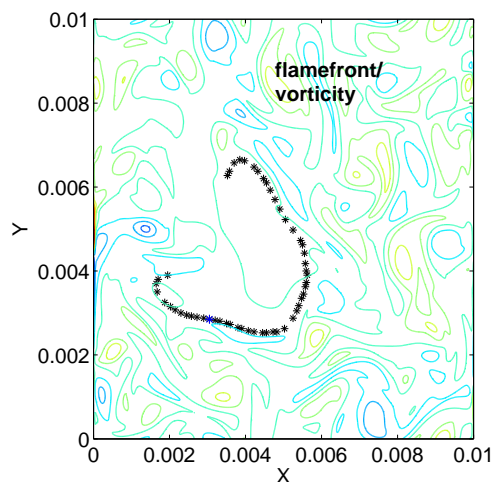


Figure 3.2: Flame front defined as crestline of  $\text{H}_2\text{O}_2$  (black stars); in the background, isolevels of vorticity magnitude

the produced data and the necessity to handle and post-process them carefully. For example for simulating an initially partially premixed  $\text{H}_2/\text{O}_2$  flame using a detailed chemical scheme of nine species in a domain of 1 cm by 1 cm and 401 grid points in each direction, we obtain an array of  $401 \times 401$  data points for each species mass fraction for each time output. The same is true for all further quantities like velocities, temperature, pressure, heat release, density, vorticity and quantities derived from them like curvature or strain rate, the flame index, the reaction progress variable or the mixture fraction. . . . Figure 3.2 shows the flame front on top of the vorticity field. The flame front is here identified by the crestline of the radical  $\text{H}_2\text{O}_2$  (crestline is explained in Section 5.2.2). Variables of interest like temperature, strain rate or curvature can be extracted along the flame front. Examples for the extraction of those variables are given in Figures 3.3 to 3.5. These extracted quantities play an important

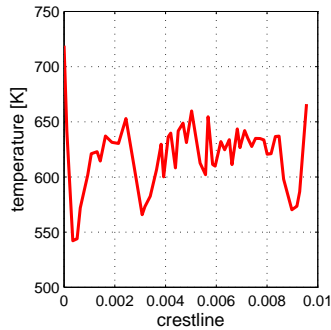


Figure 3.3: Temperature along flame front defined as crestline of  $\text{H}_2\text{O}_2$ , see Figure 3.2

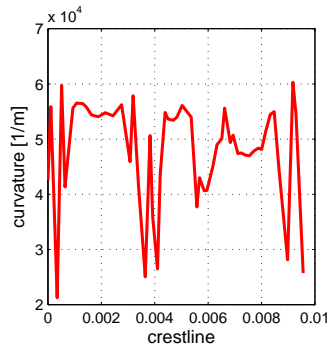


Figure 3.4: Curvature along flame front defined as crestline of  $\text{H}_2\text{O}_2$ , see Figure 3.2

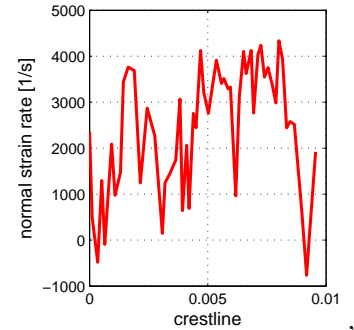


Figure 3.5: Strain rate along flame front defined as crestline of  $\text{H}_2\text{O}_2$ , see Figure 3.2

role in combustion modeling, as discussed in more details later.

### 3.1.5 Example for a 3D-direct numerical simulation of a premixed flame

Even if we use the FPI method, allowing a relative coarse grid the amount of produced data is much higher for a three dimensional simulation than for a two dimensional simulation. For example for simulating a fully premixed methane/air flame in a domain of 6.5 mm by 6.5 mm by 6.5 mm and 119 grid points in each direction we obtain a cube of more than one and a half million data points. Considering the cube as a batch of two-dimensional slices we obtain 119 arrays of 119 by 119 data points. This is true for the FPI coordinates and species mass fractions deduced from the database as well as for all quantities like velocities, temperature, pressure, heat release, density, vorticity and quantities derived from them like reaction progress variables or strain rate. . . . Figure 3.6 shows slices of the species  $\text{CO}_2$  through the domain.

In this example the flame front is defined by the isolevel 0.03 of the mass fraction of the species  $\text{CO}_2$ . Figure 3.7 shows the isosurface of the flame front defined in this manner. Extracting variables along the flame front we obtain information at more than 20 000 points for each variable. It is not an easy task to handle all this information for a single variable and it becomes even more difficult when we are interested for example in correlations between two extracted variables. Figure 3.8 shows the normal strain rate extracted along the flame front. In order to handle the information obtained in several thousands of points it is appropriate to arrange the data in an histogram. Figure 3.9 shows the histogram of the strain rate extracted along the flame front surface. If we want to define our flame front between two boundaries of course the task becomes even more complicated. At some point, it becomes impossible to analyze the corresponding data with simple methods, and advanced tools must be developed

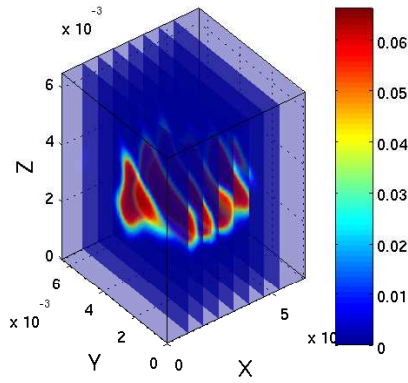


Figure 3.6: Slices of CO<sub>2</sub> mass fraction through the domain

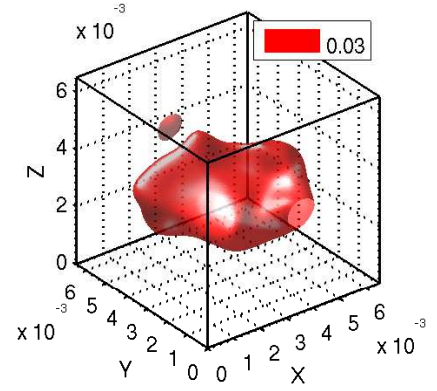


Figure 3.7: Flame front defined by the isolevel 0.03 of CO<sub>2</sub> mass fraction

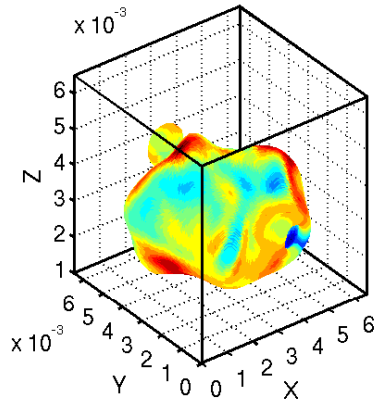


Figure 3.8: Normal strain rate along flame front defined by the isolevel 0.03 of CO<sub>2</sub>

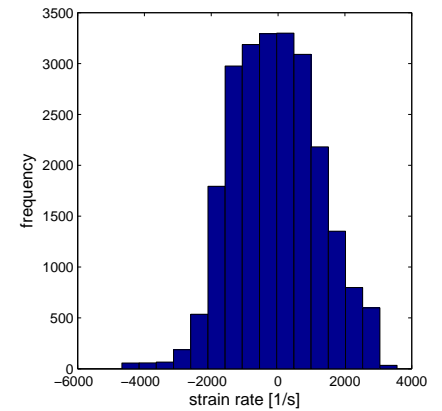


Figure 3.9: Histogram of normal strain rate extracted along the above flame front, see Figure 3.7

for this purpose as described in Chapter 5.

## 3.2 Reynolds-Averaged Navier-Stokes-methods (RANS)

### 3.2.1 Concept

Unfortunately, for real technical processes with high Reynolds numbers or more complex geometries the quantity of data obtained by DNS is too big and computational time is too long. On the other side engineers are often only interested in the mean values of the turbulent quantities but not in the time-dependent fluctuations or higher order moments.

The concept of RANS-methods is to do the statistics first and to average out the unsteadiness. According to the proposal of Osborne Reynolds [109] every variable in the Navier-Stokes equations in Section 2.3 can be written as the sum of a mean value and fluctuations about that mean value. Then, the averaged Navier-Stokes equations are solved for the mean flow field. The new conservation equations, however, contain new terms which can not be represented as functions of the mean quantities, which means that the system of equations is not closed any more. The new unknown correlation terms that describe the influence of the turbulent fluctuations on the mean flow field and on the flame need to be modeled. Detailed information about associated turbulent combustion modeling can be found for example in [34, 59, 100, 145].

In non-reacting and incompressible flows the density can be considered as constant and density fluctuations can be neglected. Then, classically ensemble-averaged equations according to Reynolds are used for mass and momentum. But in reacting turbulent systems, there are large fluctuations of density because of volume expansion and heat release. Density changes can not be neglected. In order to limit the number of unknown correlations that need to be modeled the density-weighted averaging method introduced by Favre [30] is preferred.

### 3.2.2 System of averaged balance equations

Every value is now decomposed into:

$$\phi = \tilde{\phi} + \phi'' \quad (3.5)$$

with

$$\tilde{\phi} = \frac{\overline{\rho\phi}}{\bar{\rho}} \quad \text{and} \quad \overline{\rho\phi''} = 0 \quad (3.6)$$

The mean value of a density averaged fluctuation vanishes. The Favre averaged Navier-Stokes equations are written [100]:

#### Balance equation for Mass

$$\frac{\partial}{\partial t}(\bar{\rho}) + \frac{\partial(\bar{\rho}\tilde{u}_i)}{\partial x_i} = 0 \quad (3.7)$$



### Balance equation for Momentum

$$\frac{\partial}{\partial t}(\bar{\rho}\tilde{u}_i) + \frac{\partial}{\partial x_i}(\bar{\rho}\tilde{u}_i\tilde{u}_j) = -\frac{\partial\bar{p}}{\partial x_j} + \frac{\partial}{\partial x_i}(\bar{\tau}_{ij} - \bar{\rho}u_i''u_j'') \quad (3.8)$$

### Balance equation for Enthalpy

$$\frac{\partial(\bar{\rho}\tilde{h}_s)}{\partial t} + \frac{\partial(\bar{\rho}\tilde{u}_i\tilde{h}_s)}{\partial x_i} = \bar{\dot{\omega}}_T + \frac{\overline{Dp}}{Dt} + \frac{\partial}{\partial x_i}\left(\lambda\frac{\partial\overline{T}}{\partial x_i} - \overline{\rho u_i''h_s''}\right) + \tau_{ij}\frac{\partial u_i}{\partial x_j} - \frac{\partial}{\partial x_i}\left(\overline{\rho\sum_{k=1}^{N_s}V_{k,i}Y_k h_{s,k}}\right) \quad (3.9)$$

### Balance equation for Species mass fractions

$$\frac{\partial(\bar{\rho}\tilde{Y}_k)}{\partial t} + \frac{\partial}{\partial x_i}(\bar{\rho}\tilde{u}_i\tilde{Y}_k) = -\frac{\partial}{\partial x_i}\left(\overline{\rho V_{k,i}Y_k} + \bar{\rho}u_i''\tilde{Y}_k''\right) + \bar{\dot{\omega}}_k \quad (3.10)$$

In the above equations new unknown terms occur:

- $\bar{\rho}u_i''u_j''$  is the Reynolds stress tensor,
- $\bar{\rho}u_i''\tilde{Y}_k''$  is the turbulent species transport,
- and  $\bar{\dot{\omega}}_k$  is the mean reaction rate.

These terms need to be modeled.

## 3.2.3 Closure of unknown terms

### Turbulence Closure

The first new term is the Reynolds stress tensor  $\bar{\rho}u_i''u_j''$  in the momentum equation Eq. (3.8). It is possible to formulate transport equations for this term. But these equations now contain new unknown triple-correlations like  $\bar{\rho}u_i''u_j''u_k''$ . An equation describing the triple-correlations would produce fourth-order correlations and so on. This is the closure problem of RANS modeling. Therefore, one has to break up the formulation of equations and to model the unknown values. Reviews on modeling strategies for the Reynolds stress tensor are given for example in [110, 127]. Some well-known models are among others:

- Prandtl mixing length model [105],
- Prandtl-model [106],
- k- $\epsilon$  model [57],
- second order closures [58, 68].

### Turbulent species transport models

For isotropic turbulence the transport term  $\bar{\rho} u_i'' \widetilde{Y_k''}$  is traditionally described by a gradient eddy viscosity model [21, 34, 145]. Information concerning an extension to non-isotropic turbulence can be found in [34].

### Reaction rate models

The mean reaction rate is significantly affected by turbulent fluctuations, especially fluctuations in temperature. As shown in Eq. (2.39) the rates of chemical reactions have a strong dependence on temperature. It is well known that in turbulent cases  $\bar{\omega} \neq \bar{\omega}(\bar{Y}, \bar{T})$ . Both sides of this equation can differ by orders of magnitude. Therefore, it is the main difficulty and one of the most important challenges in combustion modeling to find good models for the source term  $\bar{\omega}_k$ . Several models are reviewed in detail for example in [145]. Some well-known models are among others:

- The Eddy-Break-Up (EBU) model for premixed combustion [121, 122],
- The Magnussen model for non-premixed combustion [84],
- Flamelet modeling [95, 96],
- Bray-Moss-Libby Model [13],
- Flame surface density models [129],
- Conditional moment closures [61].

## 3.2.4 Advantages and Drawbacks

### Advantages

In engineering and industrial applications it is important to minimize time and costs, which is the main advantage of the RANS-models compared to the other methods. Because the computer requirements are not so high, RANS modeling could start earlier and there are more years of experience compared to LES and DNS. RANS models, especially the k- $\epsilon$ -model family are included into commercial codes and they are easily usable.

### Drawbacks

Because all scales must be modeled and the large scales are very sensitive to boundary and initial conditions it is nearly impossible to find universal models that are valid for several situations and geometries. The models contain empirical constants that can not be optimized for several different flows at the same time. RANS models can not describe instantaneous processes, rotation or strong curvature of, e.g., flame surfaces.

## 3.3 Large Eddy Simulation (LES)

### 3.3.1 Concept

LES is a compromise between DNS and RANS-models. The larger eddies at the beginning of the energy cascade contain most of the energy, contain also the information about initial and boundary conditions, are three-dimensional and unsteady and are responsible for the main part of the turbulent transport. All this information can be described exactly by DNS but nearly gets lost in statistical methods. On the other hand, at the end of the energy cascade the smaller eddies are much weaker concerning turbulent kinetic energy and transport. At small scale, the flow field itself can be considered to be nearly isotropic and it is easier to find an adequate model for it. Therefore, it makes sense to distinguish between a large scale and a fine scale field, to describe the large eddies exactly and to model only the effects of the smaller ones by so called subgrid scale models (Figure 3.10). Ideally the field of the large eddies should contain about 80 % of the turbulent kinetic energy. To separate the large scales from the small ones,

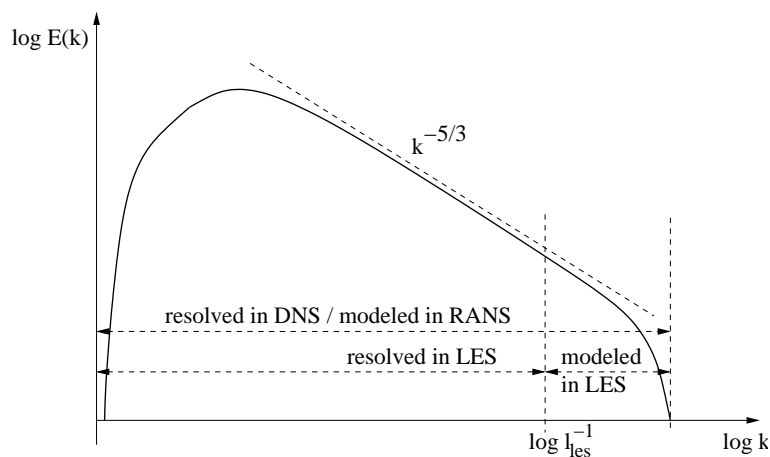


Figure 3.10: Classical energy spectrum for a homogeneous and isotropic turbulent flow

following the proposal of Leonard [72], a filtering operation is introduced, which also leads to unknown terms that need to be modeled.

Concept of and progress in Large Eddy Simulations are reviewed for example in [75, 98, 112]. The theory, filter methods and subgrid scale models is extensively exposed for example in the textbooks [14, 115] for non-reacting, incompressible flows. Large eddy simulations in compressible flows are discussed in [28]. Finally, special information concerning reacting flows can be found for example in [100, 145].

### 3.3.2 Advantages and drawbacks

#### Advantages

The first advantage of LES compared to RANS-modeling is that the large scales in which the large-scale mixing between fuel and oxidizer occurs are simulated directly and are not averaged. Mixing plays an important role in combustion. Secondly, because the small scales are modeled, the LES method is not limited to such low Reynolds numbers like DNS. The small scales can be described by less complicated and more universal models than those used in RANS-modeling where the whole spectrum must be described. Therefore, LES is a good method when DNS is too expensive because the Reynolds number is too high and when a statistical model is not accurate enough or even fails. Cases where LES can be used will increase with increasing computer capacity.

#### Drawbacks

Even if LES is not as expensive as DNS it still takes a lot of computer time and costs. One problem of LES is to handle initial and boundary conditions, particularly near walls and to take into account the backscatter effect. Methods to describe reactive flows are still under development.

## 3.4 Probability-density function methods (PDF)

### 3.4.1 Concept

The key problem in combustion modeling is to find a closure for the chemical source term in the species balance equation. Modeling of the chemical source term can be avoided by the use of probability density function (PDF) methods. PDF methods combine an exact treatment of chemical reactions with a closure for the turbulence field. Two types of PDF approaches can be distinguished: The transported PDF method of Pope [101] and the presumed PDF method. In the first one for each species a balance equation is resolved for the velocity-composition PDF wherein the chemical source term appears in closed form. The shape of the PDF may evolve freely. The one-point joint velocity composition PDFs describe the velocity components, chemical species and scalars exactly. When the velocity-composition-probability-density-function in a point is known, all statistics in that point are known.

A description of transported PDF methods can be found for example in [34, 101].

In the presumed PDF methods the shape of the PDF is given by a mathematical function defined by the first couple of moments. Typically, Gaussian or  $\beta$ -functions are in use. That is justified because in many cases the chemical source term is relatively insensitive to the shape of the PDF.

Unfortunately it is very hard to define an assumed PDF that describes the statistical distribution of all source term variables. The greatest problems arise from the coupling of temperature

and gas composition. Therefore, at the present state statistical independence of temperature and gas composition is usually assumed [37, 39], though it is questionable. A description of presumed PDF methods can be found for example in [38].

### 3.4.2 Advantages and drawbacks

The main advantage of the transported PDF method is that there is no *a priori* assumption concerning the shape of the PDF. Moreover it does not suffer from assumptions of statistical independence of temperature and species mass fractions. It is more accurate in general but it requires substantially more computational resources and time compared to the presumed PDF method. In principle all source terms of all species can be treated if the complete chemical scheme is known. But in practice, in many cases for example for hydrocarbon flames the scheme must be reduced because of computer requirements. Because of their efficiency compared to the full PDF methods the presumed PDF methods are often preferred in practical applications.

Before describing the post-processing library developed during this thesis, it is now necessary, as a last step, to explain all quantities of interest and their importance.

# Chapter 4

## Post-processed scales and quantities

In Sections 2.1 and 2.2 a phenomenological description of turbulence and flames was given. In this chapter we introduce the corresponding quantitative scales that can be calculated by the post-processing toolbox. In Section 4.1 we explain scales calculated in the turbulence part of the toolbox. Section 4.2 deals with scales calculated in the combustion part of the toolbox. Quantities describing probability are important for combustion modeling. These quantities are introduced in Section 4.3 and can be determined by the statistical part of the toolbox.

### 4.1 Scales and quantities characterizing turbulence

Scales calculated in the turbulence part of the toolbox are based on velocity components because in turbulent flow fields velocity is the most important item. In Sections 4.1.1 and 4.1.2 we explain scales derived from one-point and from two-point statistics. In Section 4.1.3 we introduce scales concerning the energy cascade. Section 4.1.4 deals with two-dimensional turbulence. Finally in Section 4.1.5 a table summarizes the quantities calculated in the turbulence part of the toolbox, while the corresponding MATLAB tools are introduced later in Section 5.2.4.

#### 4.1.1 Quantities derived from one-point statistics

According to the proposal of Reynolds [109], in turbulent flows quantities are decomposed in mean (or average) values of the quantity and deviations (or fluctuations) around those mean values. In one-point statistics mean values, fluctuations and moments at a single fixed point are considered.

- Mean value

Depending on the system of interest, different averages (in space, in time, over different realizations) must be computed. They are explained in Appendix A.

- Fluctuations

The fluctuations  $u'_i$  of the velocity component  $u_i$  are defined by:

$$u'_i = u_i - \overline{u_i} \quad (4.1)$$

By definition the mean value of the fluctuations is  $\overline{u'_i}=0$ . Therefore  $\overline{u'_i}$  is not a useful value to measure turbulence. More convenient quantities to describe turbulence is the variance, which measures the dispersion around the mean value in a distribution or the standard deviation, which measures the absolute value of the mean fluctuations.

- Variance

$$\overline{u'^2_i} = \sigma^2 = Var(u_i) = \int_{-\infty}^{\infty} (u_i - \overline{u_i})^2 \cdot f(u_i) du_i \quad (4.2)$$

The square-root of the variance  $Var(u_i)$  is called standard deviation  $u_{rms}$ .

$$u_{rms} = \sqrt{\overline{u'^2_i}} \quad (4.3)$$

Often the standard deviation is the preferred quantity because it has the same dimension as the original value.

- Turbulent kinetic energy

The variance can be used to quantify the turbulent kinetic energy  $k$ , which we know from the energy cascade:

$$k = \frac{1}{2} \overline{u'_i u'_i} \quad (4.4)$$

- Vorticity

A further important quantity in turbulent flow fields is the *vorticity*  $\omega$  which is defined as the curl or rotation of the velocity field.

$$\omega = \nabla \times \mathbf{u} = \begin{pmatrix} \frac{\partial}{\partial x_1} \\ \frac{\partial}{\partial x_2} \\ \frac{\partial}{\partial x_3} \end{pmatrix} \times \begin{pmatrix} u_1 \\ u_2 \\ u_3 \end{pmatrix} \quad (4.5)$$

Sometimes in the literature vorticity is defined as half the rotation of the velocity field. In this work and in the toolbox the factor  $\frac{1}{2}$  is not used.

### 4.1.2 Quantities derived from two-point statistics

In turbulent flow fields, influence and relations between fluctuations in neighboring points or at different instants of time are of great importance. Therefore, it is necessary to extend the consideration to several velocity components at several local points and several instants. In

statistics this dependence is described and measured by correlations. If the local or temporal distance between two local or temporal points is smaller than the size or the lifetime of the largest turbulent eddies there is a dependence or correlation between the velocity components in the two points. The correlation is different from zero. For greater distances the correlation gets lost. Correlations between velocity components as a quantity to describe turbulence were first introduced by Taylor [130]. Based upon these correlations von Kármán introduced correlation tensors [147].

Two-point correlations give information how the fluctuations in neighboring points are related. From such velocity correlations integral scales and the micro-scales of Taylor can be determined.

### Correlation functions in a general flow field

Definitions of correlation functions are given for example in [50, 113].

- General correlation function

In the most general case the correlation function for fluctuations in different directions  $u'_i, u'_j$ , at two different local points  $x_1, x_2$ , and different time instants,  $t_1, t_2$ , is defined as:

$$R_{ij}(x_1, t_1, x_2, t_2) = \overline{u'_i(x_1, t_1)u'_j(x_2, t_2)} \quad (4.6)$$

- Spatial correlation function

If the flow field is homogeneous according to space, and the averages are taken with respect to space, we do not have to consider the dependence on time. For  $t_2 = t_1 = t$  the spatial correlation function at the instant  $t$  is defined:

$$R_{ij}(x_1, x_2, t) = \overline{u'_i(x_1, t)u'_j(x_2, t)} \quad (4.7)$$

- Auto correlation function

When fluctuations in the same direction are considered  $u_i = u_j$  the correlations are called auto correlation:

$$R_{ii}(x_1, t_1, x_2, t_2) = \overline{u'_i(x_1, t_1)u'_i(x_2, t_2)} \quad (4.8)$$

- Correlation coefficients

Correlation functions can be normalized by standard deviations (here we consider spatial correlation functions):

$$\rho_{ij}(x_1, x_2, t) = \frac{R_{ij}(x_1, x_2, t)}{\sqrt{\overline{u'^2_i(x_1, t)}}\sqrt{\overline{u'^2_j(x_2, t)}}} \quad (4.9)$$

The quantities  $u'_i$  and  $u'_j$  being components of two vectors, von Kármán argued that the quantities  $R_{ij}$  and  $\rho_{ij}$  are components of a tensor and introduced the concept of correlation tensors [147].  $R_{ij}$  and  $\rho_{ij}$  are second order tensors with 9 components  $\overline{u'_i(x_1)u'_j(x_2)}$  for 3D turbulence



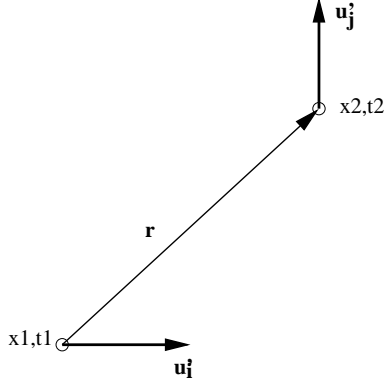


Figure 4.1: Correlation between velocity components in two points in general case

and four components for 2D turbulence. Figure 4.1 illustrates an example for a two point correlation tensor. This means that depending on location and direction there are several possibilities to define correlation tensors.

### Correlation functions in homogeneous isotropic turbulence

When the flow field is homogeneous and isotropic the problem can be simplified and the correlation tensor can be described by only two special types of correlation. Due to the condition of continuity (see Section 2.3) there is a relation between the two correlations and the tensor is completely determined by only one scalar function [148].

We follow the explanations of [2, 50, 113]. In homogeneous turbulence the correlation tensor is independent of location and only a function of the distance vector  $\mathbf{r}$ :

$$R_{ij}(\mathbf{r}) = \overline{u'_i(\mathbf{x})u'_j(\mathbf{x} + \mathbf{r})} \quad (4.10)$$

According to the definition of isotropy, any relation between turbulence quantities must be invariant under rotation of the coordinate system and under reflection with respect to the coordinate planes. This means for the correlation tensor:

- $R_{ij}(\mathbf{r}) = \overline{u'_i(\mathbf{x})u'_j(\mathbf{x} + \mathbf{r})} = 0$  for  $i \neq j$ ,
- and from the remaining three correlations  $\overline{u'_i(\mathbf{x})u'_i(\mathbf{x} + \mathbf{r})}$  two must be the same.
- The root mean square of the velocity fluctuations is the same for all directions:  
 $\sqrt{u_i'^2} = \sqrt{u_j'^2} = \sqrt{u'^2} = u_{rms}$ .

In isotropic turbulence including spherical and reflectional symmetry a second-order-two-point tensor has the following form:

$$R_{ij}(\mathbf{r}) = F(r)r_i r_j + G(r)\delta_{ij} \quad (4.11)$$

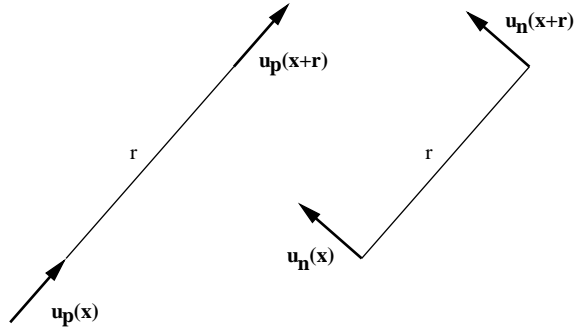


Figure 4.2: Longitudinal and transverse velocity correlation

where  $F$  and  $G$  are arbitrary scalar functions of  $r^2$ . The interested reader can find the derivation in [2, 50, 113].

### Longitudinal and transversal correlations

It is found convenient, for example in connection with experimental work, to introduce an alternative pair of scalar functions  $f(r)$  and  $g(r)$  defined by:

$$f(r) = \frac{\overline{u'_p(\mathbf{x})u'_p(\mathbf{x} + \mathbf{r})}}{\sqrt{\overline{u_p'^2}}\sqrt{\overline{u_p'^2}}}, \quad g(r) = \frac{\overline{u'_n(\mathbf{x})u'_n(\mathbf{x} + \mathbf{r})}}{\sqrt{\overline{u_n'^2}}\sqrt{\overline{u_n'^2}}} \quad (4.12)$$

where  $u_p$  and  $u_n$  denote velocity components parallel and normal respectively to the vector separation  $\mathbf{r}$  (Figure 4.2) [2]. That is,  $f(r)$  is the longitudinal auto correlation coefficient and  $g(r)$  is the transverse auto correlation coefficient for two points of distance  $r$  apart in any direction.

### Integral- or Macro-scales in isotropic Turbulence

From the two correlation coefficients  $f(r)$  and  $g(r)$ , integral lengths scales can be defined [113]:

$$L_f = \int_0^{\infty} f(r) dr \quad (4.13)$$

and

$$L_g = \int_0^{\infty} g(r) dr \quad (4.14)$$

where  $L_f$  is the longitudinal and  $L_g$  is the transverse or lateral integral scale. The relation between  $L_f$  and  $L_g$  is:

$$L_g = \frac{1}{2}L_f \quad (4.15)$$

### Micro-scales of Taylor

The second pair of length scales which can be obtained from  $f(r)$  and  $g(r)$  are the longitudinal and lateral micro-scales of Taylor:

$$\frac{1}{\lambda_f^2} = -\frac{1}{2} \left[ \frac{\partial^2 f}{\partial r^2} \right]_{r=0} \quad (4.16)$$

$$\frac{1}{\lambda_g^2} = -\frac{1}{2} \left[ \frac{\partial^2 g}{\partial r^2} \right]_{r=0} \quad (4.17)$$

Considering velocity components parallel to the coordinate axes we can write for the longitudinal micro-scale [103]:

$$\overline{\left( \frac{\partial u'_1}{\partial x_1} \right)^2} = \frac{2\overline{u'^2}}{\lambda_f^2} \quad (4.18)$$

and for the lateral micro-scale [103]:

$$\overline{\left( \frac{\partial u'_1}{\partial x_2} \right)^2} = \frac{2\overline{u'^2}}{\lambda_g^2} \quad (4.19)$$

The relation between  $\lambda_f$  and  $\lambda_g$  is:

$$\lambda_f = \lambda_g \sqrt{2} \quad (4.20)$$

## 4.1.3 Quantities characterizing the energy cascade

### The energy cascade in wave number space

In Section 2.1 a phenomenological description of the energy exchange between eddies of different sizes in the energy cascade was given. But this picture did not give us any information about the way eddies of different sizes exchange energy with each other. A way to overcome this lack of information is to consider spectra instead. The value of the spectrum at a given wavenumber is the mean energy in that wave. Spectra are decompositions of a function (for example the turbulent kinetic energy) into waves of different specific wavelengths. They can be obtained by Fourier transforms of velocity correlations of the corresponding eddies. Here, we only introduce the spectrum tensor  $\Phi_{ij}$  and the wave-number  $\boldsymbol{\kappa}$ . For homogeneous turbulence the spectrum tensor  $\Phi_{ij}$  and the correlation tensor  $R_{ij}$  from Eq. (4.10) form the following Fourier transform pair:

$$\Phi_{ij}(\boldsymbol{\kappa}) = \frac{1}{(2\pi)^3} \int_{-\infty}^{\infty} \int_{-\infty}^{\infty} \int_{-\infty}^{\infty} e^{-i\boldsymbol{\kappa}\mathbf{r}} R_{ij}(\mathbf{r}) d\mathbf{r} \quad (4.21)$$

and

$$R_{ij}(\mathbf{r}) = \int_{-\infty}^{\infty} \int_{-\infty}^{\infty} \int_{-\infty}^{\infty} \Phi_{ij}(\boldsymbol{\kappa}) e^{i\boldsymbol{\kappa}\mathbf{r}} d\boldsymbol{\kappa} \quad (4.22)$$

where  $\mathbf{r}$  is the physical variable and  $\boldsymbol{\kappa}$  is the Fourier variable or wavenumber. The wavenumber has the dimension 1/length. For the interested reader these Fourier transforms are derived in Appendix C.

The distribution of the turbulent kinetic energy on the different length scales and their corresponding wave-numbers is given by the energy spectrum (see Figure 4.3):  $E(\kappa)$  is large at low

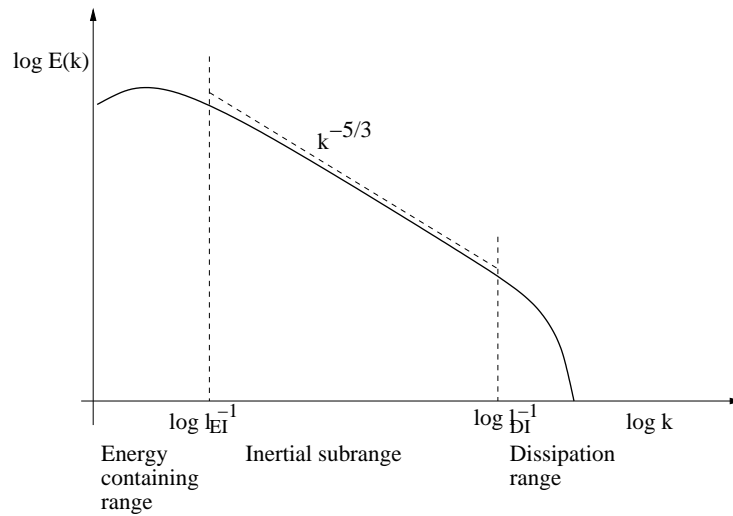


Figure 4.3: The energy spectrum,  $L_{EI}^{-1}$  is the wavenumber at the beginning of the inertial subrange and  $l_{DI}^{-1}$  the wavenumber at the end of the inertial subrange.

wavenumbers (large eddies) and low at high wavenumbers (small eddies). The area under the curve  $E(\kappa)$  over  $\kappa$  represents the turbulent kinetic energy. There is a range of wavenumbers, where the spectrum decreases as  $\kappa^{-5/3}$ . This slope is a characteristic feature of the energy spectrum and takes place in the inertial subrange introduced in the Kolmogorov hypotheses in Section 2.1. At high wavenumbers, in the dissipation range, viscous effects become important and the spectrum decays rapidly [22, 103].

In the inertial subrange the spectrum function is:

$$E(\kappa) = C\varepsilon^{2/3}\kappa^{-5/3} \quad (4.23)$$

where  $C$  is the Kolmogorov constant.

This is the famous  $\kappa^{-5/3}$  law introduced by Kolmogorov [62] and independently derived by von Weizsäcker [149].

### The dissipation rate $\varepsilon$

The turbulent kinetic energy  $k = \frac{1}{2}\overline{u'_i u'_i}$  decays if there is no continuous external energy supply for example through shear at the beginning of the cascade to compensate the dissipation at the end. The rate of dissipation of energy in a fluid at any instant depends only on the viscosity,  $\nu$ , and on the instantaneous distribution of the velocity [131]. The general expression for the rate of dissipation is:

$$\begin{aligned} \varepsilon = \nu & \left( 2\overline{\left(\frac{\partial u'_1}{\partial x_1}\right)^2} + 2\overline{\left(\frac{\partial u'_2}{\partial x_2}\right)^2} + 2\overline{\left(\frac{\partial u'_3}{\partial x_3}\right)^2} \right. \\ & \left. + \overline{\left(\frac{\partial u'_2}{\partial x_1} + \frac{\partial u'_1}{\partial x_2}\right)^2} + \overline{\left(\frac{\partial u'_3}{\partial x_2} + \frac{\partial u'_2}{\partial x_3}\right)^2} + \overline{\left(\frac{\partial u'_1}{\partial x_3} + \frac{\partial u'_3}{\partial x_1}\right)^2} \right) \end{aligned} \quad (4.24)$$

For isotropic turbulence several simplifications are possible and the dissipation rate can be expressed as follows [131]:

$$\varepsilon = 15\nu \overline{\left(\frac{\partial u'_1}{\partial x_1}\right)^2} = 7.5\nu \overline{\left(\frac{\partial u'_1}{\partial x_2}\right)^2} \quad (4.25)$$

for 3-dimensional turbulence.

### Micro-scales of Kolmogorov

In his theses Kolmogorov introduced length and time scales based only on  $\nu$  and  $\varepsilon$  by dimensional analysis.

- Time scale:

$$t_k = \left(\frac{\nu}{\varepsilon}\right)^{\frac{1}{2}} \quad (4.26)$$

- Length scale:

$$l_k = \left(\frac{\nu^3}{\varepsilon}\right)^{\frac{1}{4}} \quad (4.27)$$

### 4.1.4 Scales of 2-dimensional turbulence

#### Enstrophy

As mentioned in Section 2.1 there is no vortex stretching in 2D-turbulence. This means we have to introduce a new quantity, the enstrophy  $D$ , in order to describe the specific vorticity behavior. The enstrophy  $D$  is calculated from the vorticity  $\omega$  defined in Eq. (4.5) in the following manner [73, 74]:

$$D = \frac{1}{2}\overline{\omega^2} \quad (4.28)$$

In two-dimensional turbulence enstrophy is conserved in addition to the turbulent kinetic energy, while in three-dimensional turbulence enstrophy is not conserved. Now two kinds of

inertial transfer similarity ranges, energy transfer and vorticity (or enstrophy) transfer ranges, exist.

Kolmogorov's energy spectrum Eq. (4.23) is valid in two dimensions as well as in three:

$$E(\kappa) = C\varepsilon^{2/3}\kappa^{-5/3} \quad (4.29)$$

The alternate assumption in two dimensions is that the enstrophy spectrum depends on only  $\eta$  and  $\kappa$  and yields [64, 65, 73]:

$$E(\kappa) = C'\eta^{2/3}\kappa^{-3} \quad (4.30)$$

where  $\eta$  is the enstrophy dissipation rate.

The energy and enstrophy cascades in 2D-turbulence are discussed controversially in the literature. According to the classical papers [3, 64, 70] in 2D-turbulence the energy cascade is downward in wavenumber and the vorticity cascade is upward in wavenumber. These transfers are mutually exclusive. The energy spectrum can not transfer enstrophy and the enstrophy spectrum can not transfer energy.

However, according to for example [41, 42] there are double cascades of energy and enstrophy both in upscale and downscale directions.

### Dissipation rate

For 2D velocity fields Eq, (4.24) for the dissipation rate becomes [146]:

$$\varepsilon = 2\nu\left(\overline{\left(\frac{\partial u'_1}{\partial x_1}\right)^2} + \overline{\left(\frac{\partial u'_1}{\partial x_2}\right)^2}\right) = 8\nu\overline{\left(\frac{\partial u'_1}{\partial x_1}\right)^2} \quad (4.31)$$

### Scales

In 2D velocity fields the scale relations differ from 3D velocity-fields in the following manner: Equation (4.15) becomes [146]:

$$\mathbf{L}_g = 0 \quad (4.32)$$

Equation (4.20) becomes [146]:

$$\lambda_f = \lambda_g\sqrt{3} \quad (4.33)$$

In Section 6.1, 2D and 3D velocity fields are compared and differences are shown.

#### 4.1.5 Table of available turbulent quantities and corresponding tools to post-process them

The following table summarizes the quantities of the turbulent flow field that are calculated or visualized in the post-processing toolbox and the corresponding post-processing tools. These tools are later demonstrated in Section 5.2.4.

quantity	tool
2D-velocity field	streamlines2 quiverplot2 streamsliceplot2
3D-velocity field	streamlines3 quiverplot3 coneplot3 streamsliceplot3 streamslicebatch
2D-velocity fluctuations and std's	ekinturb2
3D-velocity fluctuations and std's	ekinturb3
2D-auto correlation functions along lines /columns	corrfuncntline corrfuncntcol
3D-auto correlation functions	corrfunctionall3all corrfuncntall3allcol
2D-Integral-length-scale	corrfuncntline corrfuncntcol spectrum2d
3D-Integral-length-scale	corrfunctionall3all corrfunctionall3allcol spectrum3d
2D-turbulent kinetic energy	ekinturb2, spectrum2d
2D-slope of kinetic energy	slope2
2D-ensrophy	ensrophy
slope of ensrophy	slope2enst
3D-turbulent kinetic energy	ekinturb3, spectrum3d
3D-slope of kinetic energy	slope3

2D-vorticity	vort2dord2 vort2dord4 vort2dord6 vort2dord6pb
3D-vorticity	vort3dord2 vort3dord4 vort3dord6
2D-dissipation rate	dissip2dord2 dissip2dord4 dissip2dord6
3D-dissipation rate	dissip3dord2 dissip3dord4 dissip3dord6
Taylor scales	taylor2 taylor3
Kolmogorov scales	kolmogorov2 kolmogorov3
spatial LES filter	lesfilter3d

Table 4.1: Tools calculating and visualizing quantities of the turbulent flow field

## 4.2 Scales and quantities describing flames

In Section 4.2.1 we introduce common and general quantities used to characterize flames and turbulent combustion. Sections 4.2.2 and 4.2.3 deal with items in order to describe premixed and non-premixed flames, respectively. Finally, in Section 4.2.4 a table summarizes the quantities calculated in the toolbox, while the corresponding MATLAB tools are introduced later in Sections 5.2.2, 5.2.3 and 5.2.5.

### 4.2.1 Common quantities for all flames

#### The flame index

The dimensionless number to distinguish premixed and non-premixed flames or regions of flames is the flame index [141, 153]:

$$fi = \nabla Y_{Fuel} \cdot \nabla Y_{Oxidizer} \quad (4.34)$$

where  $Y_{Fuel}$  and  $Y_{Oxidizer}$  are the mass fractions of Fuel and Oxidizer, respectively. For positive flame indices the flame is of a premixed type and for negative indices the flame is of a non-premixed type. The absolute value increases as the supplying rate of fuel and oxygen by



molecular diffusion increases [153]. The MATLAB tool to determine the flame index is introduced in Section 5.2.3.

### **Flame front**

When analyzing combustion processes the first question is, what is the flame and where is the flame? To define and locate the flame in the flow field and to define the flame front is not an easy task since there is no unified definition in the literature to define it. The most common possibilities to define the flame front are:

- as user-defined isolevel of the mixture fraction (see Eqs. (4.52),(4.54)),
- as user-defined isolevel of the reaction progress variable (see Eqs. (4.42),(4.43)),
- as user-defined isolevel of an arbitrary variable,
- as crestline of a variable.

The MATLAB tools to identify the flame front are introduced in Section 5.2.2.

### **Quantities influenced by turbulence**

Turbulence does not only increase transport processes and reaction rates. Through turbulence the geometrical shape of the flame is influenced and may change significantly. For example flames get stretched, that means strained and curved, an effect which can lead to quenching, partial or even total extinction of a flame.

Therefore, we have to consider the geometrical parameters carefully. The most important geometrical quantities are:

- flame length,
- surface area,
- normals to the flame front,
- flame thickness,
- flame strain,
- flame curvature,
- flame stretch.

### **Flame length and surface area**

We need to calculate the flame surface area and its rate of change when we investigate flame stretch. The MATLAB tools to calculate flame length and surface area are introduced in Section 5.2.2.

### Flame normal

The unit vector normal to the flame front  $\mathbf{n}$  is defined by the gradient of the flame surface  $\Theta_f$ :

$$\mathbf{n} = -\frac{\nabla\Theta_f}{|\nabla\Theta_f|} \quad (4.35)$$

where  $\mathbf{n}$  points by convention into the fresh gases for premixed flames [100] and into the oxidizer side for non-premixed flames. We need normal vectors because for example:

- The curvature along a flame is expressed in terms of normals and their rate of change.
- Normal vectors are used to define the direction of linear cuts in order to explore the flame structure or the flame thickness.

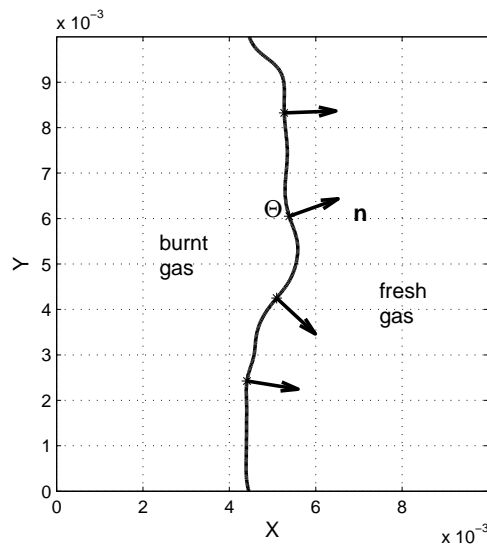


Figure 4.4: Local normals to flame front of a premixed flame pointing by convention toward fresh gases

The MATLAB tools to compute normal vectors are introduced in Section 5.2.2.

### Flame thickness

Defining and estimating a flame thickness is an obvious requirement for many numerical combustion problems because this thickness controls the required mesh resolution [100]. There are several possibilities to define the flame thickness:

- by user-defined boundaries

In the most general case the flame thickness can be defined as real flame extension along user-defined cuts between user-defined boundaries.

- thermal flame thickness

The thermal thickness  $\delta_L^0$  is obtained by using the temperature profile:

$$\delta_L^0 = \frac{T_b - T_u}{\max(|\frac{\partial T}{\partial x}|)} \quad (4.36)$$

where  $T_b$  and  $T_u$  are the burnt and the unburnt gas temperature. Since it measures temperature gradients it is usually considered as the most appropriate thickness [100].

A specific definition to determine the thickness of premixed flames is given in Section 4.2.2. The corresponding MATLAB-tools to determine the different flame thicknesses are introduced in Section 5.2.2.

### Flame stretch

Flame stretch was introduced by Karlovitz et al. as the specific rate at which the flame surface area is locally increased by turbulent motions [60]. Flame stretch is discussed, for example, in [11, 19, 100, 152]. For our definitions we follow the explanations of [19, 100]. The flame stretch  $\kappa$  is defined by the fractional rate of change of a flame surface element  $A$ :

$$\kappa = \frac{1}{A} \frac{dA}{dt} \quad (4.37)$$

### Strain rate

Flames have the tendency to become instable in regions of high velocity gradients. This instability can lead to local or even global extinction. The strain rate can be used as a parameter to describe the departure from stable burning conditions. Therefore, it is important to investigate the strain rate carefully.

The important role of strain effects due to turbulence is shown for example in [23, 114]. Along the flame front, the strain rate can be separated into tangential and normal components.

The tangential component is:

$$a_t = \mathbf{t}\mathbf{t} : \nabla \mathbf{u} = t_i t_j \frac{\partial u_i}{\partial x_j} \quad (4.38)$$

The normal component is:

$$a_n = \mathbf{n}\mathbf{n} : \nabla \mathbf{u} = n_i n_j \frac{\partial u_i}{\partial x_j} \quad (4.39)$$

where  $\mathbf{n}$  and  $\mathbf{t}$  are the unit normal and tangential vectors to the flame front and  $\mathbf{u}$  is the velocity of the flow field. For a 3D flame the tangential part consists of two orthogonal vectors defining a

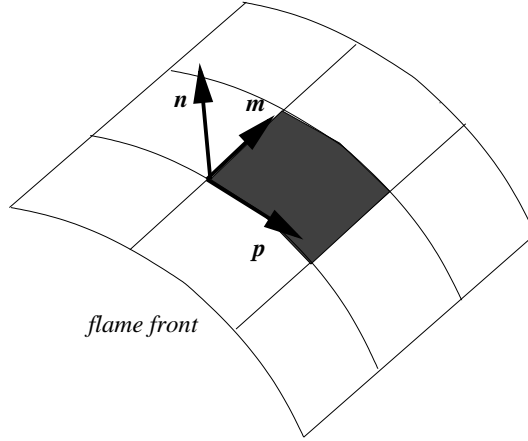


Figure 4.5: Schematic representation of an element of flame surface

tangential plane to the flame. In Figure 4.5  $\mathbf{m}$  and  $\mathbf{p}$  are the two orthonormal vectors belonging to the local tangential plane of the flame. In this thesis we define the tangential strain rate in 3D as sum of the two parts in the tangential plane following [19, 100]:

$$a_t = (\mathbf{m}\mathbf{m} + \mathbf{p}\mathbf{p}) : \nabla \mathbf{u} \quad (4.40)$$

The tools to calculate the strain rate are introduced in Section 5.2.5.

### Curvature

The role of curvature effects, in particular due to turbulence, is demonstrated for example in [23, 55, 114]. As mentioned above curvature is expressed by the normal vector and its rate of change. The term  $\nabla \cdot \mathbf{n}$  is the curvature of the flame front and is linked to the flame surface radii of curvature  $\mathcal{R}_1$  and  $\mathcal{R}_2$  by:

$$\nabla \cdot \mathbf{n} = -\left(\frac{1}{\mathcal{R}_1} + \frac{1}{\mathcal{R}_2}\right) \quad (4.41)$$

where  $\frac{1}{\mathcal{R}_1} = k_1$  and  $\frac{1}{\mathcal{R}_2} = k_2$  measure the highest surface curvature and the surface curvature in the perpendicular direction, respectively.

Often the following definitions are in use (see for example [71]):

- $\frac{1}{\mathcal{R}_1} = k_1$  and  $\frac{1}{\mathcal{R}_2} = k_2$  are called *main* or *principal curvatures*.
- $H = \frac{1}{2}(k_1 + k_2)$  is defined as *mean curvature*
- $K = \frac{1}{\mathcal{R}_1\mathcal{R}_2}$  is defined as *Gaussian curvature*.

- Following [114] the shape factor  $S$  is defined as the smallest principal curvature divided by the largest curvature.

$$S = \begin{cases} \frac{k_1}{k_2} & \text{if } |k_1| \leq |k_2| \\ \frac{k_2}{k_1} & \text{otherwise} \end{cases}$$

where

$$S = \begin{cases} -1 & \text{means the flame has a local saddle point} \\ 0 & \text{means the flame is cylindrically curved} \\ 1 & \text{means the flame is spherically curved} \end{cases}$$

How to calculate the different kinds of curvature is derived in Appendix B. By convention, a curvature is positive when the flame surface is convex toward the fresh gases. The corresponding MATLAB-tools to calculate the different curvatures and the shape factor are introduced in Section 5.2.5.

An important reason for calculating flame curvature in 3D is that three-dimensional DNS computations of reacting flows with a realistic chemistry, produce extremely high numerical costs. Therefore, two-dimensional simulations are still a very valuable alternative for all configurations where three-dimensional effects are small [100]. Knowing the curvature of the flame surface quantitatively we can find out, whether the flame front can be considered as mostly cylindrical (and thus dominated by two-dimensional features) or spherical (and therefore fully three-dimensional).

## 4.2.2 Quantities and scales to describe premixed flames

### The reaction progress variable $c$

In order to describe the propagation of a premixed flame front a variable is introduced that reproduces the progress of combustion, the so-called reaction progress variable  $c$ . The reaction progress variable takes on values between 0 for fresh and 1 for fully burnt gases. The reaction progress variable also may be used to locate the flame front. It can be defined as a reduced temperature or reduced mass fraction of fuel or a final product, for example  $\text{CO}_2$ :

$$c = \frac{T - T_u}{T_b - T_u} \quad (4.42)$$

where  $T$ ,  $T_u$  and  $T_b$  are the local, the unburnt and the burnt gas temperature respectively, or:

$$c = \frac{Y_P - Y_P^u}{Y_P^b - Y_P^u} \quad (4.43)$$

where  $Y_P, Y_P^u$  and  $Y_P^b$  are the local, the unburnt and the burnt mass fractions of a combustion product [145]. For unity Lewis numbers the two definitions are equivalent, and it becomes

possible using some complementary hypotheses to write a balance equation for the reaction progress variable  $c$ :

$$\frac{\partial(\rho c)}{\partial t} + \nabla \cdot (\rho \mathbf{u} c) = \nabla \cdot (\rho D \nabla c) + \dot{\omega} \quad (4.44)$$

The MATLAB tool to calculate the reaction progress variable is introduced in Section 5.2.3.

### Surface density function

A further important quantity is the surface density function, SDF, which is defined as the magnitude of the gradient of the reaction progress variable  $|\nabla c|$ :

$$SDF = |\nabla c| \quad (4.45)$$

The term  $|\nabla c|$  and correlations between SDF and other variables are important in combustion modeling. The MATLAB tool to calculate SDF is introduced in Section 5.2.3. Correlations between  $|\nabla c|$  and other important variables like curvature, strain rate and flame thickness are discussed in Section 6.2.2

### Scalar dissipation rate and burning rate

The burning rate may be quantified as a function of turbulent mixing described by the scalar dissipation rate  $\chi$ :

$$\chi = 2\mathcal{D}|\nabla c|^2 \quad (4.46)$$

The scalar dissipation rate directly measures the decay of fluctuations via turbulent micro mixing. Since the burning rate depends on the contact between the reactants, in many models, the scalar dissipation rate enters directly or indirectly the expression for the mean burning rate. Assuming very fast chemistry and a combustion limited by mixing the mean burning rate is proportional to the scalar dissipation rate. Dissipation rate of scalars is a key concept of turbulent combustion. Directly or indirectly,  $\chi$  appears in many tools used to model flames [145]. For example in the Eddy-Break-Up model (EBU) the burning rate is expressed as [21]:

$$\dot{\omega}_F = C_{EBU} \frac{\chi}{\tau_t} \quad (4.47)$$

### The laminar flame speed

According to [100] the flame speed can be defined in three ways:

- by the absolute flame front speed relative to a fixed reference frame,
- by the displacement speed of the flame front relative to the flow,
- by the speed at which reactants are consumed.

In this thesis we consider the displacement speed: The displacement speed measures the front speed relative to the flow, i.e., the difference between the flow speed  $\mathbf{u}$  and the front speed  $\mathbf{w}$ :

$$s_d = (\mathbf{w} - \mathbf{u}) \cdot \mathbf{n} = s_a - \mathbf{u} \cdot \mathbf{n} \quad (4.48)$$

Since the flow accelerates through the flame front the displacement speed changes too and depends on the position where it is measured. Equation (4.44) can be rewritten in the following manner [145]:

$$\frac{\partial c}{\partial t} + \mathbf{u} \cdot \nabla c = \frac{1}{\rho} \left[ \frac{\nabla(\rho D \nabla c) + \dot{\omega}}{|\nabla c|} \right] |\nabla c| = s_d |\nabla c| \quad (4.49)$$

$|\nabla c|$  is discussed and investigated in Section 6.2.2.

### The total thickness $\delta_L^t$

It is often defined as the length over which the reaction progress variable  $c$  changes from 0.01 to 0.99 between fresh and fully burnt products [100, 145]. The MATLAB tool to calculate the total thickness is introduced in Section 5.2.2.

## 4.2.3 Quantities and scales to describe non-premixed flames

In Section 2.2.1 we introduced the combustion regimes of infinitely fast and finite rate chemistry. In reactions with infinitely fast chemistry where the problem is reduced to a mixing problem a standard assumption is that the instantaneous molecular species concentrations and the temperature are functions only of a conserved scalar concentration at this instant. The statistics of all thermodynamic variables can be obtained from the knowledge of the statistics of that scalar. The need to evaluate mean reaction rates is thus removed. A typical choice for that scalar is the mixture fraction  $Z$ , which is introduced below.

In reactions with finite rate chemistry, where the reaction rate is dependent on the action of the turbulent field on the local flame structures, the conserved scalar approach is still useful, but another parameter has to be introduced to quantify the departure from infinitely fast chemistry and equilibrium condition. The two most often used parameters are the strain rate and the scalar dissipation rate  $\chi$ .

### Element mass fraction

In order to determine mixture fractions we first have to introduce element mass fractions. The element mass fraction is defined locally by the ratio between the mass  $m_{i,e}$  of an element  $i$  and the total mass  $m_{tot}$  in the mixture.

$$Z'_i = \frac{m_{i,e}}{m_{tot}} \quad (4.50)$$

$Z'_i$  can be expressed using species mass fractions as well:

$$Z'_i = \sum_{k=1}^{N_S} \mu_{ik} Y_k \quad i = 1, \dots, M \quad (4.51)$$

where  $N_S$  is the number of species and  $M$  the number of elements in the system. The coefficients  $\mu_{ik}$  are the mass percentage of the  $i$ th element in the  $k$ th species.

Element mass fractions are introduced because elements are not produced or consumed, due to chemical reactions, in contrast to species.

### Mixture fraction

Mixing is one of the most important issues in non-premixed flames. The mixture fraction  $Z$  is the variable that describes the level of mixing between the reactants in a non-premixed flame front. As a chemical reaction is only possible in a region where fuel and oxidizer are mixed adequately (nearly stoichiometric), a non-premixed flame usually lies in the vicinity of the stoichiometric iso-level. The mixture fraction  $Z$  takes on values between 0 for pure oxidizer and 1 for pure fuel. The iso-level of  $Z$  corresponding to stoichiometric conditions is often used to identify the flame front ( $Z = Z_{st}$ ).<sup>1</sup>

The mixture fraction can be calculated from the element mass fractions. Like the element mass fractions it is also a so-called passive or conserved scalar. This means that its value changes because of diffusion and convection but not because of reaction.

### Mixture fraction based on a certain element

For a problem where only the reaction of the two streams fuel (index 1) and oxidizer (index 2) is considered the mixture fraction based on element  $i$  can be calculated in the following manner [6, 7, 150]:

$$Z_i = \frac{Z'_i - Z'_{i,2}}{Z'_{i,1} - Z'_{i,2}} \quad (4.52)$$

where  $Z'_i$  is the element mass fraction of the element  $i$ , and the subscripts 1 and 2 refer to the fuel and oxidant streams. For flames with unity Lewis numbers (for all species) the mixture fractions based on different elements are equal. The balance equation for the mixture fraction at unity Lewis numbers can then be written:

$$\frac{\partial(\rho Z)}{\partial t} + \frac{\partial}{\partial x_i}(\rho u_i Z) = \frac{\partial}{\partial x_i}(\rho D \frac{\partial Z}{\partial x_i}) \quad (4.53)$$

The advantage of balance equations of conserved scalars is that they do not have a source term. For unity Lewis numbers all diffusion coefficients  $D$  are equal.

### Mixture fraction based on all elements

For flames where species have different Lewis numbers different formulations for the mixture fraction can be found in the literature. Eq. (4.52) is still valid, but different elements now have different mixture fractions. It is also possible to define a common mixture fraction based on all elements as linear combination of the different element mass fractions. The most common one

---

<sup>1</sup>In the literature the mixture fraction is sometimes also denoted as  $f$ .



is according to Bilger [7]:

$$Z = \frac{2(Z'_C - Z'_{C,2})/W_C + \frac{1}{2}(Z'_H - Z'_{H,2})/W_H - (Z'_O - Z'_{O,2})/W_O}{2(Z'_{C,1} - Z'_{C,2})/W_C + \frac{1}{2}(Z'_{H,1} - Z'_{H,2})/W_H - (Z'_{O,1} - Z'_{O,2})/W_O} \quad (4.54)$$

where  $Z'_i$  is the element mass fraction of the element  $i$ ,  $W_i$  is the atomic mass of element  $i$ , the subscripts  $C$ ,  $H$  and  $O$  refer to carbon, hydrogen and oxygen, respectively and the subscripts 1 and 2 refer to the fuel and oxidant streams, respectively.

Tools to calculate several kinds of mixture fractions are given in Section 5.2.3.

For non-unity Lewis numbers the mixture fractions based on species and the Bilger mixture fraction may differ significantly. Figures 4.6 to 4.9 show for example the mixture fractions of a  $H_2/CO/O_2$  flame at Reynolds-number of 3000 based on different elements. Figure 4.10 shows the corresponding mixture fraction according to Eq. (4.54). Such discrepancies highlight the need for clear definitions before comparisons can be proposed.

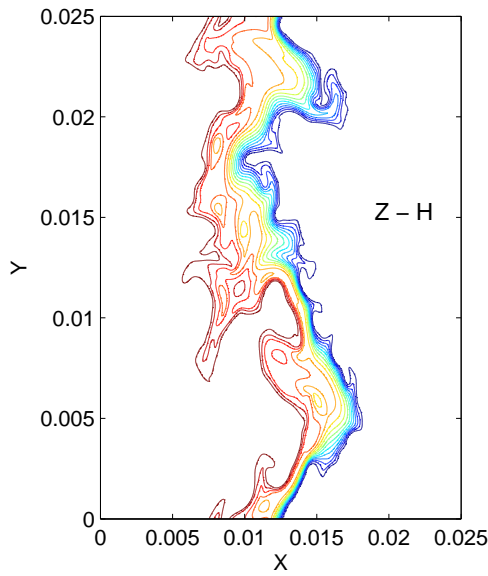


Figure 4.6: Mixture fraction based on element H

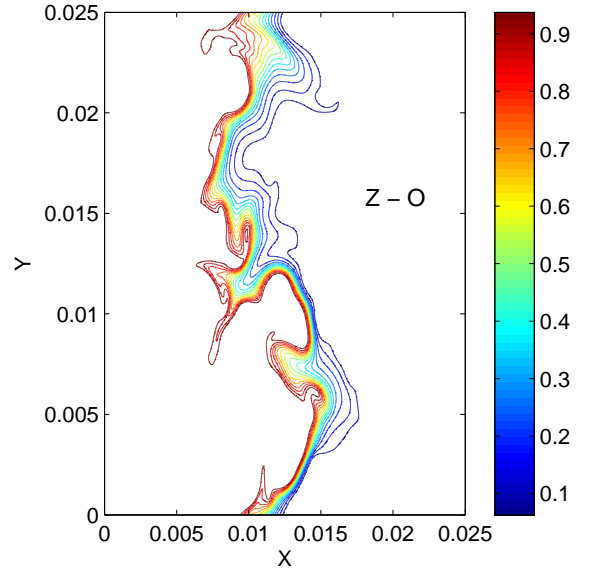


Figure 4.7: Mixture fraction based on element O

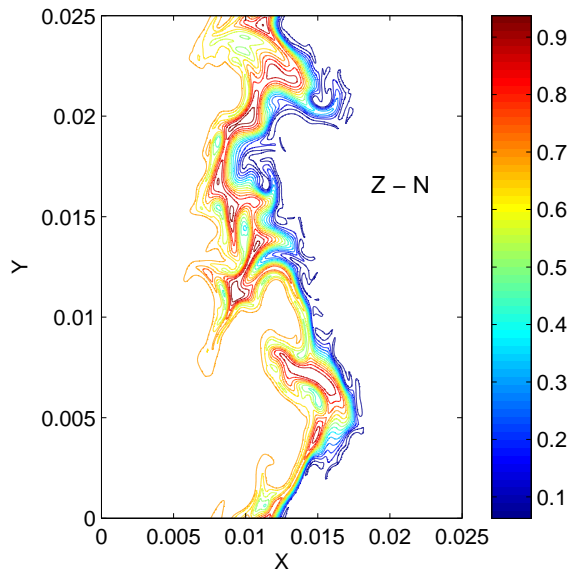


Figure 4.8: Mixture fraction based on element N

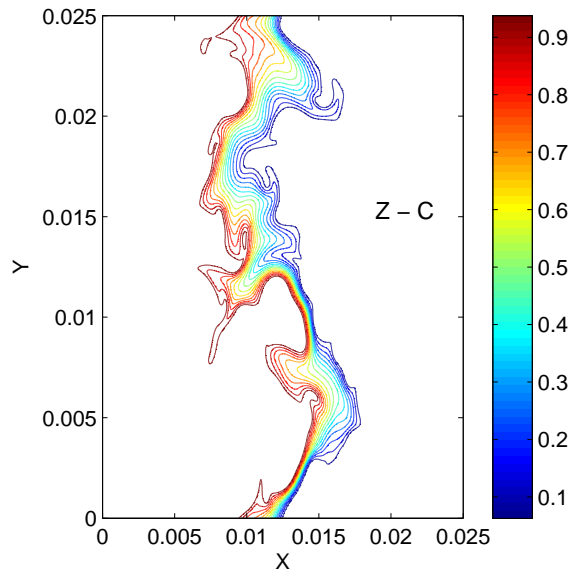


Figure 4.9: Mixture fraction based on element C

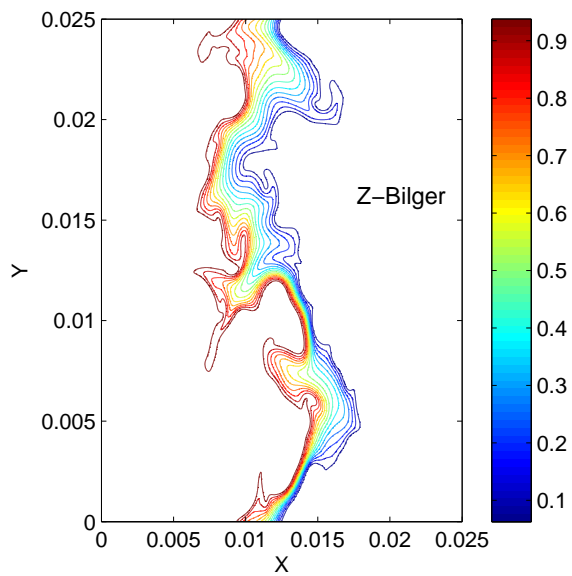


Figure 4.10: Mixture fraction according to Bilger

### Scalar dissipation rate $\chi$

This parameter describes the departure from the infinitely fast chemistry assumption. The scalar dissipation rate characterizes the local mixing rate, because it controls the gradient of  $Z$ . It is the inverse of a diffusive time and a measure for the speed at which the reactants move towards each other on a molecular level, but also the speed at which heat diffuses to and away from the reaction zone, depending on the chosen diffusion coefficient:

$$\chi = 2\mathcal{D}|\nabla Z|^2 \quad (4.55)$$

where  $\mathcal{D}$  is the local diffusion coefficient.

$\chi$  is directly influenced by strain. When the flame strain rate increases,  $\chi$  increases. In cases where each species has its own diffusion velocity and there is no unique diffusion coefficient  $\mathcal{D}$ , a reduced scalar dissipation rate  $\bar{\chi}$  is sometimes introduced:

$$\bar{\chi} = |\nabla Z|^2 \quad (4.56)$$

As a common alternative, the scalar dissipation rate is computed while choosing for  $\mathcal{D}$  the heat diffusion coefficient.

## 4.2.4 Table of available flame quantities and corresponding tools to post-process them

The following table gives an overview of quantities characterizing premixed and non-premixed flames that are calculated or visualized in the post-processing toolbox, the corresponding post-processing tools and sections where the tools are explained.

quantity	tool	section
2D-flame front	flamefront	5.2.2
	crestline	5.2.2
3D-flame front	flamefront3	5.2.2
	flamefrontslice	5.2.2
	crestbatch	5.2.2
	slicebatchorth	5.2.2
flame length	flamelength	5.2.2
	crestlength	5.2.2
flame surface area	surfarea	5.2.2
2D-flamethickness extension	flamethicklin,	5.2.2
	flamethicknonlin	5.2.2
	flamethicklincrest	5.2.2
	flamethicknonlincrest	5.2.2

2D-flamethickness thermal	flamethicklintherm flamethicknonlintherm flamethicklinthermcrest flamethicknonlinthermcrest	5.2.2 5.2.2 5.2.2 5.2.2
2D-flamethickness total	flamethicke	5.2.2
3D-flamethickness extension	flamethicklin3, flamethicknonlin3	5.2.2 5.2.2
3D-flamethickness thermal	flamethicklintherm3 flamethicknonlintherm3	5.2.2 5.2.2
3D-flamethickness total	flamethicke3	5.2.2
2D-normal vectors	normal normtoff normtorest	5.2.2 5.2.2 5.2.2
3D-normal vectors	normal3 normtoff3	5.2.2 5.2.2
2D-flame curvature	kappanew, kappanewlev curvatureall, curvaturelev	5.2.5
shape factor	shapefactor	5.2.5
3D-principal curvature 3D-gaussian curvature 3D-mean curvature	curv3new, curvlev3new	5.2.5 5.2.5
2D-strain rate	strainrateall, strainratelev	5.2.5 5.2.5
3D-strain rate	strainrate3 strnlev3	5.2.5 5.2.5
flame index	flameindex flameindex3	5.2.3
reaction progress variable	reacprog reacprog3	5.2.3
mixture fraction (Bilger) for H <sub>2</sub> flames	mixfrac mixfrac3	5.2.3
mixture fraction based on species for H <sub>2</sub> flames	mixfracspec mixfracspec3	5.2.3
mixture fraction (Bilger) for syngas-flames	mixfracsyng mixfracsyng3	5.2.3
mixture fraction based on	mixfracspecsyng	5.2.3

species for H <sub>2</sub> flames	mixfracspecsyng3	
scalar dissipation rate based on mix. frac. $Z$	scalardissZ scalardiss3Z	5.2.3
scalar dissipation rate based on react. progr. var. $c$	scalardissc scalardiss3c	5.2.3
2D-flame structure	extract	5.2.3
	crestextract	5.2.3
	flamehot	5.2.3
3D-flame structure	extractbatch	5.2.3
	extract3	5.2.3
	flamehot3	5.2.3
2D-cuts	lincut	5.2.3
	lincutcrest	5.2.3
	nonlincut	5.2.3
	nonlincutcrest	5.2.3
3D-cuts	lincut3	5.2.3
	nonlincut3	5.2.3
2D integral values along cuts	intcutlin	5.2.3
	intcutnonlin	5.2.3
	intcutlincrest	5.2.3
	intcutnonlincrest	5.2.3
3D integral values along cuts	intcutlin3	5.2.3
	intcutnonlin3	5.2.3

Table 4.2: Tools for calculating and visualizing quantities of turbulent flames

### 4.3 Scales and quantities describing probabilities

In this section some basic concepts of probability theory will be given. General background information about stochastic processes can be found for example in [29, 94, 116]. Statistical methods especially for turbulent flows can be found in [103]. Section 4.3.1 introduces the basic theory of univariate probability density functions. In combustion modeling joint probabilities and conditional probabilities are important, which are considered in Sections 4.3.2 and 4.3.3, respectively. In Section 4.3.4 a table summarizes the quantities defined in the toolbox, while the corresponding MATLAB tools are introduced in Section 5.2.6.

### 4.3.1 Univariate probability

Probability is a measure of likelihood that a variable will take on values within some range. A way to describe probabilities is to use a probability density function.

#### Probability density function (PDF)

The probability density function (PDF) of a variable  $\phi$  has the following properties.

- A valid probability density function is non-negative:  
 $f(\phi) \geq 0$
- The total area under the curve must equal 1:  
 $\int_{-\infty}^{\infty} f(\phi) d\phi = 1$
- For  $\phi$  tending to infinity or to minus infinity  $f(\phi)$  tends to zero.  
 $\lim_{\phi \rightarrow \infty} f(\phi) = \lim_{\phi \rightarrow -\infty} f(\phi) = 0$

Figure 4.11 shows schematically a PDF of a random variable  $\phi$ .

#### Probability between limits

For a discrete distribution the PDF is the probability that a variable takes a certain value. For continuous distributions the probability that a variable takes a certain value is zero. Therefore, small intervals around that value are considered instead. We thus have to calculate the integral of the variable  $f(\phi)$  over the interval of interest. For example, the probability that the variable  $\Phi$  falls in a particular interval  $[a, b]$ , is given by:

$$P(a \leq \Phi_i \leq b) = \int_a^b f(\phi) d\phi \quad (4.57)$$

The gray area in Figure 4.12 represents the probability that  $\phi$  takes on values between  $a$  and  $b$ .

#### Moments

Probability distributions can be described by moments around the mean value  $\bar{\phi}$  (or  $\mu$ ). Some moments we already know from Section 4.1, where we discussed turbulent flow fields. For a general quantity  $\phi$  moments of order  $n$  are defined by:

$$\mu_n = \int_{-\infty}^{\infty} (\phi - \mu)^n \cdot f(\phi) d\phi \quad (4.58)$$

- Mean value

In the most general case the mean value is defined by:

$$\mu = \int_{-\infty}^{\infty} \phi \cdot f(\phi) d\phi \quad (4.59)$$

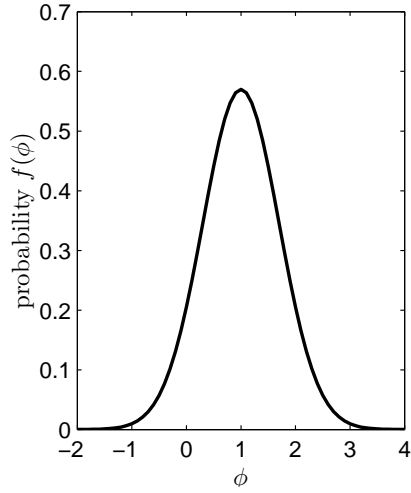


Figure 4.11: Probability density function

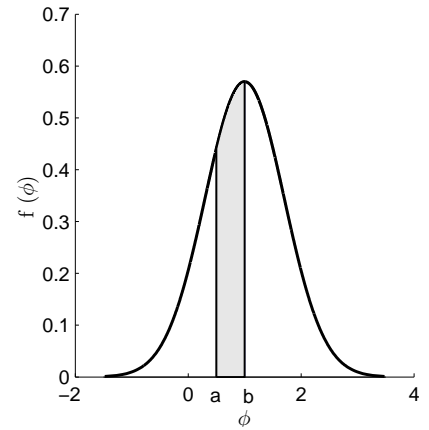


Figure 4.12: Probability  $P$  that  $\phi$  takes values between  $a$  and  $b$

Different methods of taking averages and different kinds of average or mean values are explained in Appendix A.

- Variance

The second-order moment is called variance.

$$Var = \mu_2 = \int_{-\infty}^{\infty} (\phi - \mu)^2 \cdot f(\phi) d\phi \quad (4.60)$$

Variance is a measure of dispersion in the distribution. If a random variable has a large variance, then an observed value of the random variable is more likely to be far away from the mean value  $\mu$ . The square root of the variance is called standard deviation  $\sigma$ .

- Skewness

The third-order moment is called skewness.

$$S = \mu_3 = \int_{-\infty}^{\infty} (\phi - \mu)^3 \cdot f(\phi) d\phi \quad (4.61)$$

Skewness describes the symmetry or asymmetry of the distribution. The following ratio is defined as coefficient of skewness:

$$s = \frac{\mu_3}{\mu_2^{3/2}} \quad (4.62)$$

For symmetric distributions the coefficient of skewness is zero. Distributions that are skewed to the left have a negative coefficient of skewness, and distributions that are skewed to the right have a positive value.

- Kurtosis

The fourth-order moment is called kurtosis.<sup>2</sup>

$$K = \mu_4 = \int_{-\infty}^{\infty} (\phi - \mu)^4 \cdot f(\phi) d\phi \quad (4.63)$$

Kurtosis is a measure of how outlier-prone a distribution is. The following ratio is defined as coefficient of kurtosis:

$$k = \frac{\mu_4}{\mu_2^2} \quad (4.64)$$

A coefficient of kurtosis greater than 3 indicates that the distribution is more outlier-prone than the normal- or Gaussian distribution and a coefficient of kurtosis less than 3 indicates that the distribution is less outlier-prone than the normal (or Gaussian) distribution.

### Gaussian distribution

An important distribution in statistics and engineering is the normal or Gaussian distribution. Its probability density function is given by:

$$f(\phi) = \frac{1}{\sqrt{2\pi}\sigma} \cdot e^{-(\phi-\mu)^2/2\sigma^2} \quad (4.65)$$

The shape and location of a Gaussian distribution is determined by its characteristic numbers mean value  $\mu$  and standard deviation  $\sigma$ : the curve has a symmetric bell shape, is centered at the mean value  $\mu$  and its spread is measured by the standard deviation  $\sigma$ .

The coefficient of skewness is 0:  $s = 0$ .

The coefficient of kurtosis is 3:  $k = 3$ .

The drawback of the Gaussian PDF is that it is quite inflexible in shape because it is symmetrical and has exactly one peak.

Gaussian PDFs play an important role in combustion modeling. When we have to presume the shape of the PDF the Gaussian PDF is a common candidate [77]. For homogeneous isotropic turbulence the velocity field satisfies such a Gaussian distribution [50].

### $\Gamma$ -distribution

To describe distributions that have low probabilities for intervals close to zero, increasing probability when the interval moves in positive direction and decreasing probability when the interval moves to the extreme positive side, the  $\Gamma$ -distribution is a common candidate.

The  $\Gamma$ -probability density function is given by:

$$f(\phi) = \begin{cases} \frac{1}{\Gamma(\alpha)\beta^\alpha} \phi^{\alpha-1} e^{-\phi/\beta} & \phi \geq 0 \\ 0 & \text{elsewhere} \end{cases} \quad (4.66)$$

---

<sup>2</sup>Sometimes in the literature the name flatness is used.



where  $\alpha$  and  $\beta$  are (positive) parameters that determine the specific shape of the curve. In contrast to the normal distribution also asymmetric shapes are possible now.  $\Gamma(\alpha)$  is the  $\Gamma$ -function and is defined by:

$$\Gamma(\alpha) = \int_0^{\infty} \phi^{(\alpha-1)} e^{-\phi} d\phi \quad (4.67)$$

The mean value of the  $\Gamma$ -distribution is:

$$\mu = \int_{-\infty}^{\infty} \phi f(\phi) d\phi = \int_0^{\infty} \phi \frac{1}{\Gamma(\alpha)\beta^\alpha} \phi^{\alpha-1} e^{-\phi/\beta} d\phi = \alpha\beta \quad (4.68)$$

The variance of the  $\Gamma$ -distribution is:

$$Var = \alpha\beta^2 \quad (4.69)$$

### **$\beta$ -distribution**

The most common distribution used for presumed PDF's is the  $\beta$ -distribution. The  $\beta$ -PDF is more flexible than the Gaussian and the  $\Gamma$  distribution and covers a range of different shapes depending on the values of its parameters  $\alpha$  and  $\beta$ . Also bimodal shapes are allowed. The  $\beta$ -distribution is useful to model the behavior of properties that are constrained to fall in an interval from zero to one  $[0, 1]$ . It is defined in the following manner:

$$f(\phi) = \begin{cases} \frac{\Gamma(\alpha + \beta)}{\Gamma(\alpha)\Gamma(\beta)} \phi^{(\alpha-1)} (1 - \phi)^{(\beta-1)} & 0 \leq \phi \leq 1 \\ 0 & \text{elsewhere} \end{cases}$$

where  $\alpha$  and  $\beta$  are positive constants. The constant term is necessary so that

$$\int_0^1 f(\phi) d(\phi) = 1 \quad (4.70)$$

That means (for positive  $\alpha$  and  $\beta$ ):

$$\int_0^1 \phi^{(\alpha-1)} (1 - \phi)^{(\beta-1)} d\phi = \frac{\Gamma(\alpha)\Gamma(\beta)}{\Gamma(\alpha + \beta)} \quad (4.71)$$

The mean value of a  $\beta$ -distribution is given by:

$$\mu = \int_0^1 \phi \frac{\Gamma(\alpha + \beta)}{\Gamma(\alpha)\Gamma(\beta)} \phi^{(\alpha-1)} (1 - \phi)^{(\beta-1)} d\phi = \frac{\alpha}{\alpha + \beta} \quad (4.72)$$

The variance of a  $\beta$ -distribution is given by:

$$\frac{\alpha\beta}{(\alpha + \beta)^2(\alpha + \beta + 1)} \quad (4.73)$$

The parameters  $\alpha$  and  $\beta$  are then determined as

$$\alpha = \bar{\phi} \left[ \frac{\bar{\phi}(1 - \bar{\phi})}{\bar{\phi}^2} - 1 \right] \quad (4.74)$$

and

$$\beta = \alpha \left[ \frac{1}{\bar{\phi}} - 1 \right] \quad (4.75)$$

### 4.3.2 Joint probability theory

In combustion modeling the state of the combustion is often described by two or more variables and modeled by the joint PDF of these variables. Therefore, the knowledge of the joint probability density function of a set of variables is necessary.

#### Joint Probability density function (PDF)

The joint probability density function (JPDF) of two variables  $\phi_1$  and  $\phi_2$  has the following properties.

- A valid joint probability density function is non-negative:  
 $f(\phi_1, \phi_2) \geq 0$
- The total area under the surface must equal 1:  
 $\int_{-\infty}^{\infty} \int_{-\infty}^{\infty} f(\phi_1, \phi_2) d\phi_1 d\phi_2 = 1$
- For  $\phi_1$  or  $\phi_2$  tending to infinity or to minus infinity  $f(\phi_1, \phi_2)$  tends to zero.  
 $\lim_{\phi_1 \rightarrow \infty} f(\phi_1, \phi_2) = \lim_{\phi_1 \rightarrow -\infty} f(\phi_1, \phi_2) = \lim_{\phi_2 \rightarrow \infty} f(\phi_1, \phi_2) =$   
 $\lim_{\phi_2 \rightarrow -\infty} f(\phi_1, \phi_2) = 0$

#### Probability between limits

For example, the probability that the variable  $\Phi_1$  falls in a particular interval  $[ab]$  while the variable  $\Phi_2$  simultaneously falls in a particular interval  $[cd]$  is given by:

$$P(a \leq \Phi_1 \leq b, c \leq \Phi_2 \leq d) = \int_a^b \int_c^d f(\phi_1, \phi_2) d\phi_1 d\phi_2 \quad (4.76)$$

A common way to visualize the joint PDF is to plot the data pairs  $(\phi_1, \phi_2)$  in a contourplot, where important features become evident. Figure 4.13 shows isocontours of a joint PDF of curvature and strain rate in a premixed flame as an illustration.

#### Covariance and correlation

An important quantity in joint distributions is the covariance or correlation.

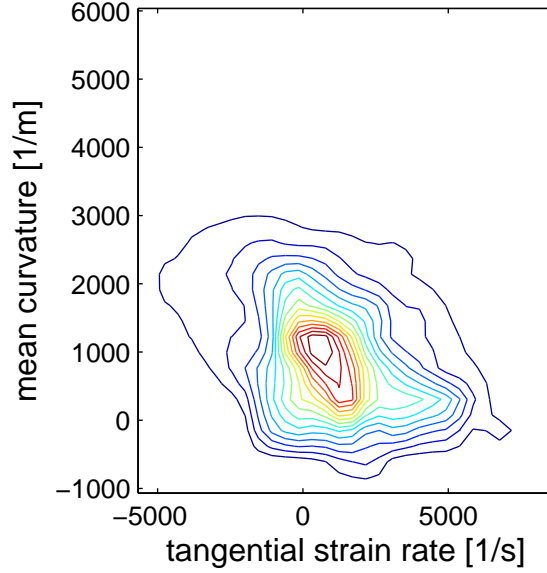


Figure 4.13: Isocontours of joint PDF of curvature and strain rate in a turbulent premixed flame

The mean value of the product of the fluctuations of two variables is called covariance or correlation.

$$\overline{\phi_1' \phi_2'} = \int_{-\infty}^{\infty} (\phi_1 - \overline{\phi_1})(\phi_2 - \overline{\phi_2}) \cdot f(\phi_1, \phi_2) d\phi_1 d\phi_2 \quad (4.77)$$

Correlations between variables in a single fixed point, for example between different velocity components or between velocity components and species mass fractions play a central role in turbulence theory and modeling. Correlations can be measured by the correlation coefficient:

$$\text{corr}(\phi_1, \phi_2) = \frac{\overline{\phi_1' \phi_2'}}{\sqrt{\overline{\phi_1'^2}} \sqrt{\overline{\phi_2'^2}}} \quad (4.78)$$

Two variables are completely correlated if the absolute value of the correlation coefficient  $|\text{corr}(\phi_1, \phi_2)| = 1$  and are completely uncorrelated if  $\text{corr}(\phi_1, \phi_2) = 0$ .

Joint-pdf's and correlations between two variables are investigated in Section 6.2.2.

### 4.3.3 Conditional probability

In combustion modeling the statistical analysis of a variable conditioned on another variable is often of particular importance.

$$P(\phi_1 | \phi_2) = \frac{P(\phi_1 \cap \phi_2)}{P(\phi_2)} \quad (4.79)$$

$P(\phi_1 | \phi_2)d\phi_1$  is the probability that the first variable  $\phi_1$  lies in the range  $d\phi_1$  around  $\phi_1$  under the condition that the second variable takes the value  $\phi_2$ . In combustion modeling variables are typically conditioned on the mixture fraction for non-premixed flames or on the reaction progress variable for premixed flames.

#### 4.3.4 Table of available statistical quantities and corresponding tools to post-process them

The following table summarizes the statistic quantities which are calculated or visualized in the post-processing toolbox and the corresponding post-processing tools. These tools are later described in Section 5.2.6

quantity	tool
moments 1-4, true pdf, Gaussian pdf of 2D-variable	varstat
moments 1-4, true pdf, Gaussian pdf of 3D-variable	varstat3
2D-conditioned moments on mixture fraction or reaction progress variable	condmeanfilt2
2D-conditioned moments on arbitrary variable	condmeanfilt22
3D-conditioned moments on mixture fraction or reaction progress variable	condmeanfilt3
3D-conditioned moments on arbitrary variable	condmeanfilt33
2D-correlation coefficient of two variables along a cut, scatterplot	correlationcut
2D-correlation coefficient of two variables along flamefront, scatterplot	correlationex
2D-correlation coefficient of two 1-d variables scatterplot	correlationgen

3D-correlation coefficient of two variables along a cut, scatterplot	correlationcut3
3D-correlation coefficient of two variables along flamefront, scatterplot	correlationex3
3D-correlation coefficient of two 1-d variables scatterplot	correlationgen3
true pdf, gaussian pdf, $\beta$ -pdf of normalized 2D-variable	compdf2of
true pdf, gaussian pdf, $\beta$ -pdf of normalized 3D-variable	compdf3of
joint probability of 2 2D-variables	statbivar2
joint probability of 3 2D-variables	statbivar3
joint probability of 2 3D-variables	statbivar3d

Table 4.3: Tools for calculating statistic quantities

# Chapter 5

## Post-processing tools for DNS data

As demonstrated in Sections 3.1.4 and 3.1.5 the results of DNS contain a huge amount of information in space and time for many variables, which we have to handle and post-process in order to gain as much useful information as possible. In this chapter we introduce our toolbox that has been developed for that purpose based on the commercial program MATLAB. In Section 5.1 the program MATLAB with its possibilities is introduced. In Section 5.2 the general procedure of post-processing is demonstrated and the most important tools are introduced. Further applications will be presented in Chapter 6.

### 5.1 The program MATLAB

MATLAB was developed by the company The MathWorks, Inc. The name MATLAB stands for matrix laboratory.

In university and research centers as well as in industry MATLAB is a wide-spread computational tool for engineering and science. The two main reasons to use MATLAB in this work are its comprehensive mathematical library and its extensive graphic tools.

MATLAB is an interactive system whose basic data element is a matrix or an array that does not require dimensioning. This allows to solve many technical computing problems, especially those with matrix and vector formulations, in a fraction of the time it would take to write a program in a scalar non interactive language such as C or Fortran.

MATLAB is a high performance language integrating computation, visualization and programming where problems and solutions are expressed in familiar mathematical notation. Typical uses include [87]:

- Applied mathematics and computation,
- Algorithm development,
- Modeling, simulation, and prototyping,

- Data analysis, exploration, and visualization,
- Scientific and engineering graphics.

Sometimes, the massive data generated by DNS or by experiments cannot be expressed directly in terms of mathematical functions. In these cases the most suitable way to analyze the data is through graphical visualization by appropriate plots. MATLAB provides many graphics functions that allow to create such plots of the data, like contour plots to visualize scalars, vector graphs for example to investigate gradients or to display velocity fields or plots for data statistics, for example histograms or scatterplots.

MATLAB also offers several volume visualization techniques to present 3D data like isosurfaces, vector plots and methods to draw 2D slices.

## 5.2 The MATLAB Toolbox

Parts of this section have already been published in [36, 155]. A detailed documentation of the toolbox is available under [154].

The toolbox developed during this project is mainly intended for post-processing data produced on a square or cubic regular grid. Values obtained on an irregular grid must be interpolated on a regular grid before continuing.

### 5.2.1 Overview on different groups of tools

The post-processing toolbox developed in this project consists of two subgroups:

- The first group contains the tools for post-processing 2D-results,
- The second group contains the tools for post-processing 3D-results.

Each group can be divided into six different sub-categories of complementary tools. We begin first by listing all these tools before illustrating the obtained results in the next section.

1. The first category contains all the tools for a direct geometrical analysis of the raw data:
  - for example tools to define and locate the flame front,
  - tools to compute all purely geometrical parameters, e.g. the flame length, flame surface area or the flame thickness,
  - tools to find crestlines or crestsurfaces,
  - tools to calculate normal vectors.
2. The second category contains all the tools to investigate the flame structure:

- for example tools to calculate the flame index,
  - tools to calculate mixture fractions for non-premixed flames,
  - tools to calculate reaction progress variables for premixed flames,
  - tools to calculate surface density function for premixed flames,
  - tools to extract the variables of interest along the flame front,
  - tools to draw linear and non linear cuts through the flame front,
  - tools to extract variables along these cuts,
  - tools to compute integral values of extracted variables along these cuts.
3. The third group contains all the tools needed to investigate and quantify the properties of turbulent flow fields:
- tools to visualize 2D-and 3D-velocity fields,
  - tools to calculate velocity fluctuations,
  - tools to calculate the turbulent kinetic energy,
  - tools to calculate the dissipation rate,
  - tools to calculate the energy spectrum,
  - tools to calculate and plot vorticity fields,
  - tools to calculate turbulent scales,
  - tools to calculate velocity correlation functions,
  - tools allowing spatial data filtering.
4. The fourth group contains tools to investigate the interaction between turbulence and flames:
- for example tools to calculate the components of the strain-rate,
  - tools to calculate curvatures of flames in 2D and 3D cases,
  - a 3D tool to calculate the shapefactor.
5. The fifth group contains tools allowing statistical investigations of the variables of interest:
- for example tools to compute the moments of order one to four of a distribution,
  - tools to represent graphically such distributions using, e.g., histograms and PDFs,
  - tools for statistical analysis of a variable conditioned on another one,
  - tools to calculate the joint PDF of two variables,



- tools to calculate correlation coefficients between two variables.
6. The sixth and last group contains tools to determine appropriate dimensions of reduced manifolds in composition space:
- tools to find nearest neighbors,
  - tools to reconstruct data in lower dimensions,
  - tools to compute correlation coefficients between original and reconstructed data,
  - tools to quantify deviations between original and reconstructed data.

In what follows, the usage of all post-processing routines is illustrated in more details.

### 5.2.2 Tools for geometrical investigations

The first group is employed for the geometrical investigation of the raw data in the light of combustion modeling. In a 2D field isocontours, i.e. lines where the variables have a certain value, must be identified. In a 3D field the corresponding equivalent to an isocontour is an isosurface.

- The main task is to find and locate the contour defining the flame front. Typical variables used to identify the flame front are for example the mixture fraction  $Z$ , the reaction progress variable  $c$ , the temperature, the mass fraction  $Y$  of a radical or the heat release. Optionally the user can define upper and lower limits for the extension of the flame by certain isolevels of the corresponding variable.

To find the flame front in a 2D-field the toolbox-tool `flamefront` is used. `Flamefront` uses the MATLAB-tools `contour` and `contourc` to calculate and display the user-defined isocontours.

In order to discover where interesting regions exist in a set of volume data sliceplanes can be employed for probing the 3D-field. The toolbox offers single slices as well as a batch modus to scan the whole domain. This is true for all coordinate directions.

In order to locate the flame front the toolbox tool `flamefrontslice` allows to take slices in several directions through the flame front at a user-defined location. The tool `slicebatchorth` allows to scan the domain along a user-defined axis by a batch of orthogonal slices.

In order to define the flame front by an isosurface of a variable we use the tool `flamefront3`. `Flamefront3` uses the MATLAB-tool `isosurface` to calculate and display the user-defined isosurface.

As an example for a 2D-flame we consider a non-premixed  $H_2/N_2/O_2$ -flame. We define the flame front by the stoichiometric isolevel  $Z=0.5$  of the mixture fraction  $Z$ . The flame front is bounded from above by the isolevel  $Z=0.9$  on the fuel side and bounded from below by the isolevel  $Z=0.1$  on the oxidizer side. In Figure 5.1 the flame front with

boundaries is shown.

As an example for a 3D-flame we consider a premixed  $\text{CH}_4$  flame. We choose the isolevel of the mass fraction  $Y(\text{CO}_2)=0.03$  as flame front. Figure 5.2 shows such a slice through the  $\text{CO}_2$  field in Y direction. In Figure 5.3 the flame front is shown. It is also possible to visualize user-defined boundaries, but they are not shown here in order to obtain a better visualization of the flame front surface.

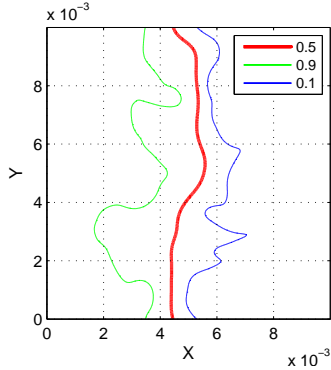


Figure 5.1: Flame front based on mixture fraction, together with flame limits, X and Y are spatial coordinates in m

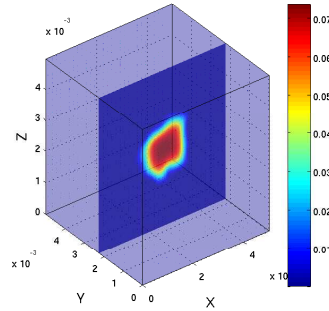


Figure 5.2: Slice through  $\text{CO}_2$  field for  $Y=\text{constant}$ , X, Y and Z are spatial coordinates in m

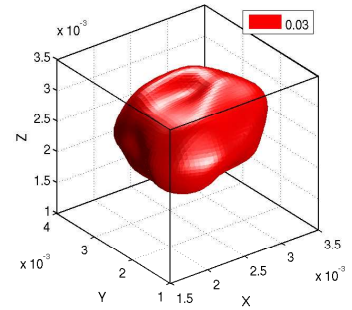


Figure 5.3: Flame front surface based on mass fraction  $Y(\text{CO}_2)=0.03$ ; X, Y and Z are spatial coordinates in m

- Additionally to isocontours the toolbox allows to define the flame front by the crestline of a variable like temperature, heat release or the mass fraction  $Y$  of a radical. Crestline is defined as the line connecting peak values of a variable, higher than a user-defined threshold.

In order to find the crestline the program starts in the absolute maximum of the variable, scans a square field of predefined size around the maximum, searches for the next highest value, jumps to the new maximum and scans a new field around that new maximum in all directions except backwards. The procedure is repeated until either the boundary of the domain is reached or the newest maximum value falls below a prescribed threshold. When the first branch is complete, the program returns to the main maximum, blocks the known branch(es) and searches for further branches. The complex underlying procedure is described in detail in [155].

The crestline can be computed using the toolbox-tool `crestline`. Figure 5.4 shows the crestline of temperature embedded in the temperature field of the flame.

The equivalent to the crestline in a 3D-field is the crestsurface of a variable. The crestsurface can be computed as a batch of slices using the toolbox-tool `crestbatchy`. Figure 5.5

shows points of the crest surface of heat release in a slice for  $Y=\text{constant}$  through the field of heat release.

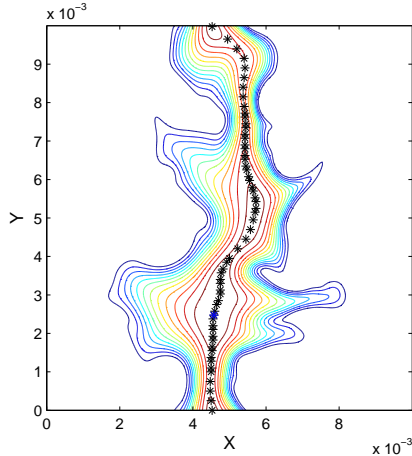


Figure 5.4: Flame front defined as crestline of temperature (black stars) embedded in temperature field of the flame, X and Y are spatial coordinates in m

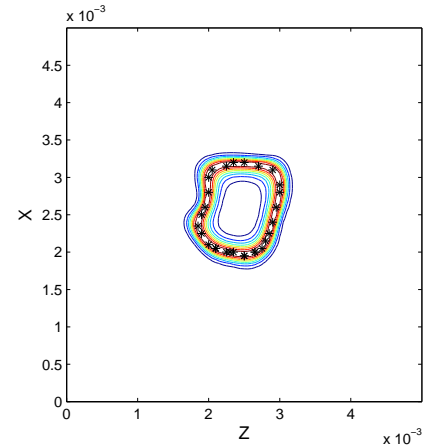


Figure 5.5: Crestpoints of heat release (black stars) in a slice in Y-direction through the flame

- The next necessary steps are to calculate flame length (for 2D-flames), or flame surface area (for 3D-flames). The flame length can be computed as the maximum of the isolevel defining the flame front using the toolbox-tool `flamelength`. The analogon to the flame length is for our 3D-flame the flame surface area. The flame surface area can be calculated using the toolbox tool `surfarea`. The flame surface is considered as a triangulated patch and the surface area is the sum of the areas of the triangles according to Eq. (B.10).
- The toolbox offers different tools to define the flame thickness in the different manners explained in Section 4.2:
  - as real extension of the flame between user-defined boundaries along linear or non-linear cuts (see later Figures 5.10 and 5.11). The appropriate toolbox-tools are `flamethicklin` and `flamethicknonlin` for 2D-flames and `flamethicklin3` and `flamethicknonlin3` for 3D-flames.
  - as thermal flame thickness based on the maximum temperature gradient. The appropriate toolbox-tools are `flamethicklintherm` and `flamethicknonlintherm` for 2D-flames and `flamethicklintherm3` and `flamethicknonlintherm3` for 3D-flames.

- as the total flame width via the reaction progress variable  $c$ . The appropriate toolbox-tools are `flamethickc` for 2D-flames and `flamethickc3` for 3D-flames.

The toolbox offers a batch modus to calculate the flame thickness at several points all over the length or the surface of the flame.

- Last but not least normal vectors to the flame front can be calculated in order to define linear cuts (see Section 5.2.3) or to prepare the calculation of curvature or strain rate (see Section 5.2.5). The unit vector normal to isolevels or isosurfaces can be determined using the toolbox-tool `normtoff` for 2D-flames or `normtoff3` for 3D-flames. By convention  $\mathbf{n}$  is pointing towards the fresh gases for premixed flames and towards the oxidizer side for non premixed flames. Figure 5.6 shows normal vectors starting in several points along the isolevel  $Z = 0.5$  of our 2D-flame. Of course their direction is to the oxidizer side. Figure 5.7 shows normal vectors starting in selected points along the flame front of our 3D flame.

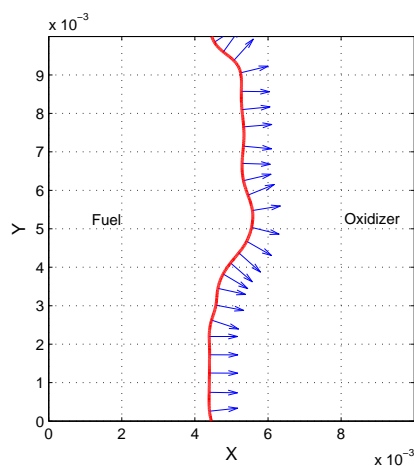


Figure 5.6: Normal vectors along 2D-flame front

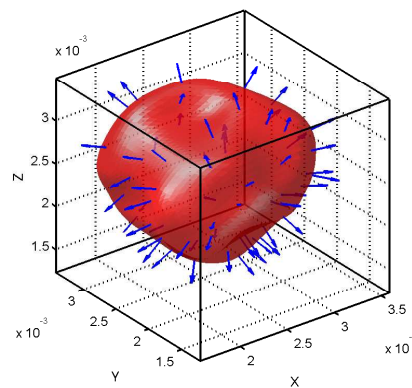


Figure 5.7: Normal vectors along 3D-flame front

The 2D flame in Figure 5.1 and the 3D flame of of Figure 5.3 will be used in the rest of this chapter to demonstrate the different tools of the toolbox.

The tools to calculate and plot geometrical features and quantities with their input and output arguments are listed in Table D.1.

### 5.2.3 Tools to investigate the flame structure

The second group is dedicated to investigations of the flame structure.

- For this purpose all the variables computed during any step of the post-processing can be extracted along the flame front either defined as a certain isovalue or as crestline or along any prescribed iso-level or iso-surface of an existing variable.

For that purpose the tools `extract` for 2D-flames and `extract3` and `extractbatch` for 3D-flames are employed. Variables of interest are for example:

- temperature profiles,
- heat release,
- mixture fraction,
- reaction progress variable,
- flame index,
- strain rate,
- flame front curvature,
- flame thickness,
- scalar dissipation rate  $\chi$ .

For a 2D-flame `extract` returns the coordinates of a user-defined isovalue, a curvilinear coordinate along this isovalue and the profile belonging to the variable extracted along the isovalue. The curvilinear coordinate and the extracted values run from the top to the bottom of the figure, that means from higher to minor values of the Y-coordinate. The tool also calculates and plots a histogram and the PDF of the extracted variable. For a 3D-flame `extract3` returns the vertices and faces of the isosurface, and the values of the variable extracted over the isosurface in the corresponding vertices, a plot of the variable extracted over the surface, a histogram and a PDF of the values of the variable. To demonstrate `extract3` we extract the normal strain rate along the flame front defined by an isosurface of the reaction progress variable. Figure 5.8 shows the normal strain rate extracted along the flame front. The distribution of this normal strain-rate is shown as an histogram in Figure 5.9, allowing a better quantification of the huge strain-rate variations. The tool `extractbatch` extracts values of a variable along an isovalue of the variable defining the flame front, in several 2D slices in a user-defined direction.

- The tools `flamehot` and `flamehot3` allow to consider a user-defined region of a flame. They determine values of a variable (for example the temperature) between boundaries defined by an other variable (for example isovalues of the mixture fraction).
- In addition to an investigation in the direction along the flame front the toolbox allows an investigation in the direction across the flame front. Linear and non linear cuts through the flame front can be calculated and visualized using the tools `lincut` and `nonlincut` for 2D-flames or `lincut3` and `nonlincut3` for 3D-flames. The direction of such a linear

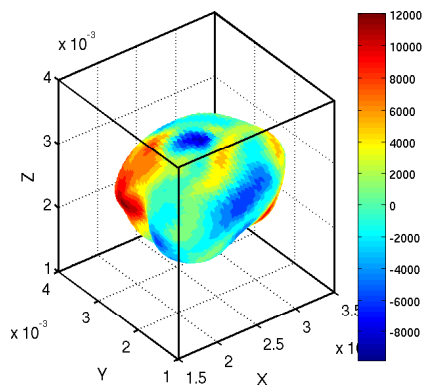


Figure 5.8: Normal strain rate (1/s) extracted along flame front

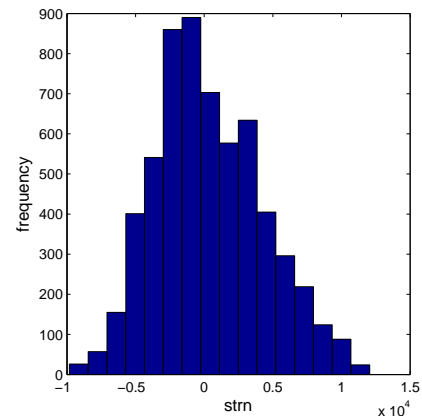


Figure 5.9: Histogram corresponding to strain rate visualized in Figure 5.8

cut is constant and normal to the iso-level or iso-surface defining the flame front.

Non-linear cuts follow the direction of the steepest gradient of a user-chosen variable.

Depending on the size and the position of the flame in the domain often only a part of the domain is of interest for values along the linear and non-linear cuts. Both linear and non linear cuts can then be limited by the boundaries of the flame front.

Figure 5.10 shows a linear cut through the flame front between the boundaries  $Z=0.1$  and  $Z=0.9$ . Of course, if required, also cuts running through the whole domain along the black dashed line are possible.

Figure 5.11 shows a nonlinear cut through the flame front, again with the limits  $Z=0.9$  and  $Z=0.1$ . Any variable of interest can be extracted and integrated along these cuts using the tools `intcutlin` and `intcutnonlin` for 2D-flames or `intcutlin3` or `intcutnonlin3` for 3D-flames.

Again, the toolbox offers a batch modus to determine the integral values along linear and nonlinear cuts all over the flame length or flame surface.

- To distinguish between premixed and non-premixed flames or parts of flames the toolbox contains a tool `flameindex` to determine the flame index. For positive values of the flame index the flame is of premixed type, for negative values the flame is of non-premixed type.
- Tools to calculate the mixture fraction can be used to describe non-premixed flames or to define the flame front. `Mixfrac` and `mixfrac3` calculate the mixture fractions according to the formula of Bilger, Eq (4.54) and plot isolevels or isosurfaces of the mixture fraction for hydrogen flames. `Mixfracspec` and `mixfracspec3` calculate the mixture fraction based on different species (N, O, H) according to Eq. (4.52) for hydrogen flames.

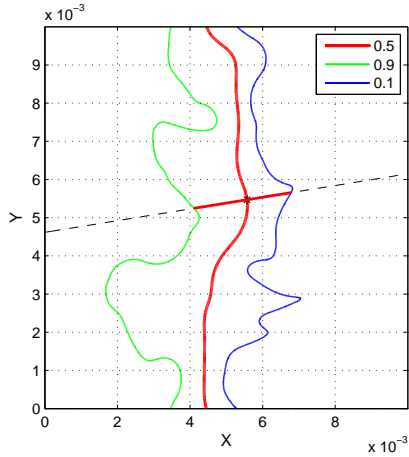


Figure 5.10: Linear cut between flame limits (fuel side, green line,  $Z=0.9$ ; oxidizer side, blue line,  $Z=0.1$ ),  $X$  and  $Y$  are spatial coordinates in m

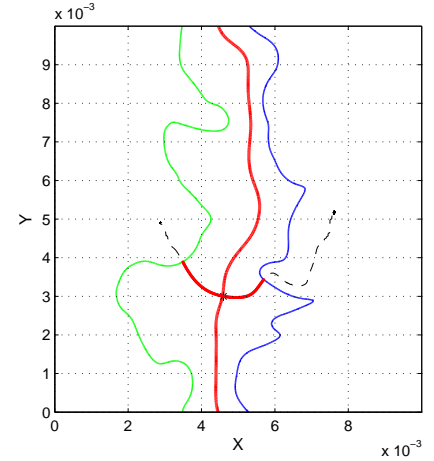


Figure 5.11: Non linear cut between flame limits (fuel side, green line,  $Z=0.9$ ; oxidizer side, blue line,  $Z=0.1$ ),  $X$  and  $Y$  are spatial coordinates in m

`Mixfracsyng` and `mixfracsyng3` calculate the mixture fractions according to the formula of Bilger for synthetic gas-flames. `Mixfracspecsyng` and `mixfracspecsyng3` calculate the mixture fraction based on different species (N, O, H, C) for synthetic gas-flames. As shown in Section 4.2.3 the different mixture fractions can differ significantly.

- For premixed flames the tools `reacprog` and `reacprog3` calculate the reaction progress variable based on temperature according to Eq. (4.42). The tools `reacprogco2` and `reacprog3co2` calculate the reaction progress variable based on the mass fraction of  $\text{CO}_2$  according to Eq. (4.43). Additionally they plot and calculate the surface density function SDF and the mean value of SDF conditioned on the reaction progress variable.

The tools to investigate the flame structure with input and output arguments are listed in Table D.2.

## 5.2.4 Tools to investigate velocity field and turbulence

As our flames are embedded in turbulent flow fields it is essential to analyze the main features of the turbulent flow. These investigations are the task of the third group.

- To start with such investigations the toolbox offers 2D as well as 3D tools to visualize the turbulent flow field and its vortical structures. Figure 5.12 shows the flame front of our 2D-flame embedded in the velocity field. We can clearly recognize large vortical

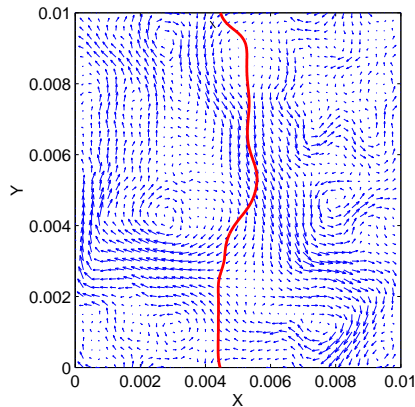


Figure 5.12: Flame front embedded in velocity field, red line flame front, blue arrows velocity field

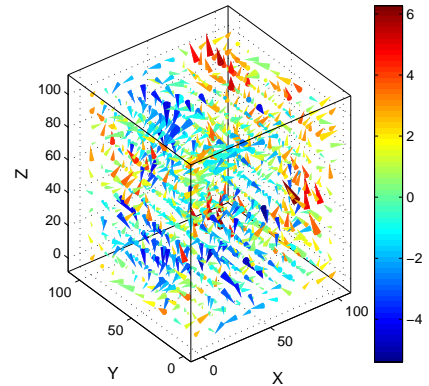


Figure 5.13: Coneplot of velocity field

structures, typical of 2D turbulence.

In order to visualize the velocity field we use the toolbox tool `quiverplot2`. Figure 5.13 visualizes the velocity field of the 3D-flame with a coneplot using the tool `coneplot3`.

- The tool `vorticity2d` calculates the vorticity values in the 2D velocity field and plots isolevels of the vorticity. The tool `vorticity3d` calculates the vorticity values in the 3D velocity field. Vorticity is calculated according to Eq. (4.5). The vorticity can be calculated in different levels of accuracy, namely with second, fourth and sixth order central schemes for the velocity gradients for 2D as well as for 3D fields.
- The toolbox offers tools to calculate the turbulent kinetic energy in physical space as well as in Fourier space. The tools `ekinturb2` and `ekinturb3` calculate velocity fluctuations and the turbulent kinetic energy in physical space. An important item belonging to the turbulent kinetic energy are spectra. The tools `spectrum2d` and `spectrum3d` calculate the turbulent kinetic energy and the energy spectrum in Fourier space, considering circles or spherical shells around the origin of wavenumber space, according to Eqs.(C.15) and (C.16) for 2D-fields and according to Eqs.(C.5) to (C.7) in the 3D case. These tools additionally compute the integral length scales according to Eqs. (C.8) and (C.17).
- The tools `slope2` and `slope3` compare the slope of the 2D- and 3D-energy cascade with the theoretical values according to Eqs. (4.23) and (4.30).
- A further important item belonging to the turbulent kinetic energy is its dissipation rate. Like vorticity the dissipation rate can be calculated in three different levels of accuracy. The tools to calculate the dissipation rate are `dissip2d` and `dissip3d`.



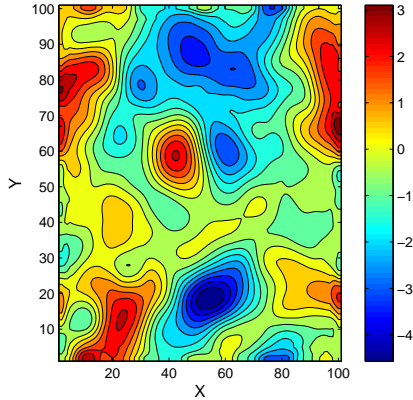


Figure 5.14: Slice in  $z$ -direction through  $x$ -velocity field, filtered by a spatial filter with a filter size of nine points in each direction

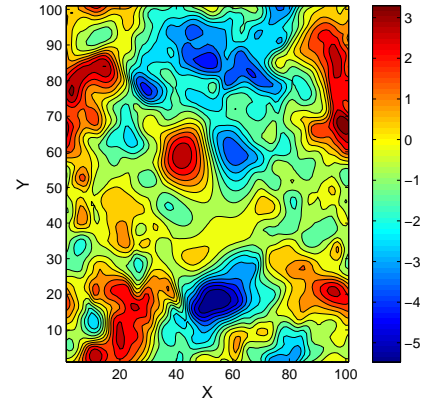


Figure 5.15: Slice in  $z$ -direction through unfiltered  $x$ -velocity field

- Taylor scales can be calculated using the tools `taylor2` and `taylor3`.
- The velocity correlation functions can be calculated along lines and along columns for longitudinal as well as for lateral correlations using the tools `corfunctline` and `corfunctcol` for a 2D-field. For 3D-fields `corfunctional3all` and `corfunctional3allcol` can be used. These tools also determine the integral length scales, as the length value where the correlation coefficient is zero.
- Data filtering tools are useful to investigate subgrid scale issues for LES modeling. The tool `lesfilter3d` allows spatial filtering of 3D DNS data with user-defined filter size. Figures 5.14 and 5.15 illustrate the filtered and unfiltered  $x$ -velocity field. We use here a spatial filter with a filter size of nine points by nine points by nine points.

The tools to visualize velocity fields and to calculate turbulent quantities are listed in Table D.3. Because turbulence is one of the most important items in turbulent flames the turbulence tools are demonstrated and discussed further in Section 6.1, where we investigate and compare 2D- and 3D turbulent velocity fields.

## 5.2.5 Tools to investigate the interaction between turbulence and flames

Flames and the turbulent flow fields interact with each other. Therefore, the fourth group of post-processing tools allows the computation of important flow variables in order to describe

and quantify this effect. In Section 4.2.1 strain rate and curvature were introduced as the most important quantities of this interaction. They can be calculated in the whole domain as well as along a certain isolevel, for example the flame front.

- In order to calculate the normal and tangential components of strain rate in a 2D field we use the toolbox-tool `strainrateall`. The tool `strainratelev` calculates and displays the normal and the tangential component of the strainrate along the curvilinear coordinate of the user-defined flame front. The tool `strainrate3` calculates the normal and tangential components of the strain rate in a 3D field. In a 3D field the tangential component consists of two parts. Here the tangential component is the sum of the two parts. We use the tool `strnlev3` in order to calculate and display the components of the strain rate over the isosurface of the flame front. The normal strain rate over the flame surface has already been shown in Figure 5.8.
- In order to calculate the curvature in a 2D field we use the toolbox-tool `kappanew`. The formula to calculate the 2D-curvature is derived in Appendix B. The tool `kappanewlev` calculates and displays the curvature along the curvilinear coordinate of the user-defined flame front.
- For 3D flames the curvature tool `curv3new` calculates all parts of the curvature, the principal curvatures, the mean- and the Gaussian curvature, respectively. The formulae to calculate the different kinds of curvature are derived in Appendix B. As already mentioned two-dimensional simulations are still a very valuable alternative, for all configurations where three-dimensional effects are small [100]. The toolbox also offers a tool to calculate the shape factor `shapefactor` in order to decide whether the flame can be considered as a cylindrical or a spherical structure.

In Section 6.2.1 the influence of turbulence on a non-premixed flame is discussed for different Reynolds numbers. In Section 6.2.2 we investigate the interaction between turbulence and a premixed flame.

The tools to calculate strain rate components and curvature are listed in Table D.4.

## 5.2.6 Tools for statistical investigations

As mentioned earlier DNS data need a statistical evaluation after computation, which is the topic of the fifth group of post-processing tools.

- In order to investigate the distribution of a variable the toolbox-tool `varstat2` and `varstat3` were developed. Applying this tool we are able to calculate moments of order one to four according to Eq. (4.58), to display the distribution in a histogram and a PDF and to compare the distribution with a Gaussian distribution. Figure 5.16 shows the distribution of the velocity component in  $x$ -direction of the 2D-flame.

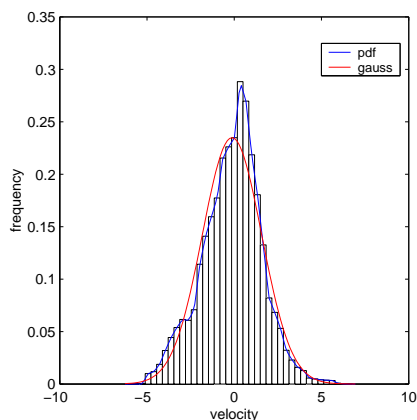


Figure 5.16: Distribution of velocity, histogram, PDF and corresponding Gaussian distribution with the same moments

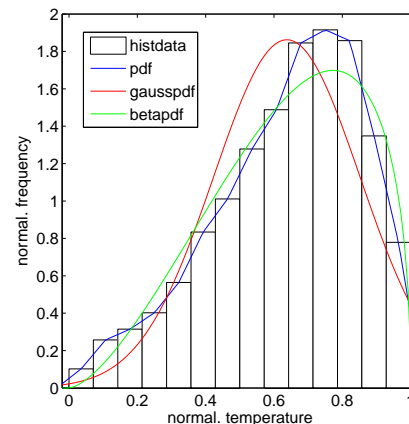


Figure 5.17: True distribution, related Gaussian distribution and  $\beta$ -distribution of normalized temperature between mixture fraction 0.5 and 0.6

- The tools `compdf2` and `compdf3` calculate and plot the true PDF, the Gaussian PDF and the  $\beta$ -PDF of a variable. As the  $\beta$ -pdf is only defined in the interval  $[0, 1]$  the input variables are normalized. Figure 5.17 shows the histogram, the true PDF, the Gaussian and the  $\beta$  distribution with the same moments for the normalized temperature of our 2D-flame. The temperature is considered in the hot burning region of the flame between mixture fractions 0.5 and 0.6.
- From a modeling point of view, the statistical analysis of a variable conditioned on another quantity, for example on the mixture fraction  $Z$  or the reaction progress variable  $c$  is necessary, since this is a central quantity for most turbulent combustion models. The toolbox-tool `condmeanfilt2` is employed to calculate the mean value, the maximum, the minimum and the standard deviation of a 2D-variable conditioned on another one. The corresponding 3D-tool is `condmeanfilt3`. Figure 5.18 shows the temperature conditioned on the mixture fraction  $Z$  of our 2D-flame.
- Often, the relationship between two variables is even more interesting than the statistics of single variables. The tool `correlationgen` displays these relationships in scatter plots and calculates the corresponding correlation coefficient.
- A further tool, `statbivar`, allows to calculate correlation coefficients and joint PDFs and to display them in contour plots. In order to demonstrate these tools we consider flame thickness and strain rate of our 2D-flame. Figure 5.19 shows a contour plot of the joint PDF of the two variables.

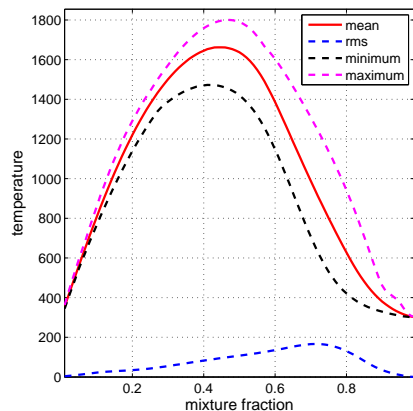


Figure 5.18: Mean value, maximum, minimum and standard deviation of the temperature conditioned on mixture fraction  $Z$  of the 2D flame

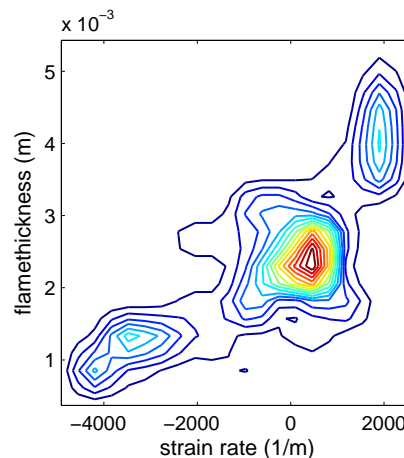


Figure 5.19: Joint PDF of flame thickness and normal strain rate displayed in a contour plot for the 2D flame

The statistic tools with their input and output arguments are listed in Table D.5.

### 5.2.7 Tools to determine appropriate dimensions of manifolds

The procedure to find the appropriate dimension for a low-dimensional manifold, allowing a reduced description of chemical processes was explained in Section 2.6.3.

- The first step was to investigate the state space and to find clouds of nearest neighbors in state space. We defined clouds in three different ways. Therefore, there are three different kinds of tools to construct our clouds.
  - Tools to investigate species mass fractions only and define clouds by a certain number of  $N$  nearest neighbors.
  - Tools to consider species mass fractions and temperature and define clouds by a certain number of  $N$  neighbors.
  - Tools to consider species mass fractions and define clouds by a prescribed radius in state space.

As we know from Section 2.6.3, weighting plays a significant role for our results.

- Therefore, there are tools considering original species mass fractions
- and tools considering weighted species mass fractions (and temperature).

The following tools are available:

- In order to find clouds for original species mass fractions the tool `cloudorgvarnb` is used. The distances in state space are calculated by Eq. (2.50). For weighted species mass fractions the tool `cloudorgvarnbweigh` is used. Weighted mass fractions  $Y_{k,w}$  are determined from the original mass fractions  $Y_k$  in the following manner:  $Y_{k,w} = \frac{Y_k - \min(Y_k)}{\max(Y_k) - \min(Y_k)}$ .

The output is a three-dimensional  $N_S$  - by -  $N$  - by -  $Cl$  matrix, where  $N_S$  is the number of species,  $N$  is the number of neighbors and  $Cl$  is the number of clouds.

- In order to consider species and temperature the tools `cloudorgvarnbtemp` and `cloudorgvarnbweightemp` are used. Because of the great difference in magnitude between temperature and species mass fractions often the weighted version is more suitable. The output is now a three-dimensional  $N_S+1$  - by -  $N$  - by -  $Cl$  matrix.

In all tools points which are nearly identical in state space are considered as one point. To summarize similar points to one point the tools call the MATLAB internal tool `iuniq`. The tools consider about 3000 cloud centers. The number of neighbors is a user-defined option. An appropriate number of neighbors is typically between twelve and 25.

- In order to find clouds defined by a prescribed radius the tools `cloudorgvarradweight` is used. As for a meaningful analysis, the number of points in the cloud must be somewhat larger than the dimension of the full state space, the tool considers only hyperspheres containing at least 12 points. Outputs are correlation coefficients, mean correlation coefficients for one to five dimensional reconstructions and the number of points in the clouds.
- In the next step we have to check whether the clouds can be approximated by a linear subspace. We use Singular Value Decompositions (SVD) of the  $Cl \ N_S \times N$  matrices and then we calculate lower dimensional approximations for those matrices according to Eq. (2.55) as described in Section 2.6.3. The appropriate tool is `svdmatrrecl`. It calculates singular values for the matrices of the original cloud and one- to five-dimensional approximations for the matrices in the cloud.
- The final step is to determine the quality of our approximations. This can be done in two ways. We can consider deviations between original and reconstructed clouds (matrices) or we can consider correlation coefficients.

- The tool to calculate the deviations is called `devorgrecl`. The deviations are normalized by the deviation for dimension zero. (Thus the deviations are independent of the cloud size). The normalized deviations are calculated according to Eq. (2.56).
- The tool to calculate the correlation coefficients and mean correlation coefficients is called `corelmatrorgmatrrecl`. The correlation coefficients are calculated according to Eq.(2.57).

The tools to investigate manifolds with their input and output arguments are listed in Table D.6.

### 5.2.8 Tools in batch mode and parallelized tools

The tools mentioned in Sections 5.2.2 and 5.2.3 calculate flame thicknesses or integral values at one certain point on the flame front. Often, we are interested in these values all over the flame front or surface. Therefore, the toolbox also offers a batch mode for these tools considering several or all points of the flame. The tools available in batch mode are listed in Table D.7. The batch computations are typically very time-consuming, especially along non linear cuts and for 3D flames. Therefore, for those tools a parallelized version was developed.

When thinking about parallel computing, we can loosely divide most algorithms used into two types: data parallel (or fine-grained parallel) and task parallel (or coarse-grained parallel) computation. Data parallelism refers to performing computations involving short, identical operations on large datasets in parallel lockstep, then communicating the results to other processors before the next operation. Task parallelism refers to performing longer, non-communicating computations in parallel, and then gathering the results at the end for analysis. The coarse grained computation is distributed uniformly over the number of parallel processors. The computations of the individual iterations are performed in complete isolation of the other iterations. Therefore, task parallelism requires that the computation being performed is independent over the iterations [53, 54]. Unrolling the for-loops in our tools working in batch mode is a typical case of task parallelism.

At the beginning the program Star-P was used for parallelizing the developed post-processing toolbox. Star-P was originally developed at the Massachusetts Institute of Technology. Interactive Supercomputing (ISC) was launched to commercialize Star-P. Star-P runs inside of MATLAB working environment. Star-P software runs on both the client and the server. To use Star-P with MATLAB, the user needs only one MATLAB license, which is installed on the client or front end. No copies of MATLAB are required on the parallel computer since Star-P uses dedicated numerical libraries to perform server-based calculations. This is the great advantage of Star-P when running parallelized tools on a cluster [53]. In 2009 ISC, and with ISC Star-P was bought by Microsoft and was not developed further. All parallel calculations were done at the Leibnitz Rechenzentrum (LRZ) in Munich. Since Star-P is not supported any more by the LRZ all parallelized tools had to be written in MATLAB. The drawback when using directly

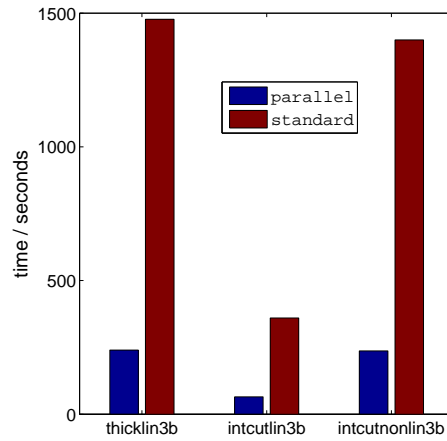


Figure 5.20: Computing time for three parallel and standard tools performing the same operation. Eight processors are used in the parallel case.

MATLAB for parallelizing is that one can only use as many workers as licensing allows. The time profit of parallelized tools compared to the standard tools is around a factor of six when using eight MATLAB-workers. Figure 5.20 shows the computing time differences for three selected parallel and standard tools. It is observed that a very good speed-up is obtained. Therefore, the end-users are encouraged to use the parallel version of the tools whenever enough MATLAB-licenses are available.

# Chapter 6

## Selected examples of applications

### 6.1 Analysis of a cold flow field

In Sections 2.1 and 4.1 we discussed the different behavior and the different scales for 2D- and 3D turbulence (especially the enstrophy and the energy cascade). In this section we demonstrate how the turbulence tools we introduced in Section 5.2.4 can be used to compare and analyze the velocity fields of a 2D and a 3D turbulent case.

- We begin with the visualization of the streamlines of both velocity fields using the tools `streamsliceplot2` and `streamlines3`. Figures 6.1 and 6.2 show the streamlines of both turbulent velocity fields.

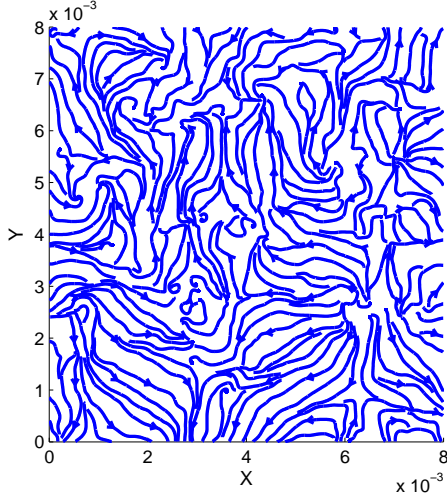


Figure 6.1: Streamlines of the 2D turbulent velocity field

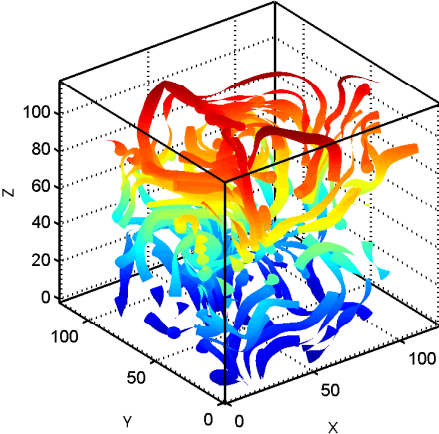


Figure 6.2: Streamlines of the 3D turbulent velocity field



- Next, we determine the following quantities for both velocity fields: (see also Table 6.1)
  - vorticity,
  - autocorrelation functions,
  - fluctuations and rms values of fluctuations,
  - turbulent kinetic energy,
  - energy spectrum,
  - integral length scale,
  - turbulent dissipation rate,
  - micro-scale of Taylor,
  - micro-scale of Kolmogorov.

- Vorticity

Figure 6.3 shows the 2D-vorticity field. The vorticity was calculated here with a fourth-order scheme using the tool `vort2dord4`. The fourth-order scheme is a good compromise

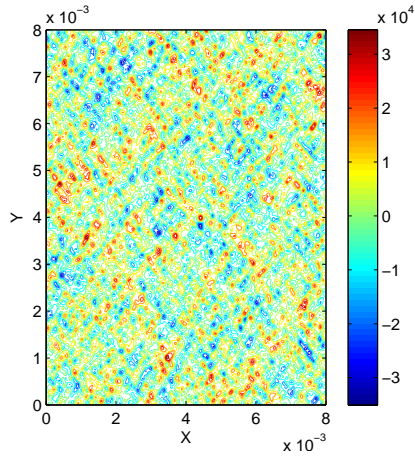


Figure 6.3: 2D vorticity field calculated with a 4th-order scheme

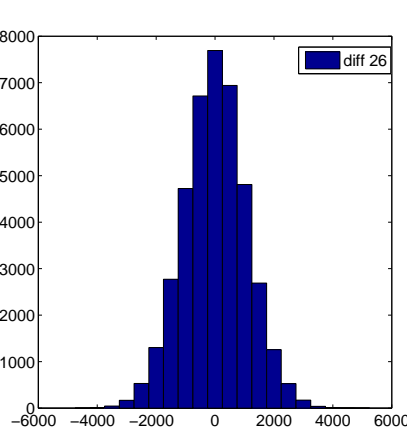


Figure 6.4: Differences in vorticity between 2nd-order and 6th-order scheme calculations

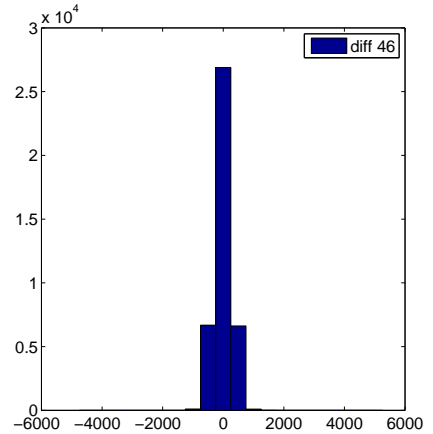


Figure 6.5: Differences in vorticity between 4th-order and 6th-order scheme calculations

because it is far more accurate than the second-order scheme and the calculation is faster than for the sixth-order scheme. Figure 6.4 shows the differences in vorticity when it is calculated with a second-order and a sixth-order scheme. Figure 6.5 shows the differences in vorticity when it is calculated with a fourth-order and a sixth-order scheme. In the second case the differences are significantly smaller than in the first one. In the first case the maximum difference is  $5.2 \cdot 10^3 \text{ s}^{-1}$  or 12.5 % of the maximum value of the vorticity

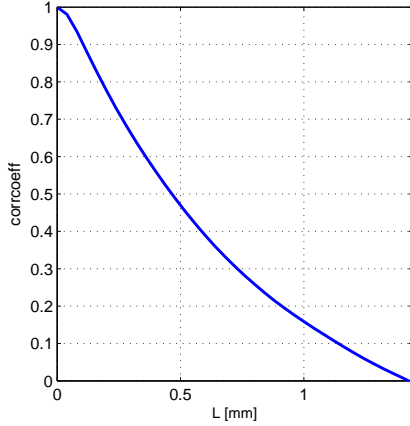


Figure 6.6: Curve of auto-correlation functions of the 2D velocity field calculated along all lines of the domain

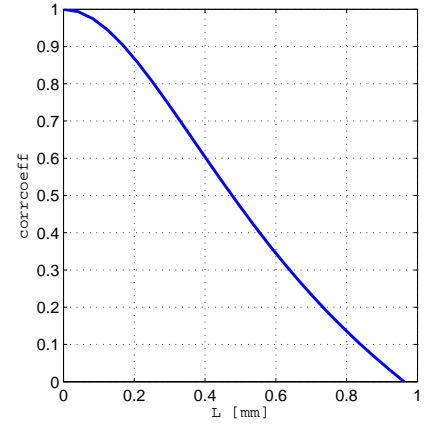


Figure 6.7: Curve of auto-correlation functions of the 3D velocity field calculated along all lines of the domain

calculated with a sixth-order scheme. In the second case the maximum difference is  $1.3 \cdot 10^3 \text{s}^{-1}$  or 3.1 % of the maximum value of the vorticity calculated with a sixth-order scheme.

From the vorticity we then calculate the enstrophy according to Eq. (4.28) using the tool `enstrophy`.

- Autocorrelation functions

For both velocity fields we compute the autocorrelation functions between two points along the lines in  $x$ -direction according to Eq. (4.12), using the tools `corrfuncnline` and `corrfuncnall3all`. From the auto-correlation functions we determine the integral length scale. Figure 6.6 shows the auto-correlation curve of the 2D field calculated along all lines of the velocity field using the tool `corrfuncnline`. Figure 6.7 shows the auto-correlation curves of the 3D velocity field. As expected the correlation coefficient is 1 when the distance between the two points is zero. The curve is monotonously decreasing until the correlation coefficient is zero when the distance is equal or greater than the integral length scale. The integral length scale is the length where the correlation coefficient is zero, leading to the values listed in Table 6.1.

- Spectra

Using the tools `spectrum2d` and `spectrum3d` we first calculate velocity fluctuations in the physical space, shift them into Fourier space and calculate the energy spectra according to Eqs.(C.5), (C.6), (C.7). Figure 6.8 shows the energy spectrum over wavenumbers for the 2D velocity field. Figure 6.9 shows the energy spectrum over wavenumbers for the 3D

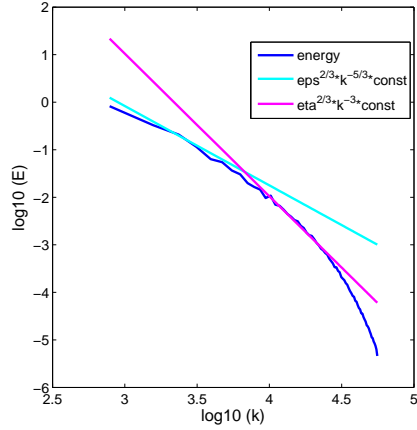


Figure 6.8: Energy spectrum of the 2D velocity field over wavenumber, slopes of energy and enstrophy cascade

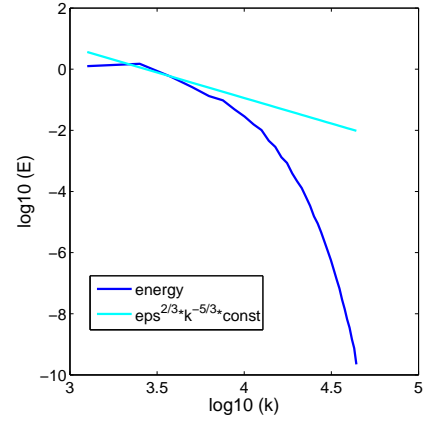


Figure 6.9: Energy spectrum of the 3D velocity field over wavenumber, slope of energy cascade

velocity field. For both curves we plot the famous  $\kappa^{-5/3}$ -Kolmogorov slope of Eq. (4.23). For the 2D fields we also represent the  $\kappa^{-3}$  slope of the enstrophy cascade according to Eq. (4.30). The 2D-slopes were determined using the tool `slope2enst`. The 3D-slope was determined using the tool `slope3`.

The `spectrum`-tools additionally calculate the integral length scales. The length scales obtained by the `spectrum`-tools are in good agreement with the length scales obtained by the `autocorrelation`-tools. (See Table 6.1).

- Turbulent dissipation rate  
Next we calculate the turbulent dissipation rates for the 2D velocity field according to Eq. (4.31) using the tool `dissip2dord4` and for the 3D field according to Eq. (4.24) using the tool `dissip3dord4`.
- Micro-scale of Taylor  
In addition to the integral scale we calculate the micro-scale of Taylor. Here, we calculate the longitudinal scales for both cases according to Eq. (4.18).
- Microscale of Kolmogorov  
We calculate the microscale of Kolmogorov according to Eq. (4.27). For the dissipation rate we used a fourth-order scheme.

quantity	in 2D-turbulence	in 3D-turbulence
rms values of fluctuations	$1.88 \frac{\text{m}}{\text{s}}$	$2.27 \frac{\text{m}}{\text{s}}$
normalized turbulent kinetic energy	$1.78 \frac{\text{m}^2}{\text{s}^2}$	$3.8 \frac{\text{m}^2}{\text{s}^2}$
normalized enstrophy	$5.0 \cdot 10^7 \frac{1}{\text{s}}$	————
turbulent dissipation rate	$3141 \frac{\text{m}^2}{\text{s}^3}$	$3900 \frac{\text{m}^2}{\text{s}^3}$
integral length scale from energy spectrum	1.6 mm	1.1 mm
integral length scale from auto-correlations	1.5 mm	0.97 mm
micro-scale of Taylor(long)	397 $\mu\text{m}$	554 $\mu\text{m}$
micro-scale of Kolmogorov	33 $\mu\text{m}$	31.6 $\mu\text{m}$

Table 6.1: Quantitative results for the analysis of 2D and 3D turbulence data

Table 6.1 quantifies the large differences found concerning the turbulence properties in the 2D and the 3D configurations.

After having demonstrated the interest of the toolbox for cold turbulence, it is time looking now at turbulent flames.

## 6.2 Analysis of flame properties

As already mentioned the toolbox allows post-processing of 2D-flames as well as of 3D-flames, for different fuels (hydrogen, hydrocarbons), for premixed as well as non-premixed flames. In order to demonstrate the flexibility of the toolbox we investigate in what follows both, a 2D non-premixed hydrogen/nitrogen/air-flame and 3D premixed flames.

### 6.2.1 Flame/turbulence interaction for a 2D non-premixed flame

#### Configuration

We investigate first a  $\text{H}_2/\text{O}_2$ -flame in a 2D velocity field. In order to obtain realistic burning conditions, the fuel ( $\text{H}_2$ ) is diluted in nitrogen. The Navier-Stokes equations are solved using centered explicit schemes of order six except at the boundaries, where the order is progressively reduced to four. Temporal integration is realized with a Runge-Kutta algorithm of order four. Boundary conditions are treated with the help of the Navier-Stokes Characteristic Boundary Condition (NSCBC) technique [5, 99]. Non-reflecting boundaries are employed in the  $x$ -direction while periodicity is assumed in the  $y$ -direction (Figures 6.10 to 6.12). The initial conditions correspond to a global mixture ratio  $\phi = 0.8$ . The stoichiometric mixture fraction given by theory is then  $Z_s = 1/(1 + \phi) = 0.55$ .

We investigate three increasing values of the Reynolds-number ( $\text{Re}_1=245$ ,  $\text{Re}_2=426$ ,  $\text{Re}_3=1800$ ).

In this manner, the influence of turbulence on flame properties can be quantified. We are mainly interested in the influence of turbulence on:

- tangential strain rate,
- flame front curvature,
- flame thickness.

As we know from Section 4.2 it is important to investigate strain and curvature carefully because these effects can lead to partial or even total extinction of a flame. We define our flame front as the stoichiometric isolevel of the mixture fraction  $Z$  at  $Z = 0.55$ . The boundaries of the flame front in order to determine the flame thickness are defined by  $Z = 0.8$  and  $Z = 0.2$ . Figures 6.10, 6.11 and 6.12 show the corresponding flame fronts at the different Reynolds num-

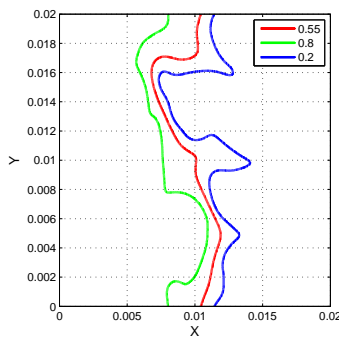


Figure 6.10: Flame front defined by stoichiometric isolevel of mixture fraction  $Z = 0.55$  at  $Re=245$

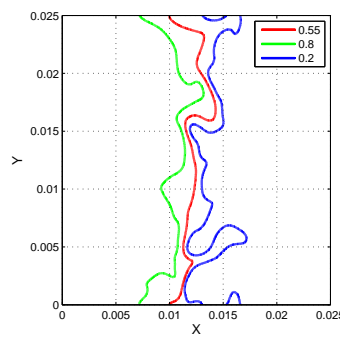


Figure 6.11: Flame front defined by stoichiometric isolevel of mixture fraction  $Z = 0.55$  at  $Re=426$

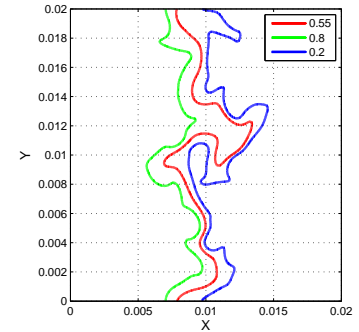


Figure 6.12: Flame front defined by stoichiometric isolevel of mixture fraction  $Z = 0.55$  at  $Re=1800$

bers. The increasing deformation of the flame with  $Re$  is clearly observed.

## Results

- Figures 6.13, 6.14 and 6.15 show the tangential strain rates extracted along the different flame fronts at the different Reynolds numbers. In order to calculate the strain rate we use the tool `strainratelev`. We clearly recognize that amplitudes and frequencies of the alterations are increasing with increasing Reynolds numbers.
- Figures 6.16, 6.17 and 6.18 show the curvatures extracted along the different flame fronts at the different Reynolds numbers. In order to calculate the curvatures we use the tool

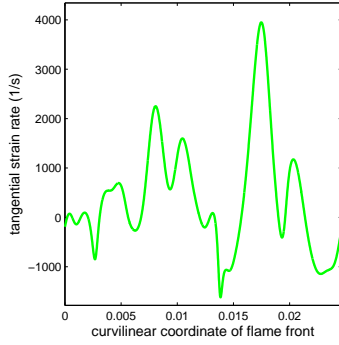


Figure 6.13: Tangential strain rate at  $Re=245$

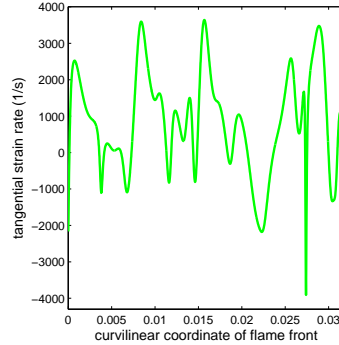


Figure 6.14: Tangential strain rate at  $Re=426$

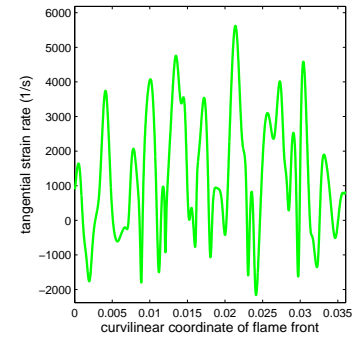


Figure 6.15: Tangential strain rate at  $Re=1800$

kappanewlev. Again, we clearly recognize that amplitudes and frequencies of the alterations are increasing with increasing Reynolds numbers, as expected.

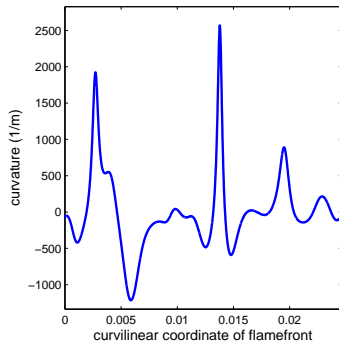


Figure 6.16: Curvature of flame front at  $Re=245$

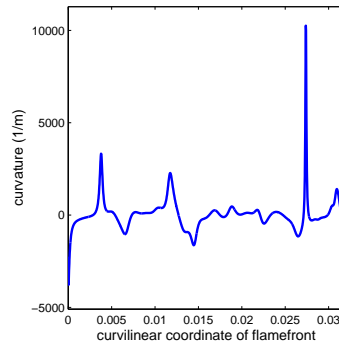


Figure 6.17: Curvature of flame front at  $Re=426$

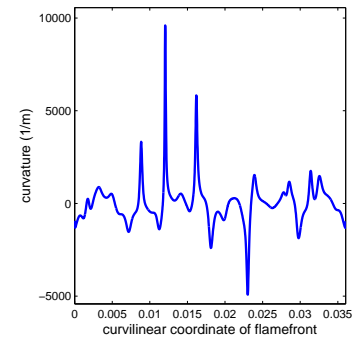


Figure 6.18: Curvature of flame front at  $Re=1800$

- Figures 6.19, 6.20 and 6.21 show the flame thicknesses along the flame fronts at the different Reynolds numbers. The flame thickness is defined as the extension of the flame between the boundaries  $Z = 0.2$  and  $Z = 0.8$  along a linear cut. In order to calculate the flame thickness in all points along the flame front we use the tool `flamethicklinb`. Concerning the influence of turbulence on the flame thickness there are contradictory observations in the literature, that are discussed for example in [25]. In our case maximum thickness is increasing with increasing Reynolds number. On the other hand the minimum thickness is decreasing with increasing Reynolds numbers as well. This means that, for higher turbulence, both thicker flames and thinner flames are observed simultaneously,

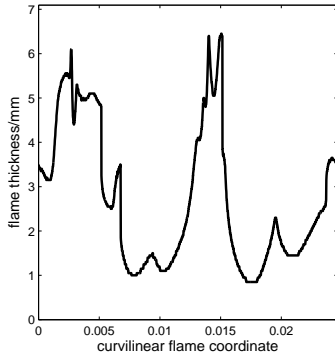


Figure 6.19: Thickness of flame front between  $Z = 0.2$  and  $Z = 0.8$  at  $Re=245$

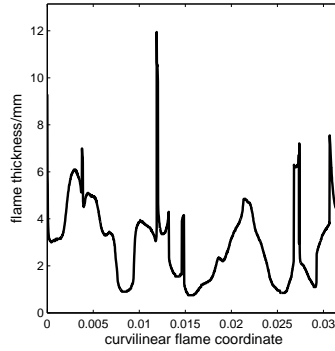


Figure 6.20: Thickness of flame front between  $Z = 0.2$  and  $Z = 0.8$  at  $Re=426$

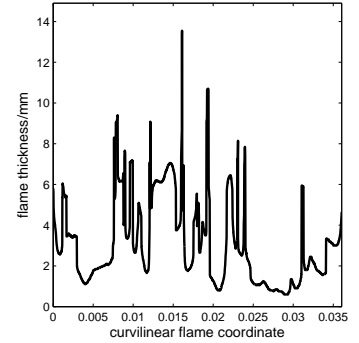


Figure 6.21: Thickness of flame front between  $Z = 0.2$  and  $Z = 0.8$  at  $Re=1800$

explaining controversial discussions in the scientific literature. Again the frequencies in alteration are increasing with increasing Reynolds numbers.

quantity	Re	min	mean	max	std
strain rate [1/s]	245	-1619	423	3949	1165
strain rate [1/s]	426	-3909	839	3641	1404
strain rate [1/s]	1800	-2161	1326	5622	1759
curvature [1/m]	245	-1215	-0.9	2570	543
curvature [1/m]	426	-4631	7.2	10260	965
curvature [1/m]	1800	-4925	4.4	9602	1147
thickness [mm]	245	0.85	2.7	6.4	1.6
thickness [mm]	426	0.75	3.0	11.9	1.6
thickness [mm]	1800	0.6	3.1	13.5	2.1

Table 6.2: Statistics of strain rate, curvature and flame thickness

As a whole, the standard deviation of all three flame properties increase with the Reynolds number, i.e. with the turbulence intensity. This is particularly true for the curvature, the flame thickness being only slightly affected.

Let us now concentrate on the more interesting case of a 3D turbulent flame.

## 6.2.2 Flame/turbulence interaction for 3D premixed flames

### Configuration

We are interested in the behavior of premixed flames expanding in a three-dimensional turbulent isotropic velocity field. This situation typifies for example the flame development after spark ignition in a gas turbine. We investigate two cases: Case 1: A methane-air flame at low Reynolds number ( $Re=110$ ) and Case 2: A synthetic gas flame at high Reynolds number ( $Re=2300$ ). In both cases we define the flame front as an isosurface of the mass fraction of  $CO_2$ :

$Y(CO_2)=0.45 \cdot \max Y(CO_2)$ . This value corresponds to the steepest temperature gradient in the associated one-dimensional laminar premixed flame.

In the first case a fully premixed methane-air flame interacts with an initially homogeneous and isotropic turbulent flow field within a three-dimensional computational domain. The length of this domain is 5 mm in each direction, discretized with 101 grid points. Figure 6.22 shows the flame front of the low Reynolds number methane-flame.

In the second case we investigate a premixed synthetic gas flame at  $Re=2300$ . The length of the domain is 15 mm in each direction, discretized with 201 grid points. Figure 6.23 shows the

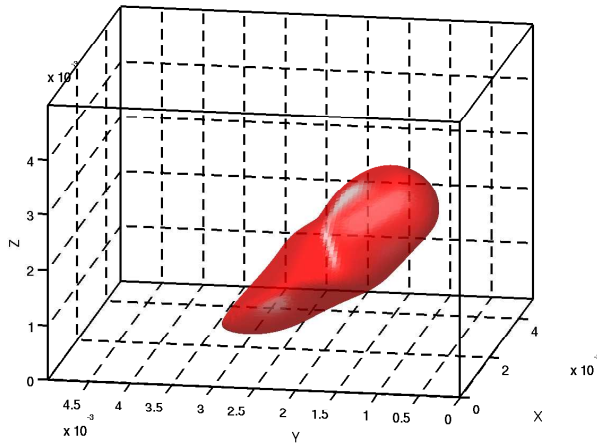


Figure 6.22: Flame front of low Reynolds number methane flame

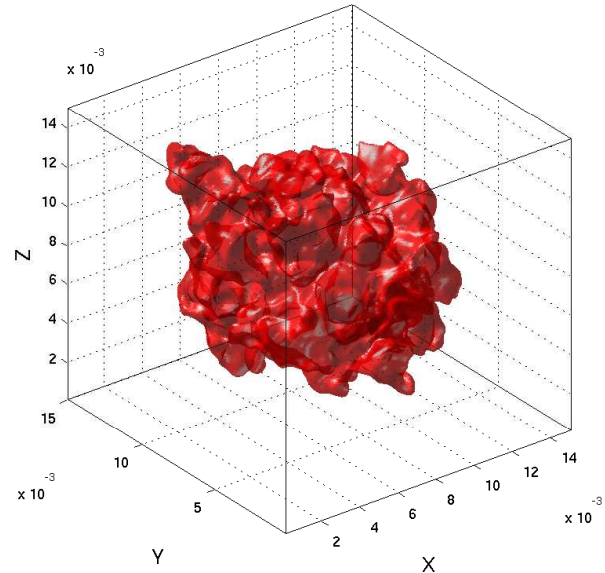


Figure 6.23: Flame front of high Reynolds number synthetic gas flame

flame front of the high Reynolds number synthetic gas flame.

We recognize clear differences in the two flame surfaces. While the surface of the low Reynolds number flame is quite smooth, the surface of the high Reynolds number flame is highly wrinkled.



We are interested in flame/turbulence interaction especially in terms of strain and curvature because they control extinction limits. As we already know, turbulent combustion modeling focuses on the closure of mean burning rates [21, 100, 145]. An important quantity to model the burning rate is the scalar dissipation rate introduced in Section 4.2. Premixed flames propagate towards the mixture of the fresh gases with the displacement speed we introduced in Section 4.2. These quantities are determined by the gradient of the reaction progress variable. Therefore, we investigate this variable carefully.

We begin with the investigation of single flame quantities. For modeling purposes, the interrelation between these quantities is even more interesting. In order to find possible correlations between our variables we will then calculate bidimensional probability density functions and correlation coefficients of the variables of interest.

### Single quantities

- We then calculate the tangential component of the strain rate according to Eq. (4.38) using the tool `strnlev3`: Figure 6.24 shows the PDF of the tangential strain rate along

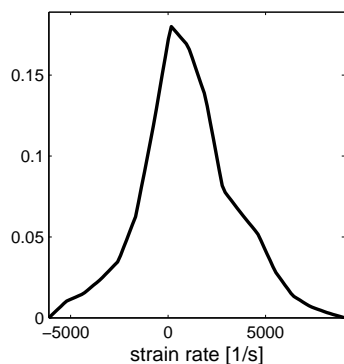


Figure 6.24: PDF of tangential strain rate along flame front of Case 1 flame

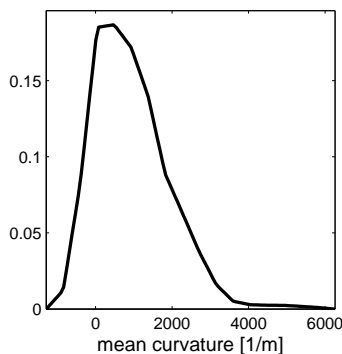


Figure 6.25: PDF of mean curvature of flame front of Case 1 flame

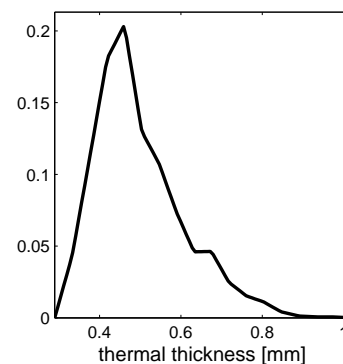


Figure 6.26: PDF of thermal flame thickness along flame front of Case 1 flame

the flame surface of the Case 1 flame. Because the surface of the high Reynolds number flame is more interesting we show for this case the tangential strain rate along the flame surface (see Figure 6.27).

- How to calculate curvatures on 3D surfaces is explained in Appendix B. The mean curvature was calculated according to Eq. (B.9). In order to calculate the curvatures we use the tool `curvlev3`. Figure 6.25 shows the PDF of mean curvature of the flame surface of the Case 1 flame. Figure 6.28 shows the mean curvature of the Case 2 flame.

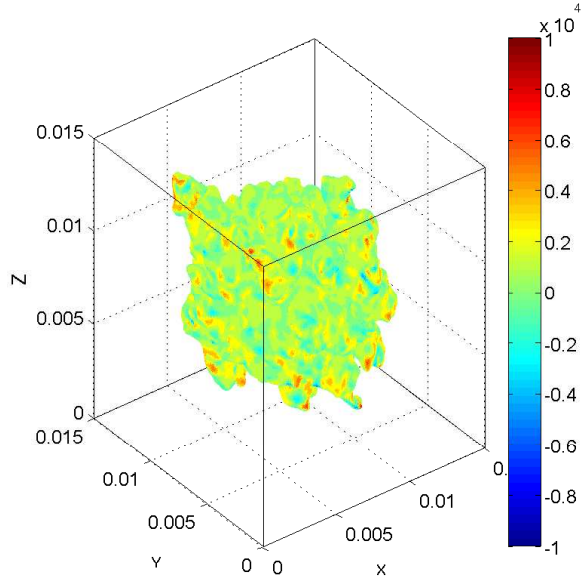


Figure 6.27: Tangential strain rate along flame front of Case 2 flame

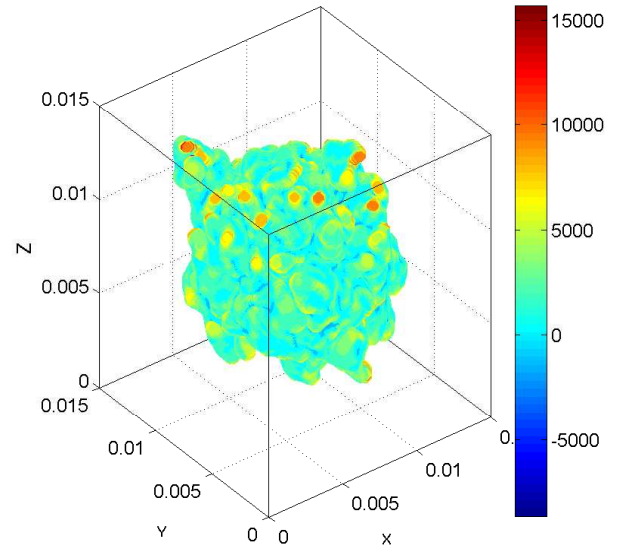


Figure 6.28: Mean curvature of flame front of Case 2 flame

- The thermal thickness  $\delta_L^0$  was introduced in Section (4.2.1) and calculated according to Eq. (4.36) using the tool `flamethicklintherm3b`. Figure 6.26 shows the PDF of the thermal flame thickness of the Case 1 flame.

In order to calculate the statistical moments we use the tool `statvar3`. Table 6.3 shows the statistical moments of order one to four for the above quantities for both flames. The deviation from a Gaussian function is particularly clear for the 3D case.

quantity	mean	std	skewness	kurtosis
Case 1: strain rate [1/s]	1024	2217	0.126	3.24
Case 2: strain rate [1/s]	2301	6164	0.402	7.57
Case 1: mean curvature [1/m]	1029	915	0.96	4.6
Case 2: mean curvature [1/m]	264	1865	-0.975	13.9
Case 1: thermal thickness [mm]	0.508	0.101	0.953	3.8
Case 2: thermal thickness [mm]	0.65	0.0845	0.786	6.26

Table 6.3: Moments of order one to four of tangential strain rate, mean curvature and thermal flame thickness of both flames

## Interrelations between the single quantities

First, we are interested in possible correlations between different flame quantities like strain rate, curvature and flame thickness. In order to find correlations we investigate the interrelation between two of the above variables by considering a bidimensional PDF of the two variables using the tool `statbivar3d`.

- Interrelation: tangential strain-rate - mean curvature

Figure 6.29 shows the plot of the bidimensional PDF of tangential strain rate and mean

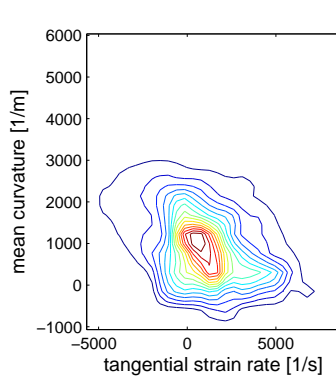


Figure 6.29: PDF of tangential strain rate and mean curvature of flame front of Case 1 flame

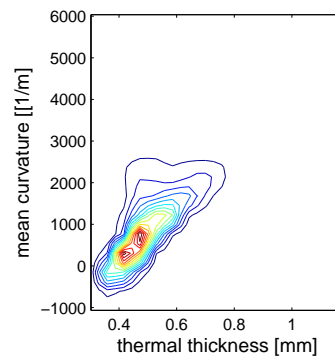


Figure 6.30: PDF of thermal flame thickness and mean curvature of flame front of Case 1 flame

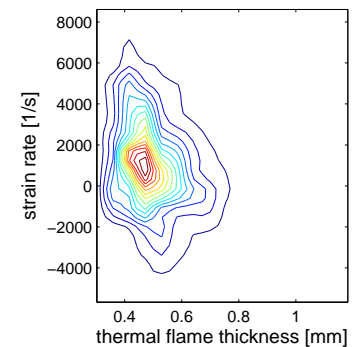


Figure 6.31: PDF of thermal flame thickness and strain rate of flame front of Case 1 flame

curvature of the Case 1 flame. We recognize a (weak) negative correlation between the two variables. This negative correlation is consistent with the literature [56].

- Interrelation: thermal flame thickness - mean curvature

Figure 6.30 shows the plot of the bidimensional PDF of thermal flame thickness and mean curvature of the Case 1 flame. Here a clear correlation between the two variables can be recognized.

- Interrelation: thermal flame thickness - strain rate

Figure 6.31 shows the plot of the bidimensional PDF of thermal flame thickness and tangential strain rate of the Case 1 flame.

For both flames a positive correlation between thermal flame thickness and mean curvature and a negative correlation between thermal flame thickness and strain rate can be recognized. This positive correlation between thermal flame thickness and mean curvature is consistent with the literature [119, 134].

quantities	correlation coefficient
Case 1: strain rate-mean curvature	-0.31
Case 2: strainrate-mean curvature	-0.081
Case 1: thickness-mean curvature	0.745
Case 2: thickness-mean curvature	0.286
Case 1: thickness-strain rate	-0.20
Case 2: thickness-strain rate	-0.163

Table 6.4: Correlations coefficients between strain rate, curvature and flame thickness for both flames

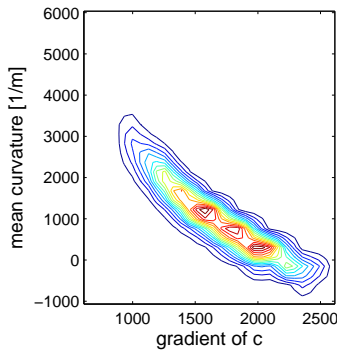


Figure 6.32: PDF of  $|\nabla c|$  and mean curvature of flame front of the Case 1 flame

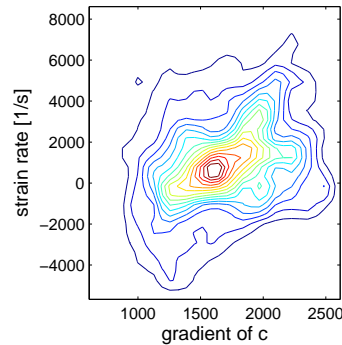


Figure 6.33: PDF of  $|\nabla c|$  and tangential strain rate of the Case 1 flame

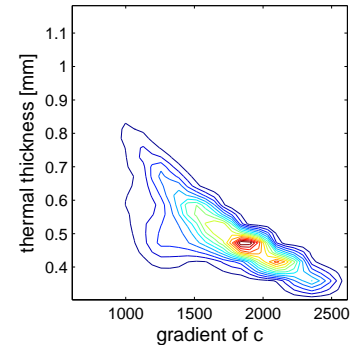


Figure 6.34: PDF of  $|\nabla c|$  and thermal flame thickness of the Case 1 flame

### Interrelation between quantities and surface density function

Secondly we are interested in correlations between the above flame quantities and the gradient of the reaction progress variable  $|\nabla c|$ .

- Surface density function

We calculate the reaction progress variable  $c$  according to Eq. (4.43) and the absolute gradient of the reaction progress variable  $|\nabla c|$ , also called surface density function (SDF). In order to calculate the reaction progress variable  $c$  and the surface density function  $|\nabla c|$  we use the tool `reacprog3co2`.

- Interrelation: gradient of  $c$  - mean curvature

Figure 6.32 shows the plot of the bidimensional PDF of  $|\nabla c|$  and mean curvature of the Case 1 flame. We recognize a clear correlation between the two variables.

quantity	correlation coefficient
Case 1: $ \nabla c $ -mean curvature	-0.94
Case 2: $ \nabla c $ -mean curvature	-0.38
Case 1: $ \nabla c $ -strain rate	0.286
Case 2: $ \nabla c $ -strain rate	0.233
Case 1: $ \nabla c $ -thickness	-0.79
Case 2: $ \nabla c $ -thickness	-0.637

Table 6.5: Correlations coefficients between quantities and  $|\nabla c|$  of both flames

- Interrelation: gradient of  $c$  - tangential strain rate  
Figure 6.33 shows the plot of the bidimensional PDF of  $|\nabla c|$  and tangential strain rate. We recognize a (weak) positive correlation between the two variables.
- Interrelation: gradient of  $c$  - thermal flame thickness  
Figure 6.34 shows the plot of the bidimensional PDF of  $|\nabla c|$  and thermal flame thickness. We recognize a clear negative correlation between the two variables.

For both flames we recognize a (strong) negative correlation between  $|\nabla c|$  and the thermal flame thickness. The negative correlation between  $|\nabla c|$  and the mean curvature and the positive correlation between  $|\nabla c|$  and the strain rate are consistent with the literature [56].

## Results

We found clear correlations:

- between the thermal flame thickness and the mean curvature of the flame surface,
- between  $|\nabla c|$  and the mean curvature,
- between  $|\nabla c|$  and the thermal flame thickness.

## 6.3 PDF modeling of a 3D nonpremixed hydrogen/air flame

Modeling correctly the PDF of mixture fraction in turbulent reacting flows is an essential issue [96, 100, 145]. PDF methods and different shapes of PDFs were discussed in Sections 3.4 and 4.3. Here we investigate the PDF of the mixture fraction in a 3D non-premixed hydrogen/air flame. The following results have been published in [35].

### Numerical configuration

A laminar nonpremixed flame of hydrogen diluted in nitrogen and burning in air (0.21O<sub>2</sub>+0.79N<sub>2</sub> in volume) is first ignited in a laminar, one-dimensional configuration. Afterwards, the resulting profiles are uniformly extended along the  $y$ - and  $z$ -directions and a three-dimensional field of synthetic turbulence is imposed on top of it. A chemical scheme involving 9 species (H<sub>2</sub>, O<sub>2</sub>, H<sub>2</sub>O, H, O, OH, HO<sub>2</sub>, H<sub>2</sub>O<sub>2</sub>, and N<sub>2</sub>) and 19 reversible elementary reactions is used to describe H<sub>2</sub> oxidation. The initial conditions correspond to a global mixture ratio  $\phi = 0.8$ . The stoichiometric mixture fraction given by theory is then  $Z_s = 1/(1 + \phi) = 0.56$ . The computational domain is a cube of sides 1.0 cm with 200 grid nodes in each direction, yielding a uniform mesh size of 50 $\mu$ m.

### PDF of mixture fraction

For most models and in particular when using the RANS approach, the form of the PDF is usually presumed, using either  $\beta$ - or  $\gamma$ -functions as given by Eqs. (6.1) and (6.2) respectively:

$$\tilde{P}_\beta(Z; \mathbf{x}, t) = \frac{Z^{a-1}(1-Z)^{b-1}}{\Gamma(a)\Gamma(b)}\Gamma(a+b) \quad (6.1)$$

$$\tilde{P}_\gamma(Z; \mathbf{x}, t) = \frac{Z^{c-1}}{d^c\Gamma(c)}\exp(-Z/d) \quad (6.2)$$

where  $\Gamma$  denotes the  $\gamma$ -function. The parameters  $a$ ,  $b$ ,  $c$  and  $d$  are determined using the Favre-averaged mean  $\tilde{Z}$  and variance  $\tilde{Z}''^2$  of the mixture fraction by

$$a = \tilde{Z}\alpha_1; \quad b = (1 - \tilde{Z})\alpha_1; \quad \alpha_1 = \frac{\tilde{Z}(1 - \tilde{Z})}{\tilde{Z}''^2} - 1$$

$$c = \alpha_2; \quad d = \alpha_2\tilde{Z}; \quad \alpha_2 = \frac{\tilde{Z}}{\tilde{Z}''^2}$$

When using turbulent combustion models,  $\tilde{Z}$  and  $\tilde{Z}''^2$  are usually obtained through supplementary, approximate transport equations. On the other hand, these quantities are readily available from the DNS data, considering the  $y$ - and  $z$ -directions as homogeneous, corresponding to separate realizations. For this analysis the central part of the numerical domain in  $x$ -direction (flame zone) is separated in 9 identical cubic sub-regions with a side length of 1/3 cm (roughly twice the integral scale of turbulence). This dimension is typical for the grid size employed in the RANS computation of a turbulent flame. In each sub-region the Favre-averaged mean  $\tilde{Z}$  and variance  $\tilde{Z}''^2$  of the mixture fraction are computed by post-processing the DNS data at  $t = 0.94\tau$ , and are afterwards used to reconstruct the PDF of  $Z$  following Eqs.(6.1) and (6.2). These reconstructed PDF are compared with the exact PDF obtained from the DNS data within the corresponding sub-region, as exemplified in Figures 6.35 and 6.36. All functions

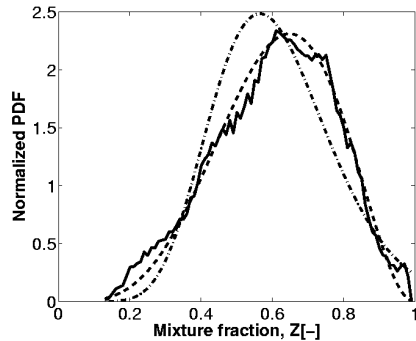


Figure 6.35: PDF of mixture fraction  $Z$  in the 6th sub-region, where the best agreement is observed with the model. DNS: solid line; reconstruction with a  $\beta$ -function: dashed line; reconstruction with a  $\gamma$ -function: dash-dotted line.

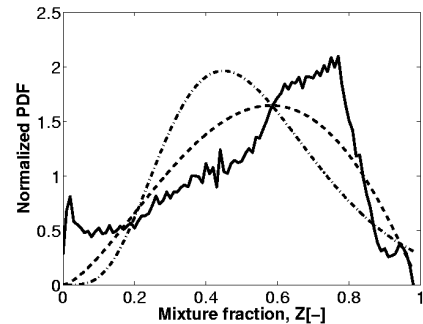


Figure 6.36: PDF of mixture fraction  $Z$  in the 9th sub-region, where the worst agreement is observed with the model. DNS: solid line; reconstruction with a  $\beta$ -function: dashed line; reconstruction with a  $\gamma$ -function: dash-dotted line.

are normalized to obtain a probability of 100% over the full  $Z$ -axis. The obtained agreement is quantified by computing the correlation between the exact and reconstructed curves. The correlation coefficients are listed in Table 6.6. The correlations demonstrate the superiority of

Sub-region number	$\beta$	$\gamma$
1	0.992	0.910
2	0.977	0.851
3	0.932	0.625
4	0.947	0.811
5	0.977	0.937
6	0.992	0.928
7	0.962	0.819
8	0.980	0.962
9	0.823	0.559
full slab	0.928	0.769

Table 6.6: Correlation coefficient between the exact PDF and the reconstructed PDF using  $\beta$ - or  $\gamma$ -function.

the  $\beta$ -function for reconstructing the PDF. Without any exception, the correlation associated with the  $\beta$ -function is considerably higher than with the  $\gamma$ -function. As a whole, the reconstruction with the  $\beta$ -function is in quite good agreement with the exact PDF, as observed for

example in Figure 6.35. Nevertheless, in one from the 9 boxes (or 11%) the agreement with both reconstructions is quite poor (Figure 6.36). This is the only case where the exact PDF exhibits three clear peaks. It is known that a good reconstruction is not possible using  $\beta$ - or  $\gamma$ -functions in such cases. The correlation obtained when carrying out the analysis for the full slab composed of the nine sub-regions is also given in Table 6.6, demonstrating again the superiority of the  $\beta$ -function reconstruction.

## 6.4 Chemistry reduction

As already mentioned in Section 2.6.3, most manifold methods are either working only for a certain dimension of the manifold or they expect that the user already knows the required dimension. We have developed a methodology to determine the appropriate dimension of a low-dimensional manifold for reaching a defined level of accuracy. When the appropriate level is found chemical source terms can be reconstructed based on that level. In order to demonstrate our methodology we investigate an extensive DNS dataset of a non-premixed  $\text{H}_2/\text{N}_2/\text{air}$ -flame. The following results were partly published in [156].

### 6.4.1 Flame configuration

To assess the influence of transport and chemistry onto the low-dimensional manifold and the required dimension for a given accuracy, the analysis is performed on two DNS datasets. In the first one we consider a flame with a detailed transport model with mixture-averaged diffusion coefficients and with Soret effect. In the second one we keep diffusion processes as simple as possible and consider a flame at unity Lewis number for all species.

In order to check the possible influence of the turbulence level on the findings, two different Reynolds numbers  $\text{Re}_t = u' l_t / \nu$ , built with the turbulent velocity  $u'$  and the Integral length scale  $l_t$ , are considered for each flame. For the flame with detailed transport (DT) model, the Reynolds numbers are 723 (Case DT-1) and 965 (Case DT-2). For the unity Lewis (UL) number flame the lowest Reynolds number is 505 (Case UL-1) and the higher Reynolds number is 1152 (Case UL-2). In both cases, a spatial discretization of  $25 \mu\text{m}$  is sufficient to resolve all relevant scales in the DNS.

Figures 6.37 and 6.38 show the temperature field and the state space for  $\text{N}_2$  and  $\text{H}_2\text{O}$  of our flame with detailed transport model at  $\text{Re}_t = 965$  for a single time step. Being embedded into a turbulent flow field, the flame displays a complex, strongly distorted structure, with high-temperature regions existing as isolated, separated islands. This strong interaction of flow and chemistry is also evident from the mass fraction scatter plot of  $\text{N}_2$  and  $\text{H}_2\text{O}$  from the same DNS data. In Figure 6.38 we plot only every tenth point for better representation and less memory requirements.



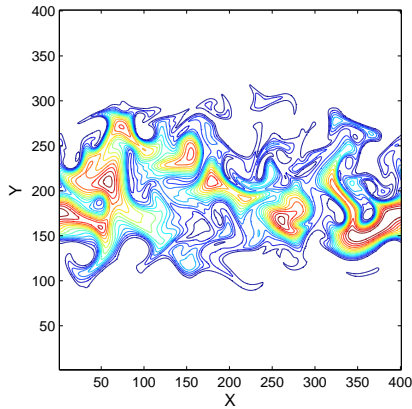


Figure 6.37: Turbulent temperature field of the flame with detailed transport model at  $Re=965$ .

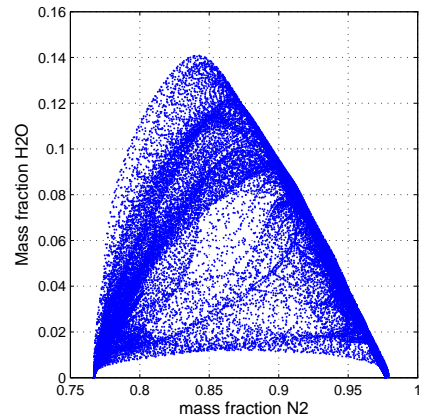


Figure 6.38: State space of the flame with detailed transport model at  $Re=965$ .

## 6.4.2 Results for detailed transport model

Let us start by stating that the Reynolds number was found to have no noticeable influence on the results in the investigated range. Exactly the same conclusions apply for Case DT-1 and DT-2. As a consequence, and in order to increase the statistical content, the results obtained for both values of  $Re$  will be combined in what follows. After initializing the computation, the DNS results obviously vary with time. For datasets from the very first time steps, the required dimension for a good reconstruction is simply one. This is understandable, since the system is still very close to the initial conditions used for the DNS, which were taken from a laminar flame.

Later on, the DNS delivers a truly turbulent flame. Five selected output times have been retained to carry out the analysis, for  $0.84\tau_t < t < 6.16\tau_t$ , where  $\tau_t = l_t/u'$  is the characteristic time of turbulence. Since it was finally found that the result was independent of the solution time step, combinations from different time outputs will be presented.

All these first results are for 15-point neighborhoods. The impact of scaling weights will be later discussed as well.

Figure 6.39 shows scatter plots of one- to nine-dimensional reconstructions vs. original species mass fractions of  $HO_2$ . All points from the considered clouds in composition space (about 3000 for each condition) are drawn.

It is seen that the reconstruction quality is improving significantly as the dimension is increased from three to four, while comparatively small further improvements are obtained for dimensions higher than four. For an ideal reconstruction, the points would reside exactly on the diagonal in each diagram.

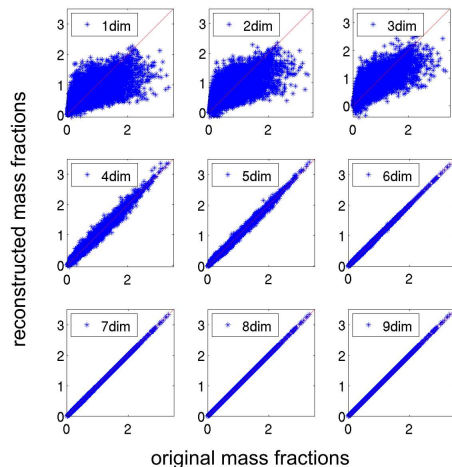


Figure 6.39: Scatter plots of original and reconstructed mass fractions of  $\text{HO}_2$  for one- to nine-dimensional locally linear reconstructions (from left to right and top to bottom). Data points sampled from DNS with detailed transport model, for both Reynolds numbers and all five output times considered (without scaling). In the diagram, the mass fractions have been scaled by a factor of 10000.

As a more comprehensive measure, Figure 6.40 shows the correlation coefficients between original and reconstructed species mass fractions (without scaling). For four-dimensional reconstructions, the mean correlation coefficients are better than 0.9 for all species. For the major species, mean correlation coefficients above 0.9 are obtained already with three dimensions. Figure 6.41 shows the mean value, taken over all clouds, of the normalized deviations  $\delta_i^{(d)}$  for all nine species mass fractions (without scaling). Deviations are normalized by deviation for zeroth-order approximation. We recognize a significant difference in the deviations of major species ( $\text{O}_2$ ,  $\text{N}_2$ ,  $\text{H}_2\text{O}$ ) and minor species ( $\text{H}_2\text{O}_2$ ,  $\text{H}$ ,  $\text{HO}_2$ ). The mean deviation averaged over all nine species is better than 10% for a four-dimensional approximation (see Figure 6.42). In order to demonstrate the influence of scaling, the analysis was repeated for a scaled version of the species mass fractions, as described in Section 2.6.3.

The influence of scaling is obvious. For three dimensional approximations, the deviation for major species  $\text{H}_2$ ,  $\text{H}_2\text{O}$ ,  $\text{N}_2$  and  $\text{O}_2$  is larger compared to the unscaled case, while for minor species, especially for  $\text{H}_2\text{O}_2$  and  $\text{HO}_2$ , the deviation is smaller compared to the unscaled case. For the scaled case, the difference between major and minor species nearly vanishes. Even  $\text{H}_2\text{O}_2$  and  $\text{HO}_2$  are now reconstructed well if a three-dimensional approximation is used.

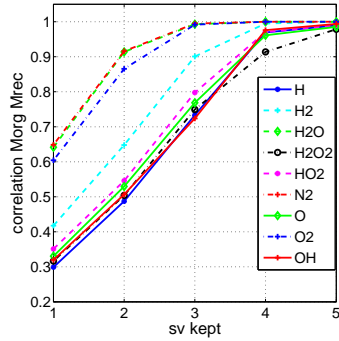


Figure 6.40: Correlation coefficients for unscaled mass fractions. DNS data from detailed transport model. Investigated neighborhood size 15 points.

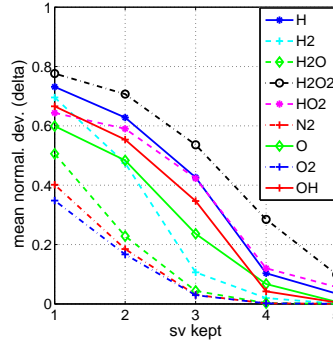


Figure 6.41: Mean normalized deviations for unscaled mass fractions. DNS data from detailed transport model. Investigated neighborhood size 15 points.

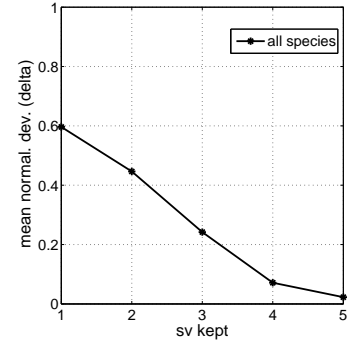


Figure 6.42: Mean normalized deviations for unscaled mass fractions from detailed transport model. Deviations are averaged over all nine species.

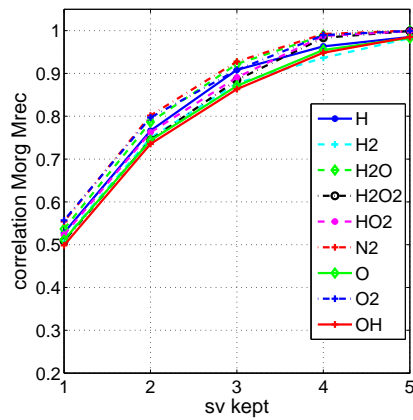


Figure 6.43: Correlation coefficients for scaled mass fractions. DNS data from detailed transport model. Investigated neighborhood size 15 points.

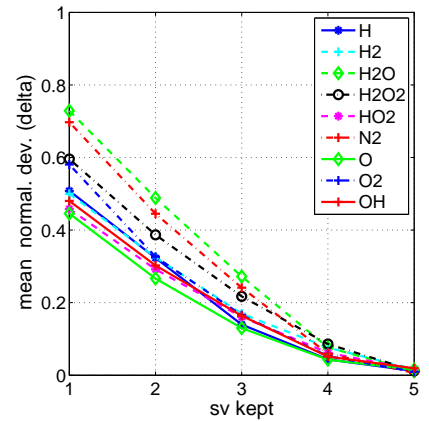


Figure 6.44: Mean normalized deviations for scaled mass fractions. DNS data from detailed transport model. Investigated neighborhood size 15 points.

Figures 6.43 and 6.44 show correlation coefficients and differences  $\delta$  for the weighted species mass fractions. Four dimensions are again required to achieve correlation coefficients better than 0.9 and mean weighted deviations better than 10% for all species. The scaling strongly influences the relative reconstruction accuracy between different species, but does not influence

the overall dimension required to meet the accuracy criterion. However, while mean deviations below 10% were only observed in the average in Figure 6.42 (without scaling), this condition is now met by all species in Figure 6.44. Therefore, scaling leads as expected to a similar behavior for all species.

### 6.4.3 Results for simplified transport model

To separately assess the influence of transport and chemistry onto the required dimension for a given reconstruction accuracy, additional DNS data have been considered from a flame that was computed with unity Lewis numbers for all species. In what follows, we again consider DNS data collected from two Reynolds numbers (505 and 1152) and five time outputs. Again, both scaled and unscaled species mass fractions were considered. Only the results for the 15-point neighborhoods are discussed.

Figures 6.45 and 6.46 show the corresponding correlation coefficients and mean deviations for the unscaled mass fractions.

Again we recognize a significant difference in the behavior of major species ( $O_2$ ,  $N_2$ ,  $H_2O$ ) and minor species ( $H_2O_2$ ,  $H$ ,  $HO_2$ ). For three-dimensional approximations, the correlation coefficients are already approaching the value one, and reconstructed and original species mass fractions become nearly identical, meeting the retained accuracy criteria: correlation coefficients are all larger than 0.9, and normalized deviations (mean value averaged over all nine species) are below 10%, in spite of the slightly higher value for  $H_2O_2$ .

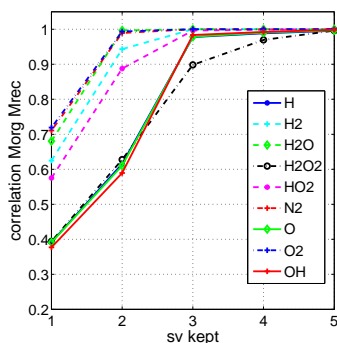


Figure 6.45: Correlation coefficients for unscaled mass fractions. DNS data from simplified transport model. Investigated neighborhood size 15 points.

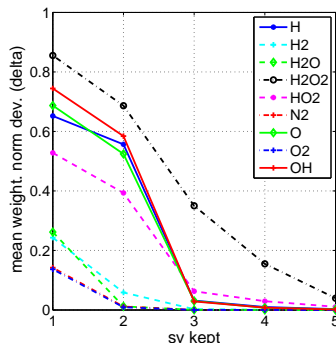


Figure 6.46: Mean normalized deviations for unscaled mass fractions. DNS data from simplified transport model. Investigated neighborhood size 15 points.

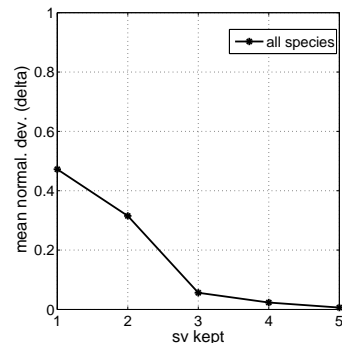


Figure 6.47: Mean normalized deviations for unscaled mass fractions from simplified transport model. Deviations are averaged over all nine species.

Figure 6.47 shows the normalized deviations averaged over all nine species. As can be seen,

the dimension required for an accurate reconstruction is three.

Considering now scaled mass fractions, the reconstruction of the major species is improving more slowly with increasing dimension, compared to the unscaled case. On the other hand, the progress is faster for the minor species. Figures 6.48 and 6.49 show correlations and mean

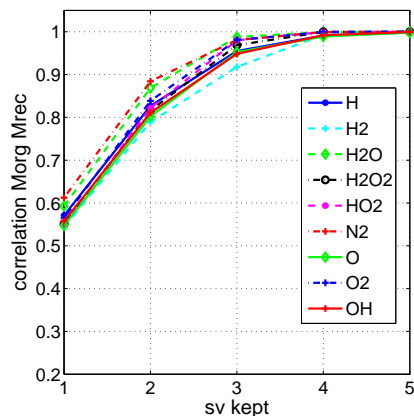


Figure 6.48: Correlation coefficients for scaled mass fractions. DNS data from simplified transport model. Investigated neighborhood size 15 points.

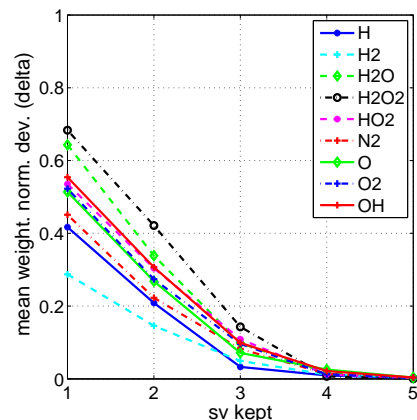


Figure 6.49: Mean normalized deviations for scaled mass fractions. DNS data from simplified transport model. Investigated neighborhood size 15 points.

deviations for the scaled case. For a three-dimensional approximation, the values for correlation coefficient and deviation of  $\text{H}_2\text{O}_2$  are now similar to the corresponding values for all other species. Both accuracy criteria are fulfilled again. Correlation coefficients for all species are greater than 0.9 and normalized deviations (mean value averaged over all nine species) are below 10%. This means, using both scaled and unscaled mass fractions, three dimensions are required to meet the accuracy criterion for all species.

Compared to the case with detailed transport, the data from the simplified transport model require one dimension less for the same reconstruction accuracy. This difference of one dimension between simplified and detailed transport model is understandable on the basis of the elemental composition of the mixture. This elemental composition (given by the mass fractions of the three elements H, O and N) can not be altered by chemical reactions, but only by mixing processes. For the simplified transport model, the element composition is (for given boundary conditions) determined by one single quantity, the mixture fraction. There is thus one degree of freedom for the mixing field. In contrast, for the detailed transport model, the three elements H, O and N can be varied independently by differential diffusion. But, since the element mass fractions have to sum up to 1, only two degrees of freedom remain for the mixing field.

Apparently, in both cases (detailed and simplified transport), two additional degrees of free-

dom (corresponding to two additional dimensions of the underlying low-dimensional manifold) are induced by the dynamics of chemistry. The combined dynamics of mixing and chemistry then yield the total of three (simplified transport model) or four (detailed transport model) dimensions for the considered hydrogen/air system.

#### 6.4.4 Analysis including temperature

In the next step, we consider the temperature as additional state vector component. Otherwise, we follow the same procedure as above, first determining neighbourhoods, applying an SVD to obtain locally linear approximations, and reconstructing data. Because of the large difference in magnitude between temperature and species mass fractions, only the scaled case is considered. The results obtained with state vectors containing temperature are almost identical to those obtained from state vectors without temperature. Again, three dimensions are needed for the simplified transport model, and four dimensions are needed for the detailed model, keeping the same quality criterion. Figures 6.50 and 6.51 show the mean correlations for the detailed transport model and the mean correlations for the simplified transport model, respectively.

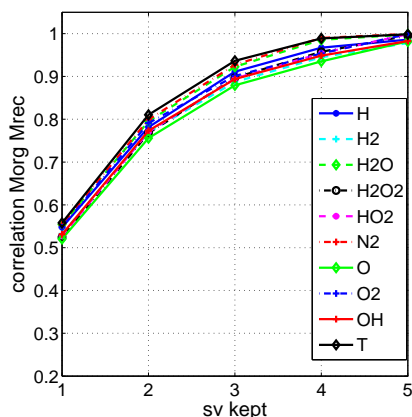


Figure 6.50: Correlation coefficients between original and reconstructed scaled mass fractions and temperature for one to five-dimensional reconstructions. DNS data from detailed transport model. Investigated neighbourhood size 15 points.

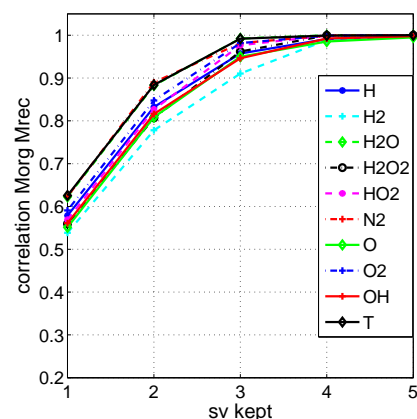


Figure 6.51: Correlation coefficients between original and reconstructed scaled mass fractions and temperature for one to five-dimensional reconstructions. DNS data from detailed transport model from simplified transport model. Investigated neighbourhood size 15 points.

### 6.4.5 Neighbourhoods based on prescribed radius

The requirement for the point clouds is that they be sufficiently small to allow a good local approximation of the manifold by a linear structure. This can be achieved by selecting a predefined small number of close points for constructing the cloud (like it has been performed in the previous sections), or also by defining a prescribed radius of the cloud. Therefore, clouds are now considered which are constructed from all data points in a state-space hypersphere of a given radius around a center point. For a meaningful analysis, the number of points in the cloud must be somewhat larger than the dimension of the full state space. Therefore, only hyperspheres containing at least 12 points are considered, a condition first met for spheres with radius 0.05. The results regarding the dimensionality are the same as for clouds based on a fixed number of neighbours: To meet the quality criterion, four dimensions are required for the detailed transport model and three dimensions are required for the simplified transport model. Note that those clouds then differ considerably in their number of neighbours. In the case of the detailed transport model the considered clouds had 114 neighbours in the average, while the maximum size exceeded 1000. Figures 6.52 and 6.53 show the mean correlations for the detailed transport model and for the simplified transport model, respectively.

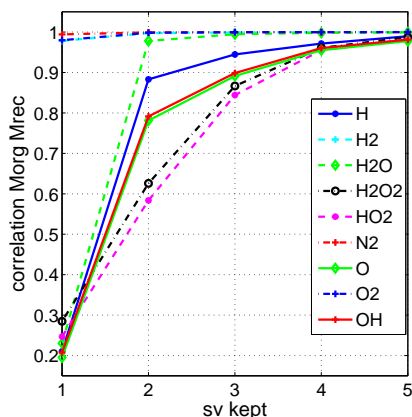


Figure 6.52: Mean correlations between original and reconstructed scaled mass fractions for one to five-dimensional reconstructions. DNS data from detailed transport model. Neighbours are sampled in a cloud of radius 0.05.

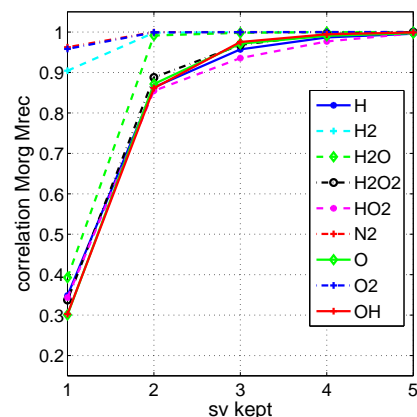


Figure 6.53: Mean correlations between original and reconstructed scaled mass fractions for one to five-dimensional reconstructions. DNS data from simplified transport model. Neighbours are sampled in a cloud of radius 0.05.

## 6.4.6 Impact of large neighborhoods

Finally, the impact of very large neighborhoods has been considered. We consider clouds with a large number of neighbors, namely 400 and clouds with a large radius in composition space, namely 0.5. Results are discussed for the detailed transport model for scaled species mass fractions only. Figure 6.54 shows the correlation coefficients for clouds with 400 neighbors, while Figure 6.55 shows the correlation coefficients for clouds with radius 0.5.

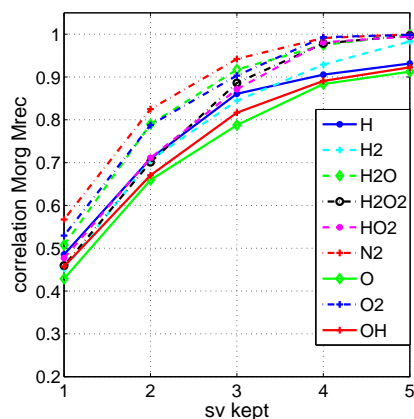


Figure 6.54: Correlation coefficients between original and reconstructed scaled mass fractions for one to five-dimensional reconstructions. DNS data from detailed transport model. Investigated neighbourhood size 400 points.

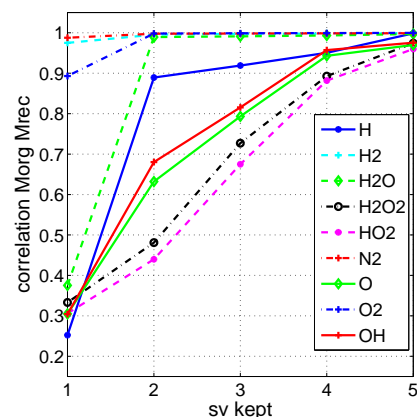


Figure 6.55: Correlation coefficients between original and reconstructed scaled mass fractions for one to five-dimensional reconstructions. DNS data from detailed transport model. Neighborhoods are sampled in a cloud of radius 0.5.

To obtain the same reconstruction quality, one dimension more is now required for the larger neighborhoods, compared to the small ones. In both cases, for clouds with 400 neighbors as well as for clouds with radius 0.5 five dimensions are now needed to obtain correlation coefficients better than 0.9, compared to four dimensions with 15-neighbor clouds (see Figure 6.43) and clouds of the small radius 0.05 (see Figure 6.52). This is a further indication of the non linearity of the evolutions in composition space.



## 6.5 Conclusion

All these examples have demonstrated the versatility and the interest of the developed MATLAB library to post-process complex DNS data describing turbulent flames. Obviously, many further examples could be included, since only a small number of more than 200 tools existing in the library have been used in Chapter 6. This will be the task of all library users listed in Table 1.1, together colleagues of the group in Magdeburg.

# Chapter 7

## Summary

In this project a large toolbox for post-processing and analyzing turbulent flames was developed using the commercial program MATLAB. The toolbox works for 2D and 3D flames, for premixed and non-premixed regimes, for hydrogen and for hydrocarbon fields. This toolbox is particularly useful to analyze DNS data, but could also be used in principle for many other cases, for instance experimental data.

A phenomenological description of turbulent flow fields, of premixed and of non-premixed flames was first given. The balance equations to describe turbulent reacting flows and methods to solve the system with the focal point on direct numerical simulations were introduced. The necessity of post-processing the huge amount of data obtained by DNS was demonstrated.

Reaction kinetics and methods to reduce reaction kinetics, in particular manifold methods were discussed. A methodology to find the appropriate dimension of a low-dimensional manifold for reaching a given level of accuracy was presented.

Scales and quantities that can be post-processed using the toolbox were explained. The program MATLAB was introduced and all the tools were presented in a systematic manner.

The toolbox contains tools for a direct geometrical analysis of the raw data,  
tools to investigate the flame structure,  
tools needed to investigate and quantify the properties of turbulent flow fields,  
tools to investigate the interaction between flames and turbulence,  
tools allowing a statistical investigation of the variables of interest and  
tools to determine appropriate dimensions of manifolds.

For the most time-intensive tools running in batch mode a parallelized version was developed. As a whole more than 200 tools are now available in the library. Twenty-seven different research groups worldwide are using the toolbox in addition to the university of Magdeburg.

Important properties of flow fields and flames were analyzed using the MATLAB toolbox. Two-dimensional and three-dimensional turbulent flow fields were investigated and compared. The interaction between turbulence and flames was investigated, for 2D and 3D flames, for premixed

and non-premixed flames with different fuels.

As a final example the determination of the appropriate dimension for a low-dimensional manifold describing the chemistry in an accurate manner was investigated. A non-premixed  $\text{H}_2/\text{N}_2/\text{air}$  flame was chosen, with two different transport models. For a simplified transport model with Lewis number one a dimension of three was found for the reduced manifold, while for a detailed transport model the required dimension was four. This difference of one dimension can be explained on the basis of the elemental composition of the mixture. For the simplified transport model the mixture fraction there is one degree of freedom for the mixing field, the mixture fraction. For the detailed transport model, the three elements H, O and N can be varied independently, but, since the element mass fractions have to sum up to 1, only two degrees of freedom remain for the mixing field.

### **Outlook**

The turbulence part of the toolbox offers tools to calculate space-dependent spectra. These tools could be expanded to time-dependent spectra as well.

The present version of the toolbox contains parallel tools to unroll for-loops and to distribute repetitive, independent tasks on different workers. The size of the datasets generated by direct numerical simulations continues to grow and their handling can lead to memory or storage problems during post-processing, especially for 3D-results. The next step could be to split the domain and to extend the toolbox to parallel jobs with distributed arrays.

We have found in our last application example the dimension of a low-dimensional manifold for hydrogen flames, but the employed methodology is also working for other flames. The investigation can now be expanded to synthetic gas and methane flames, when enough DNS data are available. When the appropriate dimension is found the next step would be to reconstruct the chemical source terms.

# Appendix A

## Methods of taking averages

There are three methods of taking averages. Which one is to be preferred depends on the flow field. If the flow field is stationary random, classically averaging with respect to time is used. In a similar manner for homogeneous turbulence averaging with respect to space is used. In cases where the flow field is neither homogeneous nor stationary, time averaging and space averaging are not possible. Instead a large number of experiments has to be considered. This kind of average is called ensemble average.

- *Space average*

For homogeneous turbulence the space averaged mean value is defined:

$$\bar{\phi}(t_0) = \frac{1}{2X} \int_{-X}^{+X} \phi(x, t_0) dx \quad (\text{A.1})$$

- *Time average*

For a stationary turbulence the time averaged mean value is defined:

$$\bar{\phi}(x_0) = \frac{1}{2T} \int_{-T}^T \phi(t, x_0) dt \quad (\text{A.2})$$

- *Ensemble average*

In the most general case the ensemble averaged mean value is defined:

$$\bar{\phi}(x_0, t_0) = \frac{1}{N} \sum_{i=1}^N \phi_i(x_0, t_0) \quad (\text{A.3})$$

For stationary and homogeneous turbulence the three methods lead to the same result. This is known as ergodic theorem.

# Appendix B

## Geometrical quantities

### Curvature

In differential geometry planar curves are often given in explicit form. For example a planar curve is described by  $y = f(x)$ . Then its curvature is defined by [15]:

$$k = \frac{y''}{(1 + (y')^2)^{3/2}} \quad (\text{B.1})$$

where  $y'$  and  $y''$  are the first and second derivatives of  $y$ .

A surface  $f$  is represented through the parameters  $u$  and  $v$  as  $f(u, v)$ . Curvatures on surfaces are more difficult to define as there are infinitely many curves and directions of curves through a point. As we know from Section 4.2.1 among them we can identify one direction of maximal curvature and one direction of minimal curvature.

These directions are called the principal directions  $t_1$  and  $t_2$ .

The magnitudes of the curvatures along the principal directions  $t_1$  and  $t_2$  are called principal curvatures  $k_1$  and  $k_2$ .

The term  $K = k_1 k_2$  is called the Gaussian curvature.

The term  $H = (k_1 + k_2)/2$  is called the mean curvature.

From section 4.2.1 we know that curvature properties depend on the direction and the rate of change of their normals. We calculate the unit normal vector  $\mathbf{n}$  as follows:

$$\mathbf{n} = \frac{\frac{\partial f}{\partial u} \times \frac{\partial f}{\partial v}}{\left\| \frac{\partial f}{\partial u} \times \frac{\partial f}{\partial v} \right\|} \quad (\text{B.2})$$

The local differential geometry, which means principal, Gaussian and mean curvature, at a point of a surface is classically described by the so-called *Weingarten matrix*. Therefore, we need to determine the Weingarten matrix.

The elements of the Weingarten matrix are the coefficients of the first and second fundamental

form of the surface [26].

The first fundamental form is defined by the following coefficients:

$$E = \frac{\partial f}{\partial u} \cdot \frac{\partial f}{\partial u} \quad F = \frac{\partial f}{\partial u} \cdot \frac{\partial f}{\partial v} \quad G = \frac{\partial f}{\partial v} \cdot \frac{\partial f}{\partial v}$$

with:  $E \geq 0$        $G \geq 0$        $EG - F^2 \geq 0$

The second fundamental form is defined by the following coefficients:

$$L = \frac{\partial^2 f}{\partial u^2} \cdot \mathbf{n} \quad M = \frac{\partial^2 f}{\partial u \partial v} \cdot \mathbf{n} \quad N = \frac{\partial^2 f}{\partial v^2} \cdot \mathbf{n}$$

As the second fundamental form contains the normal vector it describes the curvature properties of the surface.

The Weingarten matrix is calculated using the values of the first and second fundamental form as follows:

$$W = \begin{pmatrix} E & F \\ F & G \end{pmatrix}^{-1} \begin{pmatrix} L & M \\ M & N \end{pmatrix} \quad (\text{B.3})$$

Knowing the Weingarten matrix we can calculate

- the principal curvatures and principal directions that respectively correspond to the eigenvalues and eigenvectors of the matrix.
- the Gaussian curvature, which corresponds to the determinant of the matrix.
- the mean curvature, which corresponds to half the trace of the matrix.

The Gaussian curvature is hence calculated as follows:

$$K = \det \left[ \begin{pmatrix} E & F \\ F & G \end{pmatrix}^{-1} \begin{pmatrix} L & M \\ M & N \end{pmatrix} \right] = \frac{LN - M^2}{EG - F^2} \quad (\text{B.4})$$

The mean curvature is calculated as follows:

$$H = \frac{1}{2} \text{trace} \left[ \begin{pmatrix} E & F \\ F & G \end{pmatrix}^{-1} \begin{pmatrix} L & M \\ M & N \end{pmatrix} \right] = \frac{EN - 2FM + GL}{2(EG - F^2)} \quad (\text{B.5})$$

The principal curvatures are calculated by:

$$\begin{aligned} k_1 &= H + \sqrt{H^2 - K} \\ k_2 &= H - \sqrt{H^2 - K} \end{aligned} \quad (\text{B.6})$$

In computer results, however, points of planar curves and surfaces are given in implicit form:

A planar curve is then given in the form  $f(x, y) = 0$ .

A surface is then given in the form  $f(x, y, z) = 0$ .

The transfer of the above concept to implicit surfaces was derived by Dombrowski in the general case of an  $n$ -dimensional space [27]. For the 3-dimensional space it is discussed in [52, 78, 142].

To calculate the curvatures again we need first- and second-order partial derivatives of  $f$ . For convenience we use the following abbreviations:

$$\begin{aligned} f_x &= \frac{\partial f}{\partial x}, & f_y &= \frac{\partial f}{\partial y}, & f_z &= \frac{\partial f}{\partial z}, \\ f_{xx} &= \frac{\partial^2 f}{\partial x^2}, & f_{yy} &= \frac{\partial^2 f}{\partial y^2}, & f_{zz} &= \frac{\partial^2 f}{\partial z^2}, \\ f_{xy} &= \frac{\partial^2 f}{\partial xy}, & f_{xz} &= \frac{\partial^2 f}{\partial xz}, & f_{yz} &= \frac{\partial^2 f}{\partial yz}. \end{aligned}$$

Then, the curvature of a planar curve can be calculated in the following form [15]:

$$k = \frac{(2f_x f_y f_{xy} - f_x^2 f_{yy} - f_y^2 f_{xx})}{(f_x^2 + f_y^2)^{3/2}} \quad (\text{B.7})$$

The Gaussian curvature  $K$  of a surface can be calculated in the following form [78, 142]

$$\begin{aligned} K &= \frac{1}{h^2} [(f_x^2 (f_{yy} f_{zz} - f_{yz}^2) + 2f_y f_z (f_{xz} f_{xy} - f_{xx} f_{yz}) \\ &\quad + f_y^2 (f_{xx} f_{zz} - f_{xz}^2) + 2f_x f_z (f_{yz} f_{xy} - f_{yy} f_{xz}) \\ &\quad + f_z^2 (f_{xx} f_{yy} - f_{xy}^2) + 2f_x f_y (f_{xz} f_{yz} - f_{zz} f_{xy})] \end{aligned} \quad (\text{B.8})$$

The mean curvature  $H$  of a surface can be calculated as [142], [78].

$$\begin{aligned} H &= \frac{1}{2h^{3/2}} [f_x^2 (f_{yy} + f_{zz}) - 2f_y f_z f_{yz} \\ &\quad + f_y^2 (f_{xx} + f_{zz}) - 2f_x f_z f_{xz} \\ &\quad + f_z^2 (f_{xx} + f_{yy}) - 2f_x f_y f_{xy}] \end{aligned} \quad (\text{B.9})$$

where  $h = f_x^2 + f_y^2 + f_z^2$ .

The principal curvatures are calculated according to Eq. (B.6).

### Surface area

We define the flame surface by a triangulated patch consisting of vortices and faces. The total flame surface area is calculated as the sum of the areas of all triangles defined by the vortices all over the patch. The areas of the triangles are calculated by the formula of Heron [15]:

$$A = \sqrt{s(s-a)(s-b)(s-c)} \quad (\text{B.10})$$

with  $s = (a + b + c)/2$ , where  $a, b, c$  are the lengths of the sides of the triangles.

# Appendix C

## Fourier transforms

As mentioned in section 4.1.3 spectra can be obtained by Fourier transforms of velocity correlations of the corresponding eddies. The relation between correlation functions and spectrum functions as Fourier pairs was first introduced in turbulence theory by Taylor [132]. In this section spectra and the relation between correlations and spectra are summarized shortly following the explanations of Batchelor [2] and Rotta [113]. More about the theory of spectra can be found for example in [50, 103, 133].

### Three-dimensional Fourier analysis

For homogeneous turbulence the spectrum tensor  $\Phi_{ij}$  and the correlation tensor  $R_{ij}$  from Eq. (4.10) form the following Fourier transform pair:

$$\Phi_{ij}(\boldsymbol{\kappa}) = \frac{1}{(2\pi)^3} \int_{-\infty}^{\infty} \int_{-\infty}^{\infty} \int_{-\infty}^{\infty} e^{-i\boldsymbol{\kappa}\mathbf{r}} R_{ij}(\mathbf{r}) d\mathbf{r} \quad (\text{C.1})$$

and

$$R_{ij}(\mathbf{r}) = \int_{-\infty}^{\infty} \int_{-\infty}^{\infty} \int_{-\infty}^{\infty} \Phi_{ij}(\boldsymbol{\kappa}) e^{i\boldsymbol{\kappa}\mathbf{r}} d\boldsymbol{\kappa} \quad (\text{C.2})$$

where  $\mathbf{r}$  is the physical variable and  $\boldsymbol{\kappa}$  is the Fourier variable or wavenumber vector. The wavenumber has the dimension 1/length. To the nine components of  $R_{ij}$  correspond nine spectrum functions which form the energy spectrum tensor  $\Phi_{ij}$ .

Considering  $R_{ij}$  for  $|\mathbf{r}|=0$ , Eq. (C.2) becomes:

$$R_{ij}(0) = \overline{u'_i(\mathbf{x})u'_j(\mathbf{x})} = \int_{-\infty}^{\infty} \int_{-\infty}^{\infty} \int_{-\infty}^{\infty} \Phi_{ij}(\boldsymbol{\kappa}) d\boldsymbol{\kappa} \quad (\text{C.3})$$

$\Phi_{ij}$  represents a density, in wavenumber space, of contributions to  $\overline{u'_i(\mathbf{x})u'_j(\mathbf{x})}$ . A knowledge of all components of the tensor  $\overline{u'_i(\mathbf{x})u'_j(\mathbf{x})}$  is necessary and sufficient to determine the energy



associated with an arbitrary component of the velocity.

### The energy spectrum function

Three-dimensional Fourier transforms are appropriate for a function of a vector argument, but the tensors of the three-dimensional velocity spectra contain a lot of information, which is difficult to handle. A simpler though less complete description is provided by the energy spectrum function  $E(\kappa)$ , which is a scalar function of a scalar. Spectrum functions of a single scalar variable can be obtained by averaging  $R_{ij}(\mathbf{r})$  and  $\Phi_{ij}(\boldsymbol{\kappa})$  over all directions of the vector arguments  $\mathbf{r}$  and  $\boldsymbol{\kappa}$ .

$$S_{ij}(r) = \frac{1}{a\pi r^2} \int R_{ij}(\mathbf{r}) dA(r) \quad (\text{C.4})$$

$$\Psi_{ij}(\kappa) = \int \Phi_{ij}(\boldsymbol{\kappa}) dA(\kappa) \quad (\text{C.5})$$

where  $r = |\mathbf{r}|$  and  $\kappa = |\boldsymbol{\kappa}|$ , and the integration is over the surfaces of spheres of which  $dA$  is an element.  $S_{ij}(r)$  is the average correlation tensor for two points, distance  $r$  apart.  $\Psi_{ij}(\kappa)d\kappa$  is the contribution to the energy tensor  $\overline{u'_i u'_j}$  from wave-numbers whose magnitudes lie between  $\kappa$  and  $\kappa + d\kappa$ .

Of particular physical interest is the energy spectrum function, which is half the trace of  $\Psi_{ij}(\kappa)$ .

$$E(\kappa) = \frac{1}{2} \Psi_{ii}(\kappa) \quad (\text{C.6})$$

$E(\kappa)$  describes the density of contributions to the kinetic energy  $k$  from all wavenumbers  $\kappa$  in the infinitesimal shell  $\kappa \leq |\boldsymbol{\kappa}| < \kappa + d\kappa$ .

We obtain the total turbulent kinetic energy  $k$  by integration of  $E(\kappa)$  over all  $\kappa$ :

$$k = \frac{1}{2} \overline{u'_i(\mathbf{x})u'_i(\mathbf{x})} = \int_0^{\infty} E(\kappa) d\kappa \quad (\text{C.7})$$

The longitudinal integral length scale is;

$$L_{11} = \frac{\pi}{2u_{rms}^2} \int \frac{E(\kappa)}{\kappa} d\kappa \quad (\text{C.8})$$

In the Fourier space the dissipation rate  $\varepsilon$  is defined by:

$$\varepsilon = \int_0^{\infty} 2\nu\kappa^2 E(\kappa) d\kappa \quad (\text{C.9})$$

### Spectrum functions in isotropic turbulence

For isotropic turbulence [2, 113], the tensor  $\Phi_{ij}(\boldsymbol{\kappa})$  only depends on the single vector argument

$\kappa$ .  $\Phi_{ii}$  is a function of the wave number magnitude alone. The energy spectrum tensor in Eq. (C.6) becomes:

$$E(\kappa) = 4\pi\kappa^2 \frac{1}{2} \Phi_{ii}(\boldsymbol{\kappa}) \quad (\text{C.10})$$

The contribution to the total energy from that part of wave number space between spheres of radii  $\kappa$  and  $\kappa + d\kappa$  is  $E(\kappa)d\kappa$ . The function  $E(\kappa)$  can be used as the single scalar function defining  $\Phi_{ij}(\boldsymbol{\kappa})$ . The spectrum tensor becomes:

$$\Phi_{ij}(\boldsymbol{\kappa}) = \frac{E(\kappa)}{4\pi\kappa^4} (\kappa^2 \delta_{ij} - \kappa_i \kappa_j) \quad (\text{C.11})$$

### The energy cascade for two-dimensional turbulence

In Fourier space the enstrophy  $D$  is:

$$D = \int_0^{\infty} \kappa^2 E(\kappa, t) d\kappa \quad (\text{C.12})$$

The energy obeys the following conservation equation [73, 74]:

$$\frac{d}{dt} \int_0^{\infty} E(\kappa, t) d\kappa = -2\nu \int_0^{\infty} \kappa^2 E(\kappa, t) d\kappa \quad (\text{C.13})$$

The enstrophy obeys the following conservation equation [73, 74]:

$$\frac{d}{dt} \int_0^{\infty} \kappa^2 E(\kappa, t) d\kappa = -2\nu \int_0^{\infty} \kappa^4 E(\kappa, t) d\kappa \quad (\text{C.14})$$

### Spectra

Spectra in 2D turbulence are discussed for example in [146]. In 2D turbulence the energy spectrum function, Eq. (C.10), becomes:

$$E(\kappa) = \pi\kappa \Phi_{ii}(\kappa) \quad (\text{C.15})$$

where  $E(\kappa)$  corresponds to the kinetic energy integrated on a circle of radius  $\kappa$ , with:

$$\Phi_{ij}(\kappa) = \frac{1}{(2\pi)^2} \int_{-\infty}^{\infty} \int_{-\infty}^{\infty} e^{-i\boldsymbol{\kappa}\mathbf{r}} R_{ij}(\mathbf{r}) d\mathbf{r} \quad (\text{C.16})$$

The integral length scale then becomes:

$$L = \frac{2}{u_{rms}^2} \int \frac{E(\kappa)}{\kappa} d(\kappa), \quad (\text{C.17})$$

# Appendix D

## MATLAB tools

Table D.1: Geometry tools

<b>name</b>	<b>task</b>	<b>input</b>	<b>output</b>
flamefront	draws flame front and boundaries	X,Y,fdefine,level,s iso1,iso2	plot
crestline	calculates and plots crestline	X,Y,t,cut,nf	CREST,cc, plot
flamelength	calculates length(s) of (several parts) of flame	X,Y,fdefine,level,s,fig	dflength, flength
crestlength	calculates length of crestline	cc	dflength, flength
flamethicklin	calculates flame thickness defined as extension of a linear cut between boundaries iso1 and iso2 in a single point	X,Y,xs,ys,nxs,nys, fdefine, level, s, iso1, iso2	fthick
flamethicknonlin	calculates flame thickness along non linear cut between iso1, iso2 in a single point	X,Y,xs,ys,fdefine,level, s, iso1, iso2	fthick
flamethicklin crest	calculates flame thickness defined as extension of a linear cut normal to crestline in a single point	X,Y,xs,ys,nxs,nys, varbound, CREST,s, iso1, iso2	fthicker
flamethicknon lincrest	calculates flame thickness along non linear cut on crestline in a single point	X,Y,xs,ys,varbound, CREST, s, iso1, iso2	fthicker
flamethick lintherm	calculates thermal flame thickness along linear cut using the maximal temperature gradient in a single point	X,Y,xs,ys,nxs,nys, fdefine, level, s, variable, iso1, iso2	fthickth300
flamethick nonlintherm	calculates thermal flame thickness along non linear cut using the maximal temperature gradient in a single point	X,Y,xs,ys, fdefine, level, s, variable, iso1, iso2	fthickth300
flamethick linthermcrest	calculates thermal flame thickness along linear cut normal	X,Y,xs,ys,nxs,nys, varbound,CREST, s,	fthickth300

Table D.1: Geometry tools (cont.)

<b>name</b>	<b>task</b>	<b>input</b>	<b>output</b>
	to crestline using the maximal temperature gradient in a single point	variable iso1, iso2,	
flamethicknon linthermcrest	calculates thermal flame thickness along non linear cut on crestline using the maximal temperature gradient in a single point	X,Y,xs,ys, varbound CREST, s, variable iso1, iso2	fthickth300
flamethicke	calculates flame thickness based on reaction progress variable c in a single point	X,Y,xs,ys,nxs,nys, fdefine,c, level, s	fthick
normal	calculates normalized normal vectors	X,Y,variable	xn,yn
normtoff	calculates and plots normals to flame front	X,Y,fdefine,level,s	SNORM, plot
normtorect	calculates and plots normals to crestline	X,Y,CREST	CRESTN, plot
flamefront3	draws flame front and boundaries	X,Y,Z,fdefine,level,s iso1,iso2	plot
flamefrontslice	plots orthogonal slice through flame front	X,Y,Z,fdefine,level,s, dsl,lsl,iso1,iso2	plot
slicebatchorth	batch of orthogonal slices through domain	X,Y,Z,dsl,variable,v,sm	plot
crestbatch	computes and plots coordinates of crestsurface	X,Y,Z,t,level,s,cut	fcrest,p
surfarea	calculates area of a surface defined as patch	X,Y,Z,fdefine,level,s	Area
flamethicklin3	calculates flame thickness along linear cut between boundaries iso1, iso2 in a single point	X,Y,Z,xs,ys,zs,nxs,nys,nzs, fdefine,dl,level,s,iso1,iso2	fthick3

Table D.1: Geometry tools (cont.)

<b>name</b>	<b>task</b>	<b>input</b>	<b>output</b>
flamethick nonlin3	calculates flame thickness along non linear cut between iso1, iso2 in a single point	X,Y,Z,xs,ys,zs,fdefine, dl,level,s,iso1,iso2	fthick3nonlin
flamethick lintherm3	calculates 3D flame thickness along linear cut based on temperature gradient in a single point	X,Y,Z,xs,ys,zs,nxs,nys,nzs, fdefine,level,s,variable, iso1,iso2	fthickth300
flamethick nonlintherm3	calculates 3D flame thickness along non linear cut based on temperature gradient in a single point	X,Y,Z,xs,ys,zs,fdefine,dl, level,s,variable,iso1,iso2	fthickth300nl3
flamethickc3	calculates flame thickness based on reaction progress variable c in a single point	X,Y,Z,xs,ys,zs,nxs,nys,nzs, fdefine,c,dl,level,s	fthick3
normal3	calculates normalized normal vectors in a 3D field	X,Y,Z,variable	xn,yn,zn
normtoff3	calculates and plots normals to flame front	X,Y,Z,fdefine,level,s,inc	SNORM3

Table D.2: Structure tools

<b>name</b>	<b>task</b>	<b>input</b>	<b>output</b>
flameindex	calculates normalized flame index	X,Y,Y(H <sub>2</sub> ),Y(O <sub>2</sub> ), fdefine, level,s	inn, in
reacprog	calculates reaction progress variable based on temperature	X,Y, temperature	c
reacprogco22d	calculates reaction progress variable based on CO <sub>2</sub> and surface density function	X,Y, Y(CO <sub>2</sub> )	c, sdf, mv
mixfrac	calculates mixture fraction according to formula of Bilger	Y(Species) X,Y	Z(Bilger)
mixfacspec	calculates mixture fraction based on species	Y(Species)	f <sub>H</sub> , f <sub>O</sub> , f <sub>N</sub>
mixfracsyng	calculates mixture fraction according formula of Bilger	Y(Species)	Z (Bilger)
mixfacsyngspec	calculates mixture fraction based on species	Y(Species)	f <sub>H</sub> , f <sub>O</sub> , f <sub>C</sub> , f <sub>N</sub>
scalardissZ	calculates scalar dissipation rate based on mixture fraction	Z,st	chired, chiredn
scalardissc	calculates scalar dissipation rate based on reaction progress variable	c,st	chired, chiredn
crestextract	extracts a variable along crestline of another one	X,Y, crest, variable	cc, cvar, plot
extract	extracts a variable along the isolevel of another one	X,Y,fdefine,level, variable, s, fig	xiso,yiso,viso,variso fprob, plots
flamehot	calculates values of a variable in user-defined hot region of the flame	var1,hval,lval,s,var2	var1red,var2red
linextract	extracts a variable along a linear cut through whole domain normal to flame front	xmin,xmax,ymin,ymax, variable,xs,ys, nxs,nys,dl, X,Y	XX,YY,VV plot

Table D.2: Structure tools (cont.)

<b>name</b>	<b>task</b>	<b>input</b>	<b>output</b>
non linextract	extracts a variable along a non linear cut through whole domain	xmin,xmax,ymin,ymax, variable,xs,ys,nx,ny, fdefine,dl,X,Y	XX,YY,V plot
lincut	extracts a variable along a linear cut with user-defined boundaries	X,Y,xs,ys,nxs,nys, fdefine,variable,dl, level,s, iso1,iso2	xmin,xmax,ymin, ymax,xx1,yy1,vv1, vv2,vvg,plot
lincutcrest	extracts a variable along a linear cut normal to crestline with user-defined boundaries	X,Y,xs,ys,nxs,nys, varbound,variable,dl, CREST,s,iso1,iso2	xmin,xmax,ymin, ymax,xx1,yy1,vv1, vv2,vvg,plot
nonlincut	extracts a variable along a non linear cut with user-defined boundaries	X,Y,xs,ys,fdefine variable,dl,level,s, iso1,iso2	xmin,xmax,ymin, ymax,xx1,yy1,vv1, vv2,vvg,plot
nonlincut crest	extracts a variable along a non linear cut from crestline with user-defined boundaries	X,Y,xs,ys,varbound variable, dl,CREST,s, iso1,iso2	xmin,xmax,ymin, ymax,xx1,yy1,vv1, vv2,vvg,plot
intcut lin	calculates integral value along linear cut with boundaries in a single point	X,Y,xs,ys,nxs,nys, fdefine,variable,dl level,s, iso1,iso2	intvar
intcut lincrest	calculates integral value along linear cut normal to crestline with boundaries in a single point	X,Y,xs,ys,nxs,nys, varbound,variable,dl CREST,s,iso1,iso2	intvar
intcutnon lin	calculates integral value along nonlinear cut with boundaries in a single point	X,Y,xs,ys,fdefine variable, dl,level,s iso1,iso2	intvarn
intcutnon lincrest	calculates integral value along nonlinear cut from crestline with boundaries in a single point	X,Y,xs,ys,varbound variable,dl,CREST,s iso1,iso2	intvarn
flamehot3	calculates values of a variable in user defined region of a 3d flame	var1,hval,lval,s,var2	var1red,var2red



Table D.2: Structure tools (cont.)

<b>name</b>	<b>task</b>	<b>input</b>	<b>output</b>
flameindex3	calculates normalized flameindex of a 3D flame	X,Y,Z,Y(H <sub>2</sub> ),Y(O <sub>2</sub> ), fdefine,level,s	inn,variso
extractbatch	extracts values of a variable along in isovalue of another one in orthogonal 2d-slices	X,Y,Z,fdefine,variable, level,npsl,dsl,s	f,v,varisosl
extract3	extracts a variable along an iso-surface of another one	X,Y,Z,fdefine,level, variable,s,fig	variso,face,vert,fprob
lincut3	extracts a 3D-variable along a linear cut with user-defined boundaries	X,Y,Z,xs,ys,zs,nxs,nys,nzs, fdefine,variable, dl,level,s,iso1,iso2	xmin,xmax,ymin,ymax, zmin,zmax,xx1,yy1, zz1,vv1,vv2,vvg
nonlincut3	extracts a 3D-variable along a non-linear cut with user-defined boundaries	X,Y,Z,xs,ys,zs,fdefine, variable,dl,level, s,iso1,iso2	xmin,xmax,ymin,ymax, zmin,zmax,xx1,yy1, zz1,vv1,vv2,vvg
intcutlin3	calculates integral value of a 3D-variable along a linear cut with boundaries in a single point	X,Y,Z,xs,ys,zs,nxs,nys,nzs fdefine,variable,dl, level,s,iso1,iso2	intvar
intcutnonlin3	calculates integral value of a 3D-variable along a non-linear cut with boundaries in a single point	X,Y,Z,xs,ys,zs,f define,variable, dl,level,s,iso1,iso2	intvarn
mixfrac3	calculates mixture fraction of a 3D-flame according to formula of Bilger	Y(Species),X,Y,Z	mixfr
mixfracspec3	calculates mixture fraction of a 3D-flame based on species	Y(species)	f <sub>H</sub> ,f <sub>O</sub> ,f <sub>N</sub>
mixfracsyng3	calculates mixture fraction of a 3D-flame according to formula of Bilger	Y(species)	ZB
mixfracsyngspec3	calculates mixture fractions of a 3D-flame based on species	Y(Species)	f <sub>H</sub> ,f <sub>O</sub> ,f <sub>N</sub>
reacprog3	calculates reaction progress variable of a 3D-flame based on temperature	X,Y,Z,temperature,level	c

Table D.2: Structure tools (cont.)

<b>name</b>	<b>task</b>	<b>input</b>	<b>output</b>
reacprog3co2	calculates reaction progress variable of a 3D-flame based on CO <sub>2</sub>	X,Y,Z,CO2,level	c,sdf,mv
scalardiss3f	calculates scalar dissipation rate of a 3D-flame based on mixture fraction	f,st	chired,chiredn
scalardiss3c	calculates scalar dissipation rate of a 3D-flame based on react. progr. var.	c,st	chired,chiredn

Table D.3: Turbulence tools

<b>name</b>	<b>task</b>	<b>input</b>	<b>output</b>
streamlines2	plots streamlines of 2D velocity field without direction arrows	X,Y, xvelocity yvelocity	plot
quivplot2	draws vector plot of a 2D velocity field	xvelocity,yvelocity X,Y,(L1,L2,C1,C2)	plot
streamsliceplot2	plots streamlines of a 2D velocity field with direction arrows	xvelocity,yvelocity X,Y	plot
streamlines3	plots streamlines of a 3D velocity field in user-defined points	xvel,yvel,zvel, X,Y,Z, XS,YS,ZS	plot
quivplot3	draws vector plot of a 3D velocity field	xvel,yvel,zvel,X,Y,Z (L1,L2,C1,C2,P1,P2)	plot
coneplot3	draws cone plot of a 3D velocity field	xvel,yvel,zvel,X,Y,Z (L1,L2,C1,C2,P1,P2)	plot
streamsliceplot3	draws orthogonal slice through a 3D velocity field	xvel,yvel,zvel, X,Y,Z,dsl,lsl	plot
streamslicebatch	draws batch of slices through a 3D velocity field	xvel,yvel,zvel, X,Y,Z,dsl,sm	plot
ekinturb2	computes urms values, turb. kin. energy of a 2D vel. field in physical space	xvelocity, yvelocity	u1rms,u2rms ekintnorm,ekintall
ekinturb3	computes urms values, turb. kin. energy of a 3D vel. field in physical space	xvel,yvel,zvel	u1rms,u2rms,u3rms ekintnorm,ekintall
corrfuncntline	calculates and plots autocorrelation coefficients along lines in a 2D field, calculates integral length scale	xvelocity, X	meanrho, meanrhok,L
corrfuncntcol	calculates and plots autocorrelation coefficients along columns in a 2D field, calculates integral length scale	yvelocity, Y	meanrho, meanrhok,L
corrfunctionall3all	calculates and plots autocorrelation coefficients along lines in a 3D field, calculates integral length scale	xvel, X	meanmeanrho,L

Table D.3: Turbulence tools (cont.)

<b>name</b>	<b>task</b>	<b>input</b>	<b>output</b>
corrfuncall3allcol	calculates and plots autocorrelation coefficients along columns in a 3D field, calculates integral length scale	yvel, Y	meanmeanrho,L
spectrum2d	calculates fluctuations, 2D energy spectrum, integral length scale	xvelocity,yvelocity, L,nx,ny	ENVP1,S1,S,k, L11,rms
slope2	verifies slope of kinetic energy (2D)	k,tdiss,ENVP1,nx,ny	plot
spectrum3d	calculates fluctuations, 3D energy spectrum, integral length scale	xvel,yvel,zvel, L,nx,ny,nz	ENVP1,S1,S,k, L11,RMS
slope3	verifies slope of kinetic energy (3D)	k,tdiss,ENVP1,nx,ny,nz	plot
dissip2dord2	calculates turbulent dissipation rate using a 2nd order scheme in a 2D field	xvel,yvel,st,(nu)	tdiss
dissip2dord4	calculates turbulent dissipation rate using a 4th order scheme in a 2D field	xvel,yvel,st,(nu)	tdiss
dissip2dord6	calculates turbulent dissipation rate using a 6th order scheme in a 2D field	xvel,yvel,st,(nu)	tdiss
enstrophy	calculates enstrophy of a 2D vorticity field	vorticity	enstnorm,enstal
slope2enst	plots slope of enstrophy	k, vorticity, tdiss ENVP1, nx ,ny, st	plot
taylor2	calculates Taylor micro-scales in a 2D field	xvel,yvel,X,Y, L1,L2,C1,C2	lambdaf, lambdag
taylor3	calculates Taylor micro-scales in a 2D field	xvel,yvel,zvel,X,Y,Z L1,L2,C1,C2,P1,P2	lambdaf, lambdag
kolmogorov2	calculates Kolmogorov micro-scales	xvel,yvel,temp,dens	lkol, tkol, vkol

Table D.3: Turbulence tools (cont.)

<b>name</b>	<b>task</b>	<b>input</b>	<b>output</b>
	in a 2D-field	X,Y,L1,L2,C1,C2	
kolmogorov3	calculates Komlogorov micro-scales in a 3D-field	xvel,yvel,zvel,temp,dens X,Y,Z,L1,L2,C1,C2,P1,P2	lkol, tkol, vkol
dissip3dord2	calculates turbulent dissipation rate using a 2nd order scheme in a 3D field	xvel,yvel,zvel,st,(nu)	tdiss
dissip3dord4	calculates turbulent dissipation rate using a 4th order scheme in a 3D field	xvel,yvel,zvel,st,(nu)	tdiss
dissip3dord6	calculates turbulent dissipation rate using a 6th order scheme in a 3D field	xvel,yvelzvel,st,(nu)	tdiss
vort2dord2	calculates vorticity of a 2D vector field using a 2nd order scheme	X,Y,xvelocity,yvelocity	vortz
vort2dord4	calculates vorticity of a 2D vector field using a 4th order scheme	X,Y,xvelocity,yvelocity	vortz
vort2dord6	calculates vorticity of a 2D vector field using a 6th order scheme	X,Y,xvelocity,yvelocity	vortz
vort2dord6pb	calculates vorticity of a 2D vector field using a 6th order scheme, optional periodic boundary conditions	X,Y,xvelocity,yvelocity	vortz
vort3dord2	calculates vorticity of a 3D vector field using a second order scheme	xvel,yvel,xvel,step	vortx,vorty,vortz
vort3dord4	calculates vorticity of a 3D vector field using a 4th order scheme	xvel,yvel,xvel,step	vortx,vorty,vortz
vort3dord6	calculates vorticity of a 3D vector field using a 6th order scheme	xvel,yvel,zvel,step	vortx,vorty,vortz
lesfilter3d	filters a matrix in physical space with a user-defined filter size	f, step	LBOXX

Table D.4: Tools describing interaction between turbulence and flames

<b>name</b>	<b>task</b>	<b>input</b>	<b>output</b>
strainrateall	calculates components of strain rate in whole 2d field	X,Y,xvel,yvel,fdefine	strn, strt
strainratelev	calculates components of strain rate along flame front	X,Y,xvel,yvel,fdefine, level, s	siso, strnff,strtff
curvatureall	calculates components of curvature in whole 2d field	X,Y,fdefine	curv
curvaturelev	calculates components of curvature along flame front	X,Y,fdefine, level, s	siso, curv
curv3new	calculates Gaussian-, mean-, principal curvatures in a 3D field	X,Y,Z,fdefine	KG,H,K1,K2
curvlev3new	calculates Gaussian-, mean-, principal curvatures along flame surface	X,Y,Z,KG,H,K1,K2 fdefine,level,s	var1,var2,var3,var4
strainrate3	calculates strainrate components in a 3D field	X,Y,Z,xvel,yvel,zvel fdefine	strn,strt
strnlev3	computes strainrate components along flame surface	X,Y,Z,str,fdefine level,s	str3,meanstr3, stdstr3
shapefactor	computes shape factor and histogram of a 3D flame	var3,var4	s,xinterp,fp plot

Table D.5: Tools for statistical investigation

<b>name</b>	<b>task</b>	<b>input</b>	<b>output</b>
maxi	calculates coordinates and value of maximum of a variable	variable	m,ii,jj
mini	calculates coordinates and value of minimum of a variable	variable	m, ii,jj
condmeanfilt2	calculates mean and rms values of a variable conditioned on mixture fraction or reaction progress variable	X,Y, varcond, variable,dl,iso1,iso2, fu, fl	v, m, rms, mi, ma plot
condmeanfilt22	calculates mean and rms values of a variable conditioned on an arbitrary one	X,Y, varcond, variable,dl,iso1,iso2, fu, fl	v, m, rms,mi, ma plot
condmeanfilt3	calculates mean and rms values of a variable conditioned on mixture fraction or reaction progress variable	X,Y,Z varcond, variable,dl,iso1,iso2, fu, fl	v, m, rms, plot
condmeanfilt33	calculates mean and rms values of a variable conditioned on an arbitrary one	X,Y,Z varcond, variable,dl,iso1,iso2, fu, fl	v, m, rms, plot
correlationgen	calculates and displays correlation between two 1d variables	var1, var2,	cc, plot
correlationex	extracts two variables along flame front calculates and displays correlations between variables	X,Y, fdefine,level, variable1,variable2	cc, plot
correlationcut	extracts two variables along linear cut through flame front calculates and displays correlations between the variables	X,Y, fdefine, variable1,variable2 xs,ys,nxs,nys,s, iso1,iso2,fu,fl	cc, plot
compdf2of	calculates true pdf, gaussian pdf, $\beta$ -pdf of not Favre-av.2D-variable	var1	dpdf,npdf,bpdf histogram, plot
compdf3of	calculates true pdf, gaussian pdf, $\beta$ -pdf of not Favre-av.3D-variable	var1	dpdf,npdf,bpdf histogram,plot

Table D.5: Tools for statistical investigation (cont.)

<b>name</b>	<b>task</b>	<b>input</b>	<b>output</b>
varstat	calculates moments 1 to 4, plots PDF, plots histogram, plots gaussian PDF	variable1	xpdf, fprob, fgauss, STATVAR, histogram, true pdf, gaussian pdf
statbivar2	calculates joint PDF of two 2D-variables plots joint PDF	variable1,variable2	biprob, corr, xint, yint, contourplot
statbivar3	calculates joint PDF of three 2D-variables	variable1,variable2, variable3	corr, contourplot
statbivar3d	calculates joint pdf of two 3D-variables plots joint PDF	variable1,variable2	corr, contourplot



Table D.6: Tools to determine dimensions of manifolds

<b>name</b>	<b>task</b>	<b>input</b>	<b>output</b>
cloudorgvarnb	finds nearest neighbors in composition space for original mass fractions for H <sub>2</sub> -flames	$Y_{sp}$ , TEMP, NN, inc	Tref,N2ref,H2Oref, $M_{Cl}$
cloudorgvarnbsyng	finds nearest neighbors in composition space for original mass fractions for syngas-flames	$Y_{sp}$ , TEMP, NN, inc	Tref,N2ref,H2Oref, $M_{Cl}$
cloudorgvarnbweigh	finds nearest neighbors in composition space for weighted mass fractions	$Y_{sp}$ , TEMP, NN, inc	Tref,N2ref,H2Oref, $M_{Cl}$
cloudorgvarnbTnotw	finds nearest neighbors in composition space for original mass fractions and temperature	$Y_{sp}$ , TEMP, NN, inc	Tref,N2ref,H2Oref, $M_{Cl}$
cloudorgvarnbTweigh	finds nearest neighbors in composition space for weighted mass fractions and temperature	$Y_{sp}$ , TEMP, NN, inc	Tref,N2ref,H2Oref, $M_{Cl}$
cloudorgvarradweigh	finds number of neighbors and correlations in a user-defined radius in composition space for weighted species mass fractions;	$Y_{sp}$ , TEMP,rad,inc	nn,zz, m
svdmatrrecl	calculates singular values and reconstructed matrices of dimension one to five	$M_{Cl}$	s1, u1, v1 $M_{3_{1kept}}$ , $M_{3_{2kept}}$ , $M_{3_{3kept}}$ $M_{3_{4kept}}$ , $M_{3_{5kept}}$
corelmatrorgmatrrecl	calculates correlation coefficients between original and reconstructed matrices	$M_{Cl}$ , M3	cc
devorrreclnorm	calculates mean weighted deviations between original and reconstructed matrices	$M_{Cl}$ , M3	mdev <sub>sp</sub>

Table D.7: Tools in batch mode

<b>name</b>	<b>task</b>	<b>input</b>	<b>output</b>
<sup>1</sup> flamethickcb	calculates flame thickness based on reaction progress variable along flame front, plots thickness along flame front	X, Y, fdefine, level, c, s	sisok, fthick, maxfl, minfl, meanfl
flamethicklinb	calculates flame thicknesses based on linear cuts along flame front, plots thickness along flame front	X, Y, fdefine, level, s, iso1, iso2	sisok, fthick, maxfl, minfl, meanfl
flamethicknonlinb	calculates flame thicknesses based on non linear cuts along flame front, plots thickness along flame front	X, Y, fdefine, level, s, iso1, iso2	sisok, fthick, maxfl, minfl, meanfl
flamethicklinthermb	calculates thermal flame thicknesses based on linear cuts along flame front, plots thickness along flame front	X, Y, fdefine, level, s, variable, iso1, iso2	sisok, fthickth300, maxfl, minfl, meanfl
flamethicknonlinb therm	calculates thermal flame thickness based on non linear cuts along flame front, plots thickness along flame front	X, Y, fdefine, level, s, variable, iso1, iso2	sisok, fthickth300nl, maxfl, minfl, meanfl
flamethicklincrestb	calculates flame thickness based on linear cuts along crestline, plots thickness along crestline	X, Y, varbound, CRESTN, s, iso1, iso2	fthicker, maxfl, minfl, meanfl, siso
flamethicknonlin crestb	calculates flame thickness based on non linear cuts along crestline, plots thickness along crestline	X, Y, varbound, CREST, s, iso1, iso2	fthicker, maxfl, minfl, meanfl, siso
flamethicklintherm crestb	calculates thermal flame thickness based on linear cuts along crestline, plots thickness along crestline	X, Y, varbound, CRESTN, variable, s, iso1, iso2	siso, fthickth300, maxfl, minfl, meanfl
flamethicknonlin thermcrestb	calculates thermal flame thickness based on non linear cuts along crestline, plots thickness along crestline	X, Y, varbound, CRESTN, variable, s, iso1, iso2	siso, fthickth300nl, maxfl, minfl, meanfl

<sup>1</sup>Additionally periodic boundary conditions can be considered. The tools are then named "\*longp" for example flamethicklinblongp

Table D.7: Tools in batch mode (cont.)

<b>name</b>	<b>task</b>	<b>input</b>	<b>output</b>
intcutlinb	calculates integral values of a variable based on linear cuts along flame front, plots integral values vs flame front	X, Y, fdefine, variable, dl, level, s, iso1, iso2	intvar
intcutnonlinb	calculates integral values of a variable based on non linear cuts along flame front, plots integral values along flame front	X, Y, fdefine, variable, dl, level, s, iso1, iso2	intvarn
intcutlincrestb	calculates integral values of a variable based on linear cuts along crestline, plots integral values vs crestline	X, Y, varbound, variable, dl, CRESTN, s, iso1, iso2	intvar
intcutnonlincrestb	calculates integral values of a variable based on non linear cuts along crestline, plots integral values vs crestline	X, Y, varbound, variable, dl, CRESTN, s, iso1, iso2	intvarn
flamethickc3b	calculates flame thickness based on reaction progress variable along flame surface, plots histogram of thickness	X, Y, Z, fdefine, SNORM3, dl, level, s, c	fthick3, mathick, mithick, meanth
flamethicklin3b	calculates flame thickness based on linear cuts in user defined points on flame surface, plots histogram of thickness	X, Y, Z, fdefine, SNORM3, dl, level, s, iso1, iso2	fthick3, mathick, mithick, meanth
flamethicklin3b2	calculates flame thickness based on linear cuts in several points on flame surface, plots histogram of thickness	X, Y, Z, fdefine, dl, level, s, iso1, iso2	fthick3, fthickred, mathick, mithick, meanthick
flamethicklnonin3b	calculates flame thickness based on non linear cuts in user-defined points on flame surface, plots histogram of thickness	X, Y, Z, fdefine, SNORM3, dl, level, s, iso1, iso2	fthick3nonl, mathick, mithick, meanth

Table D.7: Tools in batch mode (cont.)

<b>name</b>	<b>task</b>	<b>input</b>	<b>output</b>
flamethicklnonin3b2	calculates flame thickness based on non linear cuts in several points on flame-surface, plots histogram of thickness	X, Y, Z, fdefine, dl, level, s, iso1, iso2	fthick3nonl, mathick, mithick, meanth
flamethicklin therm3b	calculates thermal flame thickness based on linear cuts in user defined points on flame surface, plots histogram of thickness	X, Y, Z, fdefine, SNORM3, dl, level, s, variable, iso1, iso2	fthickth300, mathick, mithick, meanth
flamethicklin therm3b2	calculates thermal flame thickness based on linear cuts in several points on flame surface, plots histogram of thickness	X, Y, Z, fdefine, dl, level, s, variable, iso1, iso2	fthickth300, mathick, mithick, meanth
flamethicknonlin therm3b	calculates thermal flame thickness based on non linear cuts in user defined points on flame surface, plots histogram of thickness	X, Y, Z, fdefine, SNORM3, dl, level, s, variable, iso1, iso2	fthick3nonl, mathick, mithick, meanth
flamethicknonlin therm3b2	calculates thermal flame thickness based on non linear cuts in several points on flame surface, plots histogram of thickness	X, Y, Z, fdefine, dl, level, s, variable, iso1, iso2	fthick3nonl, mathick, mithick, meanth
intcutlin3b	calculates integral values of a variable along linear cuts at several points of flame surface	X, Y, Z, SNORM3, fdefine, variable, dl, s, iso1, iso2	intvarb
intcutnonlin3b	calculates integral values of a variable along linear cuts at several points of flame surface	X, Y, Z, SNORM3, fdefine, variable, dl, s,iso1,iso2	intvarn

# Bibliography

- [1] BARLOW, R. S. Laser diagnostics and their interplay with computations to understand turbulent combustion. In *Proceedings of the Combustion Institute*, volume 31, pages 49–75, 2007.
- [2] BATCHELOR, G.K. *The Theory of Homogeneous Turbulence*. Cambridge University Press, 1953.
- [3] BATCHELOR, G.K. Computation of the energy spectrum in homogeneous two-dimensional turbulence. *Phys. Fluids, Suppl. II.*, 12:233–239, 1969.
- [4] BAUM, M. Direct numerical simulation: A tool to study turbulent reacting flows. *Ann. Rev. Comput. Physics V*, pages 25–95, 1997.
- [5] BAUM, M., POINSOT, T.J. AND THÉVENIN, D. Accurate boundary conditions for multicomponent reactive flows. *J. Comput. Phys.*, 116:247–261, 1994.
- [6] BILGER, R.W. Turbulent flows with nonpremixed reactants. In P.A. Libby and F.A. Williams, editors, *Turbulent Reacting Flows in Series: Topics in applied physics, Vol. 44*, pages 65–114. Springer-Verlag, Heidelberg, 1980.
- [7] BILGER, R.W. The structure of turbulent non-premixed flames. In *Proceedings of the Combustion Institute*, volume 22, pages 475–488, 1988.
- [8] BILGER, R.W. Turbulent diffusion flames. *Ann. Rev. Fluid Mech.*, pages 101–135, 1989.
- [9] BILGER, R.W. Future progress in turbulent combustion research. *Prog. Energy Combust. Sci.*, 26:367–380, 2000.
- [10] BIRD, R., STEWART, W. AND LIGHTFOOT, E. *Transport Phenomena*. Wiley and sons, New York, 1960.
- [11] BRAY, K.N.C. Turbulent flows with premixed reactants. In P. A. Libby and F.A. Williams, editors, *Turbulent Reacting Flows in Series: Topics in applied physics, Vol. 44*, pages 115–183. Springer-Verlag, 1980.

- [12] BRAY, K. N. C. The challenge of turbulent combustion. In *Proceedings of the Combustion Institute*, volume 26, pages 1–26, 1996.
- [13] BRAY, K.N.C., LIBBY, P.A. AND MOSS, J.B. Flamelet crossing frequencies and mean reaction rates in premixed turbulent combustion. *Combust. Sci. Techn.*, 41:143–172, 1984.
- [14] BREUER, M. *Direkte Numerische Simulation und Large Eddy Simulation auf Hochleistungsrechnern*. Shaker Verlag, 2002.
- [15] BRONSTEIN, I, SEMENDJAJEW, K. *Taschenbuch der Mathematik*. Verlag Harri Deutsch, Thun, 1987.
- [16] BYKOV, V. AND MAAS, U. The extension of the ILDM concept to reaction diffusion manifolds. *Combust. Theory Modelling*, 11:839–862, 2007.
- [17] BYKOV, V. AND MAAS, U. Extension of the ILDM method to the domain of slow chemistry. In *Proceedings of the Combustion Institute*, volume 31, pages 465–472, 2007.
- [18] BYKOV, V. AND MAAS, U. Reaction-diffusion manifolds and global quasi-linearisation: Two complementary methods for mechanism reduction. *The Open Thermodynamics Journal*, 4:92–100, 2010.
- [19] CANDEL, S. AND POINSOT, T. Flame stretch and the balance equation for the flame area. *Combust. Sci. Techn.*, 70:1–15, 1990.
- [20] CANDEL, S., THÉVENIN, D., DARABIHA, N. AND VEYNANTE, D. Problems and perspectives in numerical combustion. In *Computational methods in applied sciences '96*, pages 48–62. John Wiley and sons, 1996.
- [21] CANDEL, S., THÉVENIN, D., DARABIHA, N. AND VEYNANTE, D. Progress in numerical combustion. *Combust. Sci. Techn.*, 149:297–337, 1999.
- [22] CANT, R. S., MASTORAKOS, E. *An Introduction to Turbulent Reacting Flows*. Imperial College Press, 2008.
- [23] CANT, S. Direct numerical simulation of premixed turbulent flames. *Philos. Trans. R. Soc. London Ser. A*, 357:3583–3604, 1999.
- [24] DAMKÖHLER, G. Der Einfluss der Turbulenz auf die Flammengeschwindigkeit in Gasgemischen. *Z. Elektrochem.*, pages 601–626, 1940.
- [25] DINKELACKER, F. Experimental validation of flame regimes for highly turbulent premixed flames. *Proceedings of the European Combustion Meeting*, pages 158/1–158/7, 2003.

- [26] DO CARMO, M. *Differentialgeometrie von Kurven und Flächen*. Vieweg & Sohn Verlagsgesellschaft mbH, Braunschweig, 1993.
- [27] DOMBROWSKI, P. Krümmungsgrößen gleichungsdefinierter Untermanigfaltigkeiten Riemannscher Mannigfaltigkeiten. *Mathem. Nachr.*, 38:133–180, 1968.
- [28] ERLEBACHER, G., HUSSAINI, M.Y., SPEZIALE, C.G. AND ZANG, T.A. Toward the large-eddy simulation of compressible turbulent flows. *J. Fluid Mech.*, 138:155–185, 1992.
- [29] FAHRMEIR, L., KÜNSTLER, R., PIGEOT, I. AND TUTZ, G. *Statistik*. Springer-Verlag Berlin, 2007.
- [30] FAVRE, A.J. Statistical equations of turbulent gases. In *Problems in hydrodynamics and continuum mechanics*, pages 231–266. Society for Industrial and Applied Mathematics, 1969.
- [31] FERZIGER, H.J. AND PERIĆ, M. *Computational Methods for Fluid Dynamics*. Springer-Verlag Berlin, 1999.
- [32] FIORINA, B., BARON, R., GICQUEL, O., THÉVENIN, D., CARPENTIER, S. AND DARABIHA, N. Modelling non-adiabatic partially premixed flames using flame-prolongation of ILDM. *Combust. Theory Modelling*, 7:449–470, 2003.
- [33] FIORINA, B., GICQUEL, O., VERVISCH, L., CARPENTIER, S. AND DARABIHA, N. Approximating the chemical structure of partially premixed and diffusion counterflow flames using FPI flamelet tabulation. *Combust. Flame*, 140:147–160, 2005.
- [34] FOX, R. O. *Computational Models for Turbulent Reacting Flows*. Cambridge University Press, 2003.
- [35] FRU, G., GOUARIN, L., LAVERDANT, A., THÉVENIN, D., ZISTL, C. AND JANIGA, G. Three dimensional direct simulation of a nonpremixed hydrogen/air flame using detailed models. In *Proceedings of the Combustion Institute*, poster presentation.
- [36] FRU, G., SHALABY, H., LAVERDANT, A., ZISTL, C., JANIGA, G. AND THÉVENIN, D. Direct numerical simulations of turbulent flames to analyze flame/ acoustic interactions. In A. Schwarz and J. Janicka, editors, *Combustion noise, Fluid mechanics and its applications*, pages 239–268. Springer-Verlag, Berlin, 2009.
- [37] GERLINGER, P. Investigation of an assumed pdf approach for finite-rate-chemistry. *Combust. Sci. Techn.*, 175:841–872, 2003.
- [38] GERLINGER, P. *Numerische Verbrennungssimulation*. Springer-Verlag Berlin, 2005.

- [39] GERLINGER, P., NOLL, B. AND AIGNER, M. Assumed pdf modelling and pdf structure investigation using finite rate chemistry. *Progr. Comput. Fluid Dynamics*, 5:334–335, 2005.
- [40] GICQUEL, O., DARABIHA, N. AND THÉVENIN, D. Laminar premixed hydrogen/air counterflow flame simulations using flame prolongation of ILDM with differential diffusion. In *Proceedings of the Combustion Institute*, volume 28, pages 1901–1908, 2000.
- [41] GKIOULEKAS, E. AND TUNG, K.K. On the double cascade of energy and enstrophy, part 1: Theoretical approximation. *Discrete and dynamical systems-Series B*, 5:79–102, 2005.
- [42] GKIOULEKAS, E. AND TUNG, K.K. On the double cascade of energy and enstrophy, part 2: Approach of the KLB limit and interpretation of experimental evidence. *Discrete and dynamical systems-Series B*, 5:103–124, 2005.
- [43] GOLUB, G.H., VAN LOAN, C.F. *Matrix Computation*. The Hopkins University Press, Baltimore, London, 1989.
- [44] GOUSSIS, D. A. AND MAAS, U. Model reduction for combustion chemistry. In T. Echekki and E. Mastorakos, editors, *Turbulent Combustion Modeling*, pages 193–219. Springer-Verlag, Berlin, 2011.
- [45] HAMMING, R. W. *Numerical methods for scientists and engineers*. McGraw-Hill Book Company, 1962.
- [46] HEYWOOD, J. B. *Internal combustion engine fundamentals*. McGraw-Hill Book Company, 1988.
- [47] HILBERT, R. AND THÉVENIN, D. Influence of transport model on hydrogen/air turbulent non-premixed flames. *Proceedings of the European Combustion Meeting*, pages 1–6, 2003.
- [48] HILBERT, R. AND THÉVENIN, D. Influence of differential diffusion on maximum flame temperature in turbulent nonpremixed hydrogen/air flames. *Combust. Flame*, 138:175–187, 2004.
- [49] HILBERT, R., TAP, F., EL-RABII, H., AND THÉVENIN, D. Impact of detailed chemistry and transport models on turbulent combustion simulations. *Prog. Energy Combust. Sci.*, 30:61–117, 2004.
- [50] HINZE, J. O. *Turbulence*. McGraw-Hill Book Company, 1959.
- [51] HIRSCHFELDER, J., CURTISS, C. AND BIRD, R. *Molecular Theory of Liquids and Gases*. Wiley and sons, New York, 1954.



- [52] HUGHES, J. *Differential Geometry of Implicit Surfaces in 3D-Space, CS-03-05*. Department of computer Science, Brown university, Providence Rhode Islands 02912, 2003.
- [53] INTERACTIVE SUPERCOMPUTING. Getting started with Star-P. *Massachusetts Institute of Technology*, 2006.
- [54] INTERACTIVE SUPERCOMPUTING. Star-p programming guide for use with matlab, release 2.7. *Massachusetts institute of Technology*, 2008.
- [55] JENKINS, K.W., CANT, R.S. Curvature effects on flame kernels in a turbulent environment. In *Proceedings of the Combustion Institute*, volume 29, pages 2023–2029, 2002.
- [56] JENKINS, K.W., KLEIN, M., CHAKRABORTY, N. AND CANT, R.S. Effects of strain rate and curvature on the propagation of a spherical flame kernel in the thin-reaction-zone regime. *Combust. Flame*, 145:415–343, 2006.
- [57] JONES, W.P. AND LAUNDER, B.E. The prediction of laminarization with a two-equation model of turbulence. *Int. J. Heat Mass Transfer*, 15:301–314, 1972.
- [58] JONES, W.P. AND MUSONGE, P. Closure of the Reynolds stress and scalar flux equations. *Phys. Fluids*, 31:3589–3604, 1988.
- [59] JOOS, F. *Technische Verbrennung*. Springer-Verlag, Berlin, Heidelberg, 2006.
- [60] KARLOVITZ, B., DENNINSTON, D.W., KNAPSCHSCHAEFER, D.H., AND WELLS, F.E. Studies on turbulent flames. In *Proceedings of the Combustion Institute*, volume 4, pages 613–620, 1953.
- [61] KLIMENKO, A. Y. AND BILGER, R.W. Conditional moment closure of turbulent combustion. *Prog. Energy Combust. Sci.*, 25:595–687, 1999.
- [62] KOLMOGOROV, A.N. The local structure of turbulence in incompressible viscous fluid for very large Reynolds number. *Comptes Rendus Doclady de l'Académie des Sciences de l'URSS*, 30:301–305, 1941.
- [63] KOLMOGOROV, A.N. A refinement of previous hypotheses concerning the local structure of turbulence in a viscous incompressible fluid at high Reynolds number. *J. Fluid Mech.*, 13:82–85, 1961.
- [64] KRAICHNAN, R. H. Inertial ranges in two-dimensional turbulence. *Phys. Fluids.*, 10:1417–1423, 1967.
- [65] KRAICHNAN, R. H. AND MONTGOMERY, D. Two-dimensional turbulence. *Rep. Prog. Phys.*, 43:547–619, 1980.

- [66] KRAUSE, U., GROSSHANDLER, W. AND GRITZO, L. The international forum of fire research directors: A position paper on sustainability and fire safety. *Fire Safety Journal*, 49:79–81, 2012.
- [67] KUO, K.K. *Principles of Combustion*. Wiley and sons, New York, 1986.
- [68] LAUNDER, B., REECE, G., AND RODI, W. Progress in the development of a Reynolds-stress turbulence closure. *J. Fluid Mech.*, 68:537–566, 1975.
- [69] LECHNER, C. AND SEUME, J. *Stationäre Gasturbinen*. Springer-Verlag Berlin, 2003.
- [70] LEITH, C.E. Diffusion approximation for two-dimensional turbulence. *Phys. Fluids.*, 10:1417–1423, 1967.
- [71] LENSE, J. *Kurze Einführung in die Differentialgeometrie des Raumes*. Verlag von R. Oldenbourg, Muenchen, 1954.
- [72] LEONARD, A. Energy cascade in Large-Eddy Simulations of turbulent fluid flows. *Ad. in Geophysics*, 18:237–248, 1974.
- [73] LESIEUR, M. Introduction à la turbulence bidimensionnelle. *J. Mec. Th. Appl., Suppl.*, 28:5–20, 1983.
- [74] LESIEUR, M. *Turbulence in Fluids*. Martinus Nijhoff Publishers, 1987.
- [75] LESIEUR, M. AND MÉTAIS, O. New trends in large-eddy simulations of turbulence. *Ann. Rev. Fluid Mech.*, 28:45–82, 1996.
- [76] LIÑAN, A. AND WILLIAMS, F.A. *Fundamental Aspects of Combustion*. Oxford University Press, New York, Oxford, 1993.
- [77] LOCKWOOD, F.C. AND NAGUIB, A.S. The prediction of the fluctuations in the properties of free, round-jet, turbulent, diffusion flames. *Combust. Flame*, 24:109–124, 1975.
- [78] LOHMANN, G. *Volumetric Image Analysis*. Wiley, Teubner, 1998.
- [79] MAAS, U. Efficient calculation of intrinsic low-dimensional manifolds for the simplification of chemical kinetics. *Comput. Vis. Sci.*, 1:69–81, 1998.
- [80] MAAS, U. *Automatische Reduktion von Reaktionsmechanismen zur Simulation reaktiver Strömungen*. Fakultät für Energietechnik, Universität Stuttgart, 2002.
- [81] MAAS, U. AND POPE, S.B. Simplifying chemical kinetics: Intrinsic low-dimensional manifolds in composition space. *Combust. Flame*, 88:239–264, 1992.

- [82] MAAS, U. AND THÉVENIN, D. Correlation analysis of direct numerical simulation data of non-premixed flames. In *Proceedings of the Combustion Institute*, volume 27, pages 1183–1189, 1998.
- [83] MAAS, U. AND TOMLIN, A. S. Time-scale splitting-based mechanism reduction. In *Cleaner Combustion*, pages 467–484. Springer-Verlag, London, 2013.
- [84] MAGNUSSEN, B.F. AND MJERTAGER, B.H. On mathematical modeling of turbulent combustion with special emphasis on soot formation and combustion. In *Proceedings of the Combustion Institute*, volume 16, pages 719–727, 1976.
- [85] MA, KL., ROSS, R., HUANG, J., HUMPHREYS G., MAX, N., MORELAND, K., OWENS, J.D. AND SHEN, HW. Ultra-scale visualisation: Research and education. *J. of Physics, Conf. Ser.*, 012088, 78:1–6, 2007.
- [86] MA, KL., WANG, C., YU, H. AND TIKHONOVA, A. In-situ processing and visualization for ultrascale simulations. *J. of Physics, Conf. Ser.*, 012043, 78:1–10, 2007.
- [87] MATHWORKS (2005). *Using Matlab 7*. The MathWorks Inc. Natick, MA, 2005.
- [88] MOIN, P. AND MAHESH, K. Direct numerical simulation: A tool in turbulent research. *Ann. Rev. Fluid Mech.*, 30:539–578, 1998.
- [89] MÜNZBERG, H. *Flugantriebe*. Springer-Verlag Berlin, 1972.
- [90] NAVIER, C.L.M.H. Mémoire sur les lois du mouvement des fluides. *Mém. de l'Académie*, 6:389–440, 1822.
- [91] NOLL, B. *Numerische Strömungsmechanik*. Springer-Verlag Berlin, 1993.
- [92] OBOUKHOV, A.M. Some specific features of atmospheric turbulence. *J. Fluid Mech.*, 13:77–81, 1961.
- [93] ORSZAG, S. A. AND PATTERSON, G. S. (JR.). Numerical simulation of turbulence. In M. Rosenblatt and C. van Atta, editors, *Statistical Models and Turbulence*, pages 127–147. Springer-Verlag, Berlin, 1972.
- [94] PAPULA, L. *Mathematik für Ingenieure und Naturwissenschaftler*, volume 3. Vieweg, Wiesbaden, 2001.
- [95] PETERS, N. Laminar Flamelet Concepts in Turbulent Combustion. In *Proceedings of the Combustion Institute*, volume 21, pages 1231–1250, 1986.
- [96] PETERS, N. *Turbulent Combustion*. Cambridge University Press, Cambridge, 2000.

- [97] PFADLER, S., BEYRAU, F., DINKELACKER, F. AND LEIPERTZ, A. A-priory testing of an eddy viscosity model for the density-weighted subgrid scale stress tensor in turbulent premixed flames. *Exp. Fluids*, 49:839–851, 2010.
- [98] PIOMELLI, U. Large-eddy simulation: achievements and challenges. *Progr. Aerospace Sci.*, 35:335–362, 1999.
- [99] POINSOT, T. AND LELE, S. Boundary conditions for direct simulation of compressible viscous flows. *J. Comput. Phys.*, 101:104–129, 1992.
- [100] POINSOT, T. AND VEYNANTE, D. *Theoretical and Numerical Combustion*. R.T. Edwards, Philadelphia, 2001.
- [101] POPE, S.B. PDF methods for turbulent reactive flows. *Prog. Energy Combust. Sci.*, 11:119–192, 1985.
- [102] POPE, S.B. Turbulent premixed flames. *Ann. Rev. Fluid Mech.*, 19:237–270, 1987.
- [103] POPE, S.B. *Turbulent Flows*. Cambridge University Press, 2001.
- [104] POPE, S.B. Small scales, many species and the manifold challenges of turbulent combustion. In *Proceedings of the Combustion Institute*, volume 34, pages 1–31, 2013.
- [105] PRANDTL, L. Bericht über Untersuchungen zur ausgebildeten Turbulenz. *Zeitschrift für angewandte Mathematik und Mechanik (ZAMM)*, 5:136–139, 1925.
- [106] PRANDTL, L. AND WIEGHARDT, K. Über ein neues Formelsystem für die ausgebildete Turbulenz. *Nachrichten der Akad. Wiss.*, pages 6–19, 1945.
- [107] REN, Z. AND POPE, S.B. The use of slow manifolds in reactive flows. *Combust. Flame*, 147:243–261, 2006.
- [108] REYNOLDS, O. An experimental investigation of the circumstances which determine whether the motion of water shall be direct and sinuous, and the law of resistance in parallel channels. *Philos. Trans. R. Soc. London Ser. A*, 174:935–982, 1883.
- [109] REYNOLDS, O. On the dynamical theory of incompressible viscous fluids and the determination of the criterion. *Philos. Trans. R. Soc. London Ser. A*, 186:123–164, 1895.
- [110] REYNOLDS, W. C. Computation of turbulent flows. *Ann. Rev. Fluid Mech.*, 8:183–208, 1976.
- [111] RICHARDSON, L.F. *Weather prediction by numerical processes*. Cambridge University Press, 1922.

- [112] ROGALLO, R. AND MOIN, P. Numerical simulation of turbulent flows. *Ann. Rev. Fluid Mech.*, 16:99–137, 1984.
- [113] ROTTA, J.C. *Turbulente Strömungen*. Teubner-Verlag Stuttgart, 1972.
- [114] RUTLAND, C.J. AND TROUVÉ, A. Direct simulations of premixed turbulent flames with nonunity Lewis numbers. *Combust. Flame*, 94:41–57, 1993.
- [115] SAGAUT, P. *Large Eddy Simulation for Incompressible Flows*. Springer-Verlag, Berlin, 2001.
- [116] SCHEAFFER, R.L. AND MCCLAVE, J.T. *Probability and Statistics for Engineers*. Duxbury Press Belmont, California, 2007.
- [117] SCHIESSL, R. AND MAAS, U. Von Elementarreaktionen zum technischen Verbrennungssystem, Die Verbrennung. *Physik in unserer Zeit*, 44:12–18, 2013.
- [118] SCHIESTEL, R. *Modeling and Simulation of Turbulent Flows*. ISTE Ltd London, 2008.
- [119] SHALABY, H. AND THÉVENIN, D. Statistically significant results for the propagation of a turbulent flame kernel using direct numerical simulation. *Flow Turbulence Combust.*, pages 357–367, 2010.
- [120] SMAGORINSKY, J.S. General circulation experiments with the primitive equations, 1. The basic experiment. *Monthly Weather Review.*, 91:99–164, 1963.
- [121] SPALDING, D.B. Mixing and chemical reaction in steady confined turbulent flames. In *Proceedings of the Combustion Institute*, volume 13, pages 649–657, 1971.
- [122] SPALDING, D.B. Development of the eddy-break-up model of turbulent combustion. In *Proceedings of the Combustion Institute*, volume 16, pages 1657–1663, 1976.
- [123] SPECHT, E. Die Beherrschung des Feuers als Schlüssel zur Entwicklung der Menschheit und die Auswirkung auf die Umwelt. *Magdeburger Wissenschaftsjournal.*, 1:33–37, 1999.
- [124] SPECHT, E. Simulation und Messung von Prozessen in Industrieöfen. *Gaswaerme Int.*, 50:174–177, 2001.
- [125] SPECHT, E. AND JESCHAR, R. Reaktionsmechanismen und Abbrandgeschwindigkeit mit Luft angeströmter Kohlenstoffteilchen. *Steel Research*, 57:148–159, 1986.
- [126] SPECHT, E. AND JESCHAR, R. Ermittlung der geschwindigkeitsbestimmenden Mechanismen bei der Verbrennung von dichten Kohlentelchen. In *VDI Berichte, Verbrennung und Feuerungen*, volume 645, pages 45–56, 1987.

- [127] SPEZIALE, C.G. Analytical methods for the development of Reynold-stress-closures in turbulence. *Ann. Rev. Fluid Mech.*, 23:107–157, 1991.
- [128] STOKES, G.G. On the theory of internal friction of fluids in motion, and of the equilibrium and motion of elastic solids. *Trans. Cambridge Philos. Soc.*, 8:935–982, 1845.
- [129] TAP, F., HILBERT, R., THÉVENIN, D. AND VEYNANTE, D. A generalized flame surface density modelling approach for the auto-ignition of a turbulent non-premixed system. *Combust. Theory Modelling*, 8:165–193, 2004.
- [130] TAYLOR, G.I. Diffusion by continuous movements. *Proc. Lond. Math. Soc.*, 20:196–212, 1921.
- [131] TAYLOR, G.I. Statistical theory of turbulence. *Proc. Roy. Soc. Loandon,A*, 151:421–478, 1935.
- [132] TAYLOR, G.I. The spectrum of turbulence. *Proc. Roy. Soc.London,A*, 164:476–490, 1938.
- [133] TENNEKES, H. AND LUMLEY, J.L. *A First Course in Turbulence*. MIT Press, Cambridge, Mass., 1972.
- [134] THÉVENIN, D. Three dimensional direct simulations and structure of expanding turbulent methane flame. In *Proceedings of the Combustion Institute*, volume 30, pages 629–637, 2005.
- [135] THÉVENIN, D. Modelling internal reacting flows. In *Conference on modelling fluid flow, CMFF'06*, pages 12–25, Budapest, Hungary, 2006.
- [136] THÉVENIN, D. AND CANDEL, S. Optimization procedure of a parallel direct simulation code to investigate reactive flows. In M. Bubak and J. Muscinski, editors, *Proc. SUP EUR 96*, pages 268–274. ACC Cyfronet, Krakow, 1999.
- [137] THÉVENIN, D., BAUM, M. AND POINSOT, T.J. Description of accurate boundary conditions for the simulation of reactive flows. In T.J. Poinsot, T. Baritaud, and M. Baum, editors, *Direct Numerical Simulation of Turbulent Reacting Flows*. Editions Technip, 1996.
- [138] THÉVENIN, D., BEHRENDT, F., MAAS, U., PRZYWARA, B. AND WARNATZ, J. Development of a parallel direct simulation code to investigate reactive flows. *Computers & Fluids*, 25:485–496, 1996.
- [139] THÉVENIN, D., GICQUEL, O., DE CHARENTANY, J., HILBERT, R. AND VEYNANTE, D. Two- versus three-dimensional direct simulations of turbulent methane flame kernels using realistic chemistry. In *Proceedings of the Combustion Institute*, volume 29, pages 2021–2039, 2002.

- [140] THÉVENIN, D., HILBERT, R. AND GICQUEL, O. Three-dimensional direct simulations of turbulent flames using realistic chemistry modeling. *IUTAM Symposium on Turbulent Mixing and Combustion*, pages 279–286, 2002.
- [141] THÉVENIN, D., HILBERT, R., SHALABY, H. AND JANIGA, G. Initial flame propagation in a turbulent flow. In *1st ECCOMAS Thematic Conference on Computational Combustion*, pages 25/1–25/20. Instituto Tecnico, Lisbon, 2005.
- [142] THIRION, J., GOURDON, A. *The 3D Marching lines algorithm and its application to crest lines extraction, Rapport de Recherche N 1672*. Institut National de Recherche en Informatique et en Automatique, Unité de Recherche Inria-Rocquencourt, 1992.
- [143] VAN OIJEN, J.A AND DE GOEY L.P.H. Modelling of premixed counterflow flames using the flamelet-generated manifold method. *Combust. Theory Modeling*, 6:463–478, 2002.
- [144] VERVISCH, L. AND POINSOT, T. Direct numerical simulation of non-premixed turbulent flames. *Ann. Rev. Fluid Mech.*, 30:655–691, 1998.
- [145] VEYNANTE, D. AND VERVISCH, L. Turbulent combustion modeling. *Prog. Energy Combust. Sci.*, 28:193–266, 2002.
- [146] v. KALMTHOUT, E., POINSOT, T. AND CANDEL, S. Turbulence 2d: Théorie et simulation directe. *Internal Report, Ecole Centrale Paris*, 1995.
- [147] v. KÁRMÁN, T. The fundamentals of the statistical theory of turbulence. *J. Aero. Sci.*, 4:131–138, 1937.
- [148] v. KÁRMÁN, T. AND HOWARTH, L. On the statistical theory of isotropic turbulence. *Proc. Roy. Soc. London, A*, 164:192–215, 1938.
- [149] v. WEIZSÄCKER, C.F. Das Spektrum der Turbulenz bei grossen Reynoldsschen Zahlen. *Z. Phys.*, 124:614–627, 1948.
- [150] WARNATZ, J., MAAS, U. AND DIBBLE, R.W. *Verbrennung*. Springer-Verlag Berlin, 2001.
- [151] WESTBROOK, C. K., MIZOBUCHI, Y., POINSOT, T. J., SMITH, P. J., WARNATZ, J. Computational combustion. In *Proceedings of the Combustion Institute*, volume 30, pages 125–157, 2005.
- [152] WILLIAMS, F.A. *Combustion Theory*. Benjamin Cummings, 1985.

- [153] YAMASHITA, H., SHIMADA, M. AND TAKENO, T. A numerical study on flame stability at the transition point of jet diffusion flames. In *Proceedings of the Combustion Institute*, volume 26, pages 27–34, 1996.
- [154] ZISTL, C., FRU, G., JANIGA, G. AND THÉVENIN, D. Anaflame documentation. <http://www.ovgu.de/isut/LSS/anaflame>, 2013.
- [155] ZISTL, C., HILBERT, R., JANIGA, G. AND THÉVENIN, D. Increasing the efficiency of post-processing for turbulent reacting flows. *Comput. Vis. Sci.*, 12:383–395, 2009.
- [156] ZISTL, C., SCHIESSL, R., FRU, G. AND THÉVENIN, D. The dimension of low dimensional manifolds in state space: a study using DNS data. In *Proceedings of the European Combustion Meeting*, pages P4–88/1–6, Lund, Sweden, 2013.



## Own Publications

FRU, G., ZISTL, C., JANIGA, G. AND THÉVENIN, D., Direct numerical simulations of methane flames using tabulated chemistry, in DNS and LES of reacting flows, Maastricht, The Netherlands, 2008, pp:65–66.

FRU, G., GOUARIN, L., LAVERDANT, A., THÉVENIN, D., ZISTL, C. AND JANIGA, G., Three dimensional direct simulation of a nonpremixed hydrogen/air flame using detailed models, in Proceedings of the Combustion Institute, 2008, vol. 32, poster presentation.

ZISTL, C., HILBERT, R., JANIGA, G. AND THÉVENIN, D., Increasing the efficiency of post-processing turbulent reacting flows, in Comput. Vis. Sci., 2009, vol.12, pp:383–395.

FRU, G., SHALABY, H., LAVERDANT, A., ZISTL, C., JANIGA, G. AND THÉVENIN, D., Direct numerical simulations of turbulent flames to analyze flame/ acoustic interactions, in Combustion noise, in Fluid mechanics and its applications, Schwarz, A. and Janicka, J., eds. Springer-Verlag, Berlin ”, 2009, pp:239–268.

FRU, G., THÉVENIN, D., ZISTL, C., JANIGA, G., GOUARIN, L. AND LAVERDANT, A., 3D direct simulations of a non-premixed hydrogen flame with detailed models, in Direct and Large Eddy Simulation VII, Armenio, V. Geurts, B. and Fröhlich, J., eds., ERCOFTAC Series, Springer-Verlag, 2010, pp:433–437.

ZISTL, C., FRU, G., JANIGA, G. AND THÉVENIN, D., Anafame Documentation, in <http://www.ovgu.de/isut/LSS/anafame>, 2014.

ZISTL, C., SCHIESSL, R., FRU, G. AND THÉVENIN, D., The dimension of low dimensional manifolds in state space: a study using DNS data, in Proceedings of the European Combustion Meeting, Lund, Sweden, 2013, pp:P4-88/1–6.